Stochastic models for cellular networks planning and performance assessment

Jean-Sébastien Gomez

ParisTech
INSTITUT DES SCIENCES ET TECHNOLOGIES
PARIS INSTITUTE OF TECHNOLOGY

TELECOM ParisTech

2018-ENST-0026

EDITE - ED 130

Doctorat ParisTech

T H È S E

pour obtenir le grade de docteur délivré par

TELECOM ParisTech

Spécialité “Informatique et Réseaux”

présentée et soutenue publiquement par

Jean-Sébastien GOMEZ

le 15 mai 2018

Modèles stochastiques pour le dimensionnement et l’évaluation des performances des réseaux mobiles.

Directeur de thèse : **Philippe MARTINS**

Jury

Mme Catherine GLOAGUEN, Ingénieur HDR, Orange, France	Rapporteur
M. Xavier LAGRANGE, Professeur, IMT Atlantique, France	Rapporteur
M. Jérôme BROUET, Ingénieur, Thales communications, France	
M. Philippe GODLEWSKI, Professeur, Télécom ParisTech, France	
M. Brian MARK, Professeur, GMU, États-Unis	
M. Philippe MARTINS, Professeur, Télécom ParisTech, France	Directeur de thèse
Mme Anaïs VERGNE, Maître de Conférences, Télécom ParisTech, France	Encadrant de thèse

TELECOM ParisTech
école de l’Institut Mines-Télécom - membre de ParisTech
46 rue Barrault 75013 Paris - (+33) 1 45 81 77 77 - www.telecom-paristech.fr

T H È S E

Stochastic models for cellular networks planning and performance assessment

Jean-Sébastien GOMEZ

RESUME : Avec l'explosion des solutions nomades autour de l'Internet des objets, les systèmes et réseaux sans-fils se doivent de supporter le développement exponentiel d'un éco-système numérique. L'évaluation et l'optimisation des performances radio de tels systèmes, véritable colonne vertébrale du monde des objets connectés, revêtent un caractère crucial. Le but de cette thèse est d'introduire de nouvelles méthodes théoriques et numériques afin d'approfondir notre compréhension au niveau réseau.

En effet, l'évaluation des performances des réseaux et plus spécifiquement des réseaux radio-mobiles est en général vu sous l'angle de la capacité du canal. Grâce à la géométrie stochastique, l'influence du facteur spatial, c'est à dire l'influence de la position des interféreurs, est prise en compte. Dans cette thèse, nous utiliserons le processus ponctuel β-Ginibre pour modéliser la position des stations de base dans le plan. Le β-Ginibre est un processus ponctuel répulsif, dont la répulsion est contrôlée par le coefficient β. Lorsque β tend vers 0, le processus ponctuel converge en loi vers un processus ponctuel de Poisson. Si β est égal à 1, alors c'est un processus ponctuel de Ginibre. L'analyse numérique des données réelles collectées en France montrent que la position des stations de base peut être modélisée par un processus de β-Ginibre. De plus, il est prouvé que la superposition de processus ponctuels de β-Ginibre tend vers un processus de Poisson, comme il est observé sur les données réelles. Une interprétation qualitative de la qualité du déploiement du réseau peut aussi être déduite de cette analyse.

Le paramètre β, représentant la stratégie de déploiement d'un opérateur, est aussi un indicateur de la qualité globale du signal : plus le déploiement est régulier, meilleure sera la qualité du signal. Le gain de performance induit par un β plus proche de 1 est quantifié dans le cadre d'un réseau mobile uniquement limité par les interférences et l'affaiblissement. Afin de généraliser l'évaluation des performances réseau, nous proposons une nouvelle méthode d'allocation et de dimensionnement des ressources dans les réseaux 4G, basée sur les équilibres de Cournot-Nash. Pour cette méthode, seule la qualité du signal entre les équipements communicants est nécessaire pour déterminer la stratégie d'allocation des ressources. La fourniture des ressources ainsi que les besoins en trafic sont modélisés par des mesures de probabilité. C'est le couplage entre ces deux mesures qui permet de déduire une stratégie d'allocation de ressources optimale, par minimisation d'une fonction de coût quadratique. L'analyse numérique révèle qu'il existe un point de fonctionnement optimal, où la satisfaction des utilisateurs est égale à la part d'occupation du réseau.

ABSTRACT : With the booming of the ubiquitous and nomad Internet of Things, wireless systems and networks must support the limitless development of a digitalized eco-system. Being the backbone of the connected devices, asserting and optimizing wireless network performance is of a major importance. This dissertation aims at introducing methods and numerical analysis frameworks to enhance our comprehension of performance at a network level.

Indeed, network performance has been widely explored from the point of view of the link capacity. Thanks to stochastic geometry and point process, we are able characterize the influence of the positions of the antennas. In this dissertation, the β-Ginibre point process is chosen to model the locations of the base stations in the plain. The β-Ginibre is a repulsive point process in which repulsion is controlled by the β parameter. When β tends to zero, the point process converges in law towards a Poisson point process. If β equals to one it becomes a Ginibre point process. Simulations on real data collected in France show that base station locations can be fitted with a β-Ginibre point process. Moreover we prove that their superposition tends to a Poisson point process as it can be seen from real data. Qualitative interpretations on deployment strategies are derived from the model fitting of the raw data. The β parameter that represents the deployment strategy of a operator, is also an indicator of the overall signal quality in the network : the more regular the deployment is, the better the overall signal quality. In order to quantify the gain in performance induced by a higher β, a interference limited network model based on marked point process and loss probability has been introduced.

In order to generalize performance analysis to any networks, a scheme based on the Cournot-Nash equilibria is investigated. Under this general framework, only the signal quality between nodes is required to derive a resource allocation strategy for the overall network. Supply in resources of the network and traffic requirements are modeled by probability measures. The optimal resource allocation strategy is derived by the coupling between the two probability measures that minimizes a specific quadratic objective function. Numerical analysis highlights that there exists an optimal working point, where users satisfaction and network occupancy are equal.

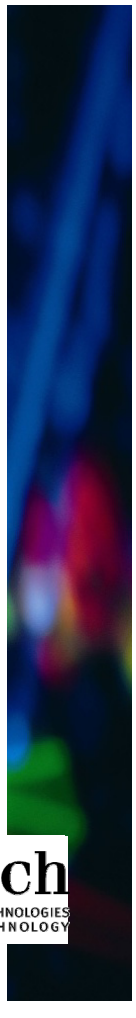

TELECOM ParisTech

EDiTE

ParisTech
INSTITUT DES SCIENCES ET TECHNOLOGIES
PARIS INSTITUTE OF TECHNOLOGY

Remerciements

Je tiens tout particulièrement à remercier :

Dr. Catherine Gloaguen et Prof. Xavier Lagrange qui, par leur relecture de qualité et leurs conseils avisés, ont grandement contribué à l'amélioration de ce document,

Prof. Philippe Godlewski pour son aide précieuse dans la préparation de la soutenance,

Mes directeurs de thèse, Prof. Philippe Martins, Dr. Anaïs Vergne, ainsi que Prof. Laurent Decreusefond, qui m'ont permis d'apprécier l'horizon de la connaissance comme un nain perché sur les épaules de géants.

Contents

Chapter 1

Introduction

1.1 Scope

The beginning of the 21st century has seen the rise of the Internet that brought a wide range of ubiquitous services. Mobile networks, mainly oriented towards voice and message services now carry data with point-to-point bit-rates that are expected to reach gigabits per second with the coming of 5th generation networks. The so-called Internet of Things is now becoming a tangible reality with the rapid development of common devices with embedded connection capabilities. To fulfill such demand of bandwidth implies providing better theoretical tools to tackle and understand frontier engineering challenges, in particular, dense cellular networks. This type of network advocates for the development of novel mathematical models to assess and predict performance on a network level.

Current performance analysis schemes and research are mostly based on models that implement a vision of a radio medium that is oriented towards the optimization of the link capacity between a pair of agents. Shannon's capacity theorem applied on the radio medium conveniently links the channel capacity C with the bandwidth W and the signal quality $SINR$.

However, interference on the radio channel must be taken into account as it is implied by the $SINR$ term. Macroscopic effects of the position of potential interferers are most of the time quantified through deterministic models. For instance, base stations are sometimes considered to be placed on a hexagonal grid. In real network deployment, the positions of the base stations are not only related to the positions of the roads, buildings and hot spots but also to local regulations, public acceptance and other externalities. Therefore, positions of the base stations are random by nature. Stochastic geometry can advantageously describe the inherent randomness of the antennas location. More precisely, the spatial properties of cellular network deployment and their implication on signal quality and network performance are studied in this document under the light of point processes.

When considering a wireless network, interference is not the only limiting factor on the overall system performance. Scarcity of the electromagnetic spectrum and its related cost has the most dramatic impact. As a consequence, the overall number of resources that is offered in the network at a given time may not be enough to fulfill the users' needs. In this situation, the network is then limited by its own resources and thus has to choose which users to satisfy. The theory of optimal transport and its extension on Cournot-Nash equilibria can be used to dimension users demand in resources while maximizing their individual throughput.

1.2 Main contributions

1.2.1 Cellular networks and β-Ginibre point processes

The performance of a cellular network is strongly linked to the spatial repartition of its agents (base stations and users). On the downlink, the spatial repartition of the antennas plays a major role. Localization of the base stations are indeed random, however, this randomness is tied by externalities and engineering choices such as the density and the spatial repartition of users to serve, the locations that are available to set up an antenna, and the overall interference in the network.

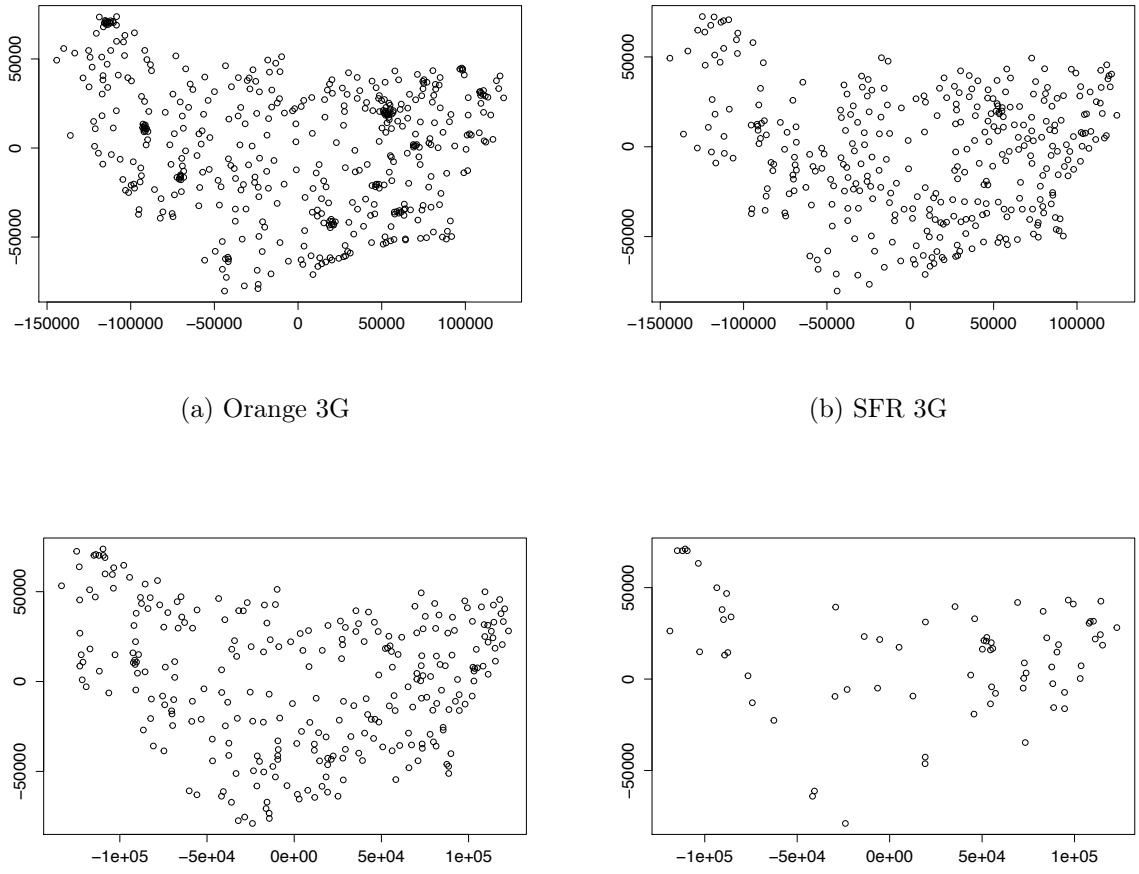

(a) Orange 3G

(b) SFR 3G

(c) Bouygues Télécom 3G

(d) Free 3G

Figure 1.1: 3G deployment for rural areas for the Haute-Saône, la Haute-Marne and Vosges perfectures, France for the four operators (distances are in meters).

On a macroscopic (regional) scale, it is obvious that cells are placed not only along communications routes such as freeways and roads, but also in villages and local cities. Figure 1.1 gives an insight on how antennas are placed in a rural region. Coverage is the main issue,

therefore cells are placed far from one another to maximize their footprint. Cities, on the other hand concentrate users on a small area. If antennas are still placed along streets, they are regularly spread in the city in order to limit the interference with one another. In this situation, signal degradation due to inter-cell interference is a real challenge that has to be traded-off with the local increase in the density of antenna on hot-spots, aimed at fulfilling local capacity needs. Figure 1.2, that gives the deployment in Paris for the operator SFR, illustrates this phenomenon.

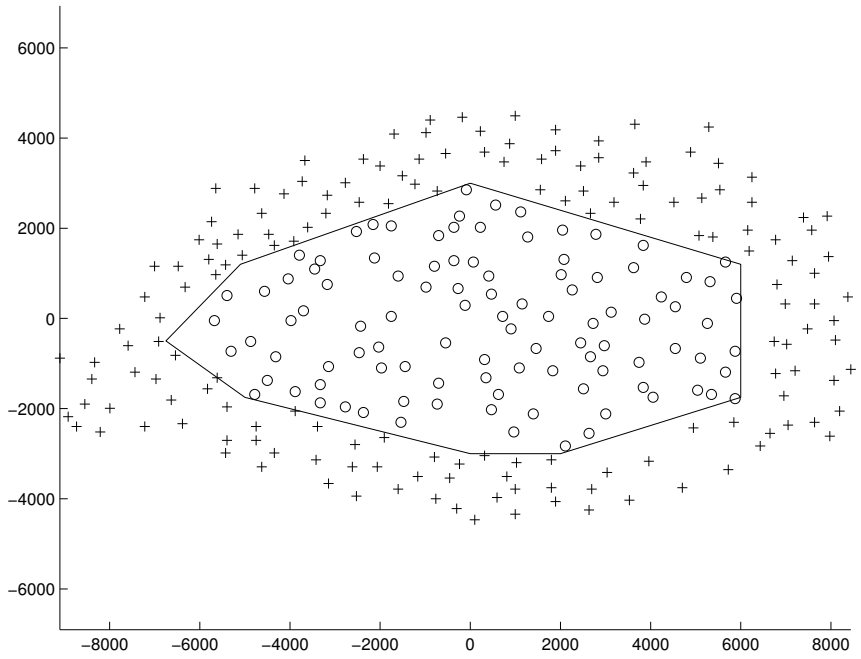

Figure 1.2: SFR UMTS 900 MHz network deployment over Paris (distance in meters).

Network models that describe the locations of the base stations are based on point processes. Base stations are placed as points in a plane. The law of the underlying point process provides statistical properties that can be linked with the overall network performance. The mostly used and widespread model that is considered in many research papers and models is the hexagonal grid. The honeycomb conjecture indeed states that the hexagonal shape is the best way to divide a surface into regions of equal area with the least total perimeter. This theorem embodies the antagonist forces that leads network deployment engineering (the trade-off between signal quality and inter-cell interference) to its deterministic ideal. Although this model is an easy way to conceive and use in numerical simulations, general results on networks are complex to obtain theoretically [69]. Even the honeycomb conjecture itself has only been proven in 1999 [55].

The Poisson point process that has been introduced for cellular network applications by Baccelli et al. [6], constitutes the stochastic counterpart of the hexagonal model. Closer to the inherent reality of deployed networks, it introduces a wide range of mathematical tools to understand cellular networks. A homogeneous Poisson point process is easy to simulate: let A be a compact in the plane and $|A|$ is area. We designate by $\lambda > 0$ the density of points per

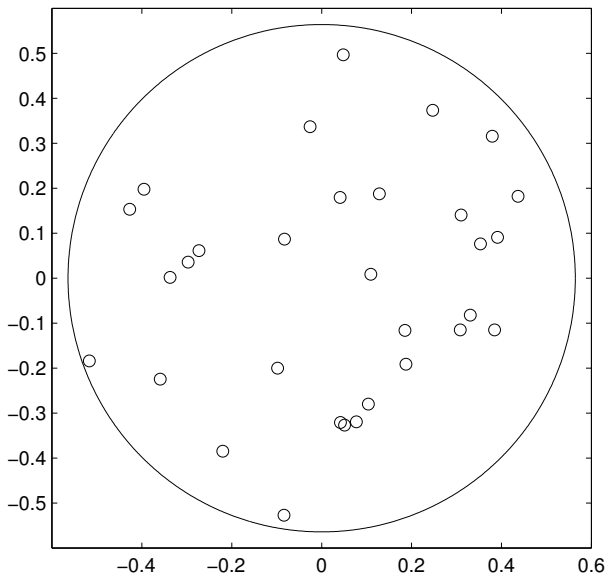

Figure 1.3: Realization of a Poisson point process.

unit of surface. The number of points to be drawn in the plane is given by a Poisson law with intensity $\lambda|A|$. Points are drawn uniformly and independently in the chosen compact. Figure 1.3 gives a realization of a Poisson point process. The property that points are independent between one another, provides the Poisson point process its tractable mathematical properties. It is also because of this very property that the Poisson point process lacks realism. Since there is no dependency between points, a repulsive force between them does not exist. Therefore, cluster of points can occur with high probability, which is sub-optimal in terms of inter-cell interference and does not comply with the fact that while engineering a cellular network, one must place antennas in order to maximize their coverage while fulfilling traffic needs. Hence, An underlying dependency between the positions of the base stations must exist, even though it is in a less rigid way than in the hexagonal model.

Using the Poisson point process as a base process, one can derive new point processes where clusters of points are avoided. For example, Mattern hard core type I and II point processes have been studied [47]. For a type I Mattern hard core point process, a distance d is considered. Then, for each point of a given Poisson point process realization, the point is kept if there is no other point at a distance smaller than d. For type II Mattern hard core point process, a random mark is associated with each point, and a point of the parent Poisson point process is deleted if another point exists within the hard-core distance d with a smaller mark. Such kind of transformation based on an exclusion area qualifies the resulting point processes as hard core. Since the points near one another are removed during the thinning, the resulting realization does not contain clusters of points. However, even if realizations of Mattern hard core Type I and II point processes are easily computed, theoretical results are proven to be complex to derive.

Another candidate family of point processes, the α-stable point processes, has been fitted on Chinese [85] and European networks [19] and some conclusions about network exploitation

costs have been derived. Comparative studies between point processes also exist [86, 20].

Point processes have also a wide range of applications, one of which is quantum physics. The determinantal point process family that was introduced by Shirai et al. [76]. Among them, the Ginibre point process models positions of the electrons trapped in space. Since electrons possess a negative electric charge, their positions in the plane is the result of the equilibrium between the trap and the particle repulsive interaction. These two antagonist effects are analogous to the ones that drive the deployment of networks. And since many theoretical results are available [52, 14, 57, 15, 51, 75], the Ginibre point process model was later introduced to describe wireless networks [68]. This model on the contrary of the Poisson point process introduces too much dependency between points. Clusters of points that might exist in real deployment occur empirically with a higher probability than in a realization of a Ginibre point process but with lower probability than in a Poisson process.

The β-Ginibre model fills that middle ground between the Ginibre point process and the Poisson point process. A realization of a β-Ginibre point process can be obtained from a realization of a Ginibre process. A thinning is performed on the parent Ginibre point process such that each point is kept independently from each other with a probability β. A re-scaling with parameter $\sqrt{\beta}$ is performed to preserve the intensity. If β is equal to one, the resulting point process is a Ginibre point process. For β decreasing, each point is kept with smaller and smaller probability. Therefore, neighbor dependency between points tends to disappear. The resulting point process thus tends to a Poisson process. Figure 1.4 gives three realizations for three different values of β.

The flexibility of the β-Ginibre model along with an existing mathematical literature [76, 68, 39, 43, 42, 51, 56, 31, 24, 41, 78, 64] make it an interesting candidate to describe wireless networks with finesse. Only two parameters are required: β that rules the equilibrium between repulsiveness and local densification, and the intensity λ which can be linked to the underlying traffic. Many theoretical results were derived especially on signal quality in wireless networks. In this dissertation, the relevance of the β-Ginibre is first discussed. Thanks to Cartoradio [4] and the ANFR (French national electromagnetic spectrum regulator), positions of base stations are made available to the general public. This data is accurate since it is mandatory for any French operator to declare the positions of their operational base stations. A fitting is performed on data collected on several environments (dense urban area (Paris), suburban and rural areas) and on each technology. Couples of values (λ, β) are deduced for each network. By comparing the relative values of the couples, conclusions are drawn on the deployment strategies of each network. The superposition of all the antennas deployed by every operators is also analyzed. We show that on a global scale, the Poisson point process model still holds for superpositions, confirming the theorem on the superposition of realization of independent β-Ginibre point processes [44].

The parameter β gives also insights on the overall signal quality in the network. Indeed, for a given threshold $\theta > 0$, there is a dependence between the coverage probability $\mathbb{P}(SINR > \theta)$ and the parameter β. The limit capacity on a point to point link defined by Shannon is a function of the bandwidth and also of the *SINR* at the point of the network considered. Since the *SINR* and the demand for traffic (for instance from users in the network) are constraints that are difficult to adjust in real time, it is spectrum that is dynamically allocated to users to fulfill their needs. For instance, in LTE networks, the number of resource blocks allocated to a given user in a sub-frame defines the throughput on the link. A dependence thus exists between the parameter β and the point to point capacity and consequently on the number of resource blocks allocated to users during a sub-frame. As the number of resource blocks are

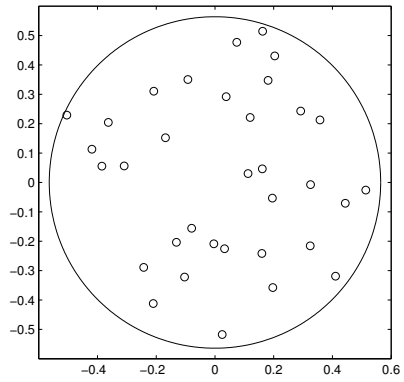

(a) 1/4-Ginibre

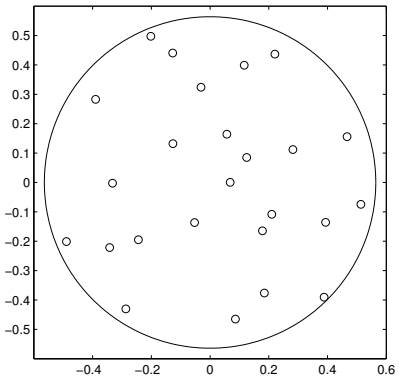

(b) 1/2-Ginibre

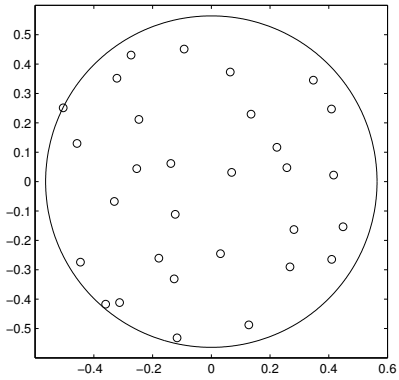

(c) 3/4-Ginibre

Figure 1.4: Examples of β-Ginibre point process realizations.

in a limited number, the parameter β influences therefore network performance and capacity.

While most of the works tend to characterize only the signal quality in the network [46, 40], we analyze the influence of the β parameter on the overall resources and potential throughput of the network. Since the simulations must take place in a reference cell (typically a cell that is placed in the middle of the network), we introduce a new simulation scheme to obtain realizations of β-Ginibre with a point at the origin of the plane. In this cell, the outage probability is taken as our main metric to understand the effects of spatial repartition on the overall performance of the network. We also provide tools to estimate the best dimensioning strategy provided a given outage probability and a couple (λ, β).

1.2.2 Resource allocation and optimal transport

In this dissertation, we also consider a method allocate resources in downlink. In order to increase the overall throughput of the network, we consider that base stations cooperate with one another. In the case of an OFDMA network, a user can then receive resource blocks from multiple base stations. One has then to know which resource block is allocated to which user from which base station. That is what we call the routing problem. We focus on a

novel approach that jointly optimizes bandwidth allocation and resource routing in OFDMA networks. The originality of this framework lies in the fact that the analysis is performed on rough assumptions (only the *SINR* of the link is required) and that performance analysis takes into account the influence of the β-parameter. On a theoretical point of view, we propose an original quadratic formulation of the resource allocation problem. We aim at finding the optimal coupling that links the supply of network resource and the traffic demand. Since the coupling also shapes the quantity of resource that is allocated to each user, this problem is solved thanks to optimal transport theory and Cournot-Nash equilibria.

The Cournot-Nash equilibria was first introduced by Antoine Augustin Cournot in 1838, to model the supply and demand of bottled water companies. This market being a duopoly implied that slight modifications of the supply had consequences on the structure of the demand, as well as the repartition of the market shares. The Cournot model highlights the equilibria points (that were proven to be a subset of Nash equilibria [66]) where the market was the most efficient [23, 79]. Blanchet et al. have recently investigated the Cournot-Nash equilibria [11, 8, 9] under a modern formulation introduced by Mas-Collel [62]. Methods to reach the equilibria solutions are also discussed [10, 12, 81]. The originality of their approach is to formulate the Cournot-Nash equilibria under the light of Optimal transport thanks to the coupling that exists between supply and demand.

Optimal transport has been introduced by Monge in 1781 [65]. The formulation of the problem is simple: given that there is a pile of sand and a hole in the ground, what is the path that each grain of sand must follow in order to minimize the energy to transfer the pile into the hole? This problem was solved by Kantorovich [54] during World War II. Optimal transport is nowadays widely applied in imaging to synthesize images and textures [73, 71, 72, 35] and has been recently widely developed on a mathematical point of view by numerous works [25, 58] and by Villani [80]. In the field of wireless networks, Optimal transport has been applied to find the position of base stations placed in floating air balloons considering the user repartition [67] and to solve traffic congestion [77].

1.3 Outline

This dissertation is organized in four parts: Chapter 2 gives the mathematical tools to manipulate the point processes, Chapter 3 overviews the relevance of the β-Ginibre model on real data and introduces the convergence theorem for a superposition of β-Ginibre. In Chapter 4, the link between the parameter β and the performance of the network is described for networks based on resource block allocation. In Chapter 5, a general performance analysis scheme is introduced thanks to Optimal transport and the Cournot-Nash equilibium framework. Finally, we conclude in Chapter 6.

Chapter 2

Point processes

Stochastic geometry and more precisely random point processes have raised interest in the wireless network community. Point processes are used to model the positions of the base stations or users in the plane. Two models have gained popularity thanks to their mathematical properties as well as practical characteristics: the Poisson point process [6] and the β-Ginibre point process [63]. Far from excluding one another, they are strongly bounded by several convergence theorems [31]. In this chapter, we introduce the formal definitions of the Poisson point process and the β-Ginibre point process. Numerous tools to analyze and characterize point processes such as the summary statistics and the Palm measure are also introduced. Finally, a novel theorem on the superposition of realizations of β-Ginibre point processes is exposed as well as a novel simulation framework to obtain realizations of β-Ginibre point processes under the Palm measure.

2.1 Introduction to point process theory

In this section, we provide definitions and notations to formally define point processes and give their main characteristics.

2.1.1 Configuration space and point processes

Let E be an Euclidian space such as $\mathbb{R}^2$ or $\mathbb{C}$. We first introduce the notions of configuration and configuration space.

Definition 2.1 (Configuration)**.** *A configuration, denoted ϕ, is a finite or countable-infinite collection of points, without accumulation.*

Hence a configuration is a set of points $\phi = \{x_1, x_2, \ldots\}$, with each $x_i \in E$. The non-accumulation property means that the number of points in any bounded subset $A \subset E$ is finite. For instance, the set of points $\{z = 1/n \mid n \in \mathbb{N}^*\}$ is not a configuration since 0 is an accumulation point. Indeed, the number of points in the unit ball is infinite.

We denote the number of points of a configuration ϕ in the subset $A \subset E$ by $\phi(A)$. A way to calculate the quantity $\phi(A)$ is given by

$$\phi(A) = \sum_{x \in \phi} \delta_x(A),$$

where δ_x is the Dirac measure on A such that $\delta_x(A) = 1$ if x lies in A, and $\delta_x(A) = 0$ otherwise. Thanks to the Dirac measure, we are able to compute functions defined on E with configuration of points such that for all functions f defined on E, we have:

$$\int_E f(x)\phi(\mathrm{d}x) = \sum_{x\in\phi} f(x).$$

Definition 2.2 (Configuration space $\mathfrak{N}_E$)**.** *The configuration space $\mathfrak{N}_E$ is the space of all the configurations on E.*

We now introduce the definition of point processes that stochastic processes:

Definition 2.3 (Point process)**.** *A point process Φ is an $\mathfrak{N}_E$-valued random variable.*

An outcome of a point process is also called a *realization*. Since a point process is a random variable on the configuration space $\mathfrak{N}_E$, its law is denoted by:

$$\forall \phi \in \mathfrak{N}_E, \quad \mathbb{P}_\Phi(\phi) = \mathbb{P}(\Phi = \phi). \tag{2.1}$$

In other terms, if $\mathcal{F}$ is the Borel σ-algebra on $\mathfrak{N}_E$, and $\mathbb{P}_\Phi$ the law of Φ, the point process Φ is a canonical random variable on $(\mathfrak{N}_E, \mathcal{F}, \mathbb{P}_\Phi)$.

Characterizing a point process with its law is often difficult in practice, since direct calculation on $\mathfrak{N}_E$ is not convenient. The Laplace transform fully defines a point process and allows calculations on the usual space E.

Definition 2.4 (Laplace transform)**.** *The Laplace transform of a point process Φ is defined for all continuous non-negative function f on E such that*

$$\begin{aligned}\mathcal{L}_\Phi(f) &= \mathbb{E}_\Phi\left[e^{-\int_E f(x)\phi(\mathrm{d}x)}\right], \\ &= \mathbb{E}_\Phi\left[e^{-\sum_{x\in\phi} f(x)}\right], \\ &= \int_{\mathfrak{N}_E} e^{-\sum_{x\in\phi} f(x)} \mathrm{d}\mathbb{P}_\Phi(\phi).\end{aligned}$$

2.1.2 The Poisson point process

The Poisson point process can be defined by its Laplace transform.

Definition 2.5 (Laplace transform of the Poisson point process)**.** *Let Λ be a measure. For all continuous function f on E, the Laplace transform of the Poisson point process Φ_P is given by*

$$\mathcal{L}_{\Phi_P}(f) = e^{-\int_E (1-e^{-f(x)})\Lambda(\mathrm{d}x)}.$$

For instance, the measure Λ is often the intensity measure $\Lambda(\mathrm{d}x) = \lambda \mathrm{d}x$, with $\lambda > 0$ and $\mathrm{d}x$ being the Lebesgue measure. In this document, we will only consider the homogeneous Poisson point process. Therefore, we always assume that $\Lambda(\mathrm{d}x) = \lambda \mathrm{d}x$.

Thanks to the Laplace transform of a Poisson point process, we can derive the Campbell formula:

Theorem 2.1 (Campbell formula [70]). *For all function $f \in L^1(E, \Lambda)$, the space of Λ-measure integrable functions, and Φ_P a Poisson point process,*

$$\mathbb{E}_{\Phi_P}\left[\int_E f(x)\mathrm{d}\phi(x)\right] = \int_E f(x)\mathrm{d}\Lambda(x).$$

While the Laplace transform comprehensively characterizes the law of a point process in a calculation point of view, it does not provide an intuitive definition of it.

For instance, an alternate and more common definition of the Poisson point process is the following:

Definition 2.6 (Poisson point process). *Let Λ be a measure. The point process Φ_P is a Poisson point process, if and only if*

$$\mathbb{P}\left\{\Phi_P(A_1) = n_1, \ldots, \Phi_P(A_k) = n_k\right\} = \prod_{i=1}^{k} e^{-\Lambda(A_i)}\frac{\Lambda(A_i)^{n_i}}{n_i!},$$

for every $k \in \mathbb{N}^*$, $n_1, \ldots n_k \in \mathbb{N}$ and all bounded mutually disjoint subsets of E: $A_1, \ldots, A_k$.

The Poisson distribution can be easily recognized in the previous definition. Furthermore, the number of points of a Poisson point process is deduced in the following proposition.

Proposition 2.1. *For all compact $A \subset E$, we have*

$$\mathbb{P}\left(\phi(A) = n\right) = \frac{(\Lambda(A))^n}{n!}e^{-\Lambda(A)}.$$

2.1.3 Operations and properties on point processes

Point processes are stochastic processes, thus notions of stationarity, ergodicity and convergence in law can be defined.

Definition 2.7 (Stationarity). *Let Φ be a point process and $\phi = \{x_i\}_{i\in\mathbb{N}}$ be a realization of Φ. For all $t \in E$, we denote by $\Phi + t$ the point process with realization $\phi + t = \{x_i + t\}_{i\in\mathbb{N}}$. The point process Φ is stationary if and only if Φ and $\Phi + t$ have the same law.*

Definition 2.8 (Ergodicity). *Let Φ be a point process and ϕ be a realization of Φ. A point process Φ is ergodic if for any family of subsets $\{A_n\}\, n \in \mathbb{N}$, such that $A_1 \subset A_2 \subset \ldots \subset E$, and for any function $f : E \times \mathfrak{N}_E \to E$, the following limits exist and verify:*

$$\lim_{n\to\infty}\frac{1}{|A_n|}\int_{A_n} f(t, \phi - t)\mathrm{d}t = \lim_{n\to\infty}\frac{1}{\phi(A_n)}\int_{A_n} f(t, \phi - t)\phi(\mathrm{d}t)$$

The left hand side of the equation is to the mean of f on E, while the right hand side is the mean of f on the realization ϕ of the point process.

Definition 2.9 (Convergence in law). *Let $\{\Phi_n\}_{n\in\mathbb{N}}$ be a family of point processes, and Φ a point process. The family $\{\Phi_n\}_{n\in\mathbb{N}}$ converges in law towards Φ, written $\Phi_n \xrightarrow{n\to\infty} \Phi$, if for all bounded continuous function $f : \mathfrak{N}_E \to \mathbb{R}$, we have:*

$$\lim_{n\to\infty}\mathbb{E}_{\Phi_n}\left[f\right] = \mathbb{E}_{\Phi}\left[f\right] \quad \Leftrightarrow \quad \lim_{n\to\infty}\int_{\mathfrak{N}_E} f(\phi)\mathrm{d}\mathbb{P}_{\Phi_n}(\phi) = \int_{\mathfrak{N}_E} f(\phi)\mathrm{d}\mathbb{P}_{\Phi}(\phi).$$

Point processes are also configurations, thus notions of scaling, superposition and independent thinning can be defined.

Definition 2.10 (Scaling). *Let Φ be a point process and ϕ one of its realization. Let $s > 0$. We denote by Ψ_s the point process with realization $\psi_s = \sum_{x\in\phi} \delta_{sx}$. Then, the point process Ψ_s is a scaling of Φ.*

Definition 2.11 (Superposition). *Let Φ and Ψ be two point processes and ϕ and ψ be one of their realizations. The point process $\Phi + \Psi$ with realization $\phi + \psi$, which is the union of the two sets of points ϕ and ψ, is the superposition of Φ and Ψ.*

The reverse operation is the superposition is called a thinning.

Definition 2.12 (Independent thinning). *Let Φ be a point process and ϕ one of its realization. Let $(U_x, x \in \phi)$ be a family of $\{0, 1\}$-valued independent and identically distributed (i.i.d) random variables, independent of the realization ϕ, with $p(x) = \mathbb{P}(U_x = 1)$. The point process Ψ with realization $\psi = \sum_{x\in\phi} U_x\delta_x$ is an independent thinning of Φ with probability p.*

Points of the thinning of a realization are selected independently from one another.

The Poisson point process illustrates the previous definitions with the following properties:

Proposition 2.2 (Properties of the Poisson point process [70]).

- *The homogeneous Poisson point process is stationary and ergodic.*
- *An independent thinning of a Poisson point process of parameter Λ with probability p is a Poisson point process with intensity $p\Lambda$.*
- *A superposition of several independent Poisson point processes is also a Poisson point process whose intensity is the sum of the underlying point processes intensities.*

2.1.4 Correlation functions and Palm measure

Point processes can also be defined thanks to their correlation functions.

Definition 2.13 (Correlation functions). *Let Φ be a point process and Λ be a measure on E. The correlation functions of Φ in respect to the measure Λ, denoted $\rho_k : \mathfrak{N}_E \to \mathbb{R}$ for $k \in \mathbb{N}^*$, are given by:*

$$\mathbb{E}_\Phi\left[\prod_{i=1}^{k}\phi(B_i)\right] = \int_{B_1\times\ldots\times B_k} \rho_k(x_1,\ldots,x_k)\Lambda(\mathrm{d}x_1)\ldots\Lambda(\mathrm{d}x_k), \tag{2.2}$$

for any family of mutually disjoint compact $B_1, \ldots B_k \subset E$.

For any finite configuration $\{x_1, \ldots x_k\}$, the k-th correlation function $\rho_k(x_1, \ldots x_k)$ of a point process Φ is the probability to have exactly k points in the vicinity of each one of the $\{x_1, \ldots x_k\}$.

For instance, the correlation functions of a Poisson point process of intensity λ, where $\Lambda(\mathrm{d}x) = \lambda\mathrm{d}x$ are computed thanks to Equation (2.2). Using previous notations, since Poisson point processes on disjoint sets are independent,

$$\mathbb{E}_\Phi\left[\prod_{i=1}^{k}\phi(B_i)\right] = \prod_{i=1}^{k}\mathbb{E}_\Phi\left[\phi(B_i)\right].$$

Thanks to the Campbell formula,

$$\mathbb{E}_\Phi\left[\prod_{i=1}^{k}\phi(B_i)\right] = \lambda^k\prod_{i=1}^{k}|B_i| = \int_{B1\times\ldots\times B_k}\lambda\,\mathrm{d}x_1\ldots\lambda\,\mathrm{d}x_k.$$

Therefore, by identification with Equation (2.2), the correlation functions of the Poisson point process are for any $k\in\mathbb{N}^*$

$$\rho_k(x_1,\ldots,x_k)=1.$$

The correlation functions can indicate the repulsiveness or attractiveness of a point process.

Definition 2.14 (Repulsive and attractive point process)**.** *A point process with correlation functions ρ_k, for $k\in\mathbb{N}^*$, is repulsive (resp. attractive) if for x, y in E, we have :*

$$\rho_2(x,y)\leq\rho_1(x)\rho_1(y)\quad(\text{resp. }\rho_2(x,y)\geq\rho_1(x)\rho_1(y))$$

From the correlation functions, we can derive the following definition of the Palm measure.

Definition 2.15 (Palm measure [21])**.** *Let Φ be a point process with correlation functions $(\rho_k, k\geq 1)$. The Palm measure of Φ is the law of the point process whose correlations functions are given by*

$$\rho_k^0(x_1,\ldots,x_k)=\frac{\rho_k(x_1,\ldots,x_k)}{\rho_1(0)}.$$

The Palm measure can be interpreted as the distribution of Φ given that $\Phi(\{0\})=1$.

Since its correlation functions are all equal to 1, the Palm measure of a Poisson point process is given by the following proposition.

Theorem 2.2 (Slivnyak-Mecke Theorem)**.** *The Palm measure of a Poisson point process Φ is its own law. As a result, to obtain a realization of a Poisson point process under the Palm measure, it suffices to add the point $\{0\}$.*

2.2 Point process characterization via statistical inference

Statistical inference is performed thanks to summary statistics functions that are defined below. They are used to infer properties and characterize a point process from the observation of its realizations. One can remark that, when studying a given realization, properties may differ given the point of view of the observer. We provide a short example below.

Let ϕ be a configuration of points of integer coordinates $\phi=\{(i,j)\}_{(i,j)\in\mathbb{Z}^2}$, as represented on Figure 2.1.

Let us consider z a point in $\mathbb{C}$. We denote by $d(\phi,z)$ the distance between the nearest point of the configuration ϕ that is not z and the point z. Considering the infinity norm $\|\ \|_\infty$,

$$d(\phi,z)=\min_{\substack{x\in\phi\\x\neq z}}\|z-x\|_\infty,$$

$$d(\phi,z)=\min_{\substack{x\in\phi\\x\neq z}}\max(\Re(z-x),\Im(z-x)).$$

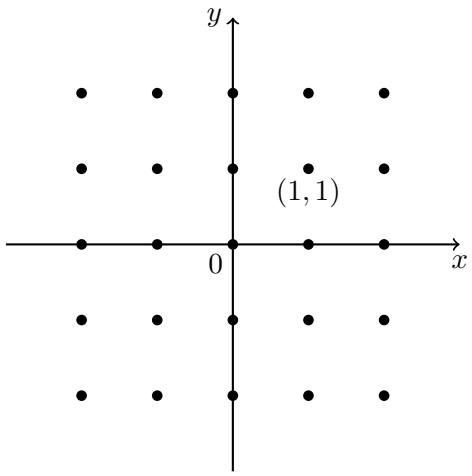

Figure 2.1: Configuration $\phi = \{(i,j)\}_{(i,j)\in\mathbb{Z}^2}$

If z is in $\mathbb{C}$, $d(\phi, z) > 0$ and depends of the position of z. Meanwhile, if z is in ϕ, $d(\phi, z) = 1$.

Hence, interpretations of the properties of a configuration may differ according to the point of view from which is observed. Therefore we consider the following summary statistic functions:

Definition 2.16 (Contact distribution function F [64])**.** *Let ϕ be a realization of a stationary point process Φ. The contact distribution is the probability that for any point x of E, no point lies in an open ball of center x and radius r, denoted $b(x,r)$. For $r > 0$,*

$$F(r) = \mathbb{P}\left(\Phi(b(x,r)) > 0\right).$$

Since the point process is stationary, we can choose x to be $o = (0,0)$.

Example: For the Poisson point process of intensity λ, we have for all $r > 0$:

$$F(r) = 1 - e^{-\lambda\pi r^2}.$$

Definition 2.17 (Nearest neighbor distance distribution function G [64])**.** *Let ϕ be a realization of a stationary point process Φ. For x in ϕ, we denote by Φ_x the point process with realization $\phi \setminus \{x\}$. The nearest neighbor distance distribution is the probability that for any point x of ϕ, no other point lies in an open ball of center x and radius r. For $r > 0$,*

$$G(r) = \mathbb{P}\left(\Phi_x(b(x,r)) > 0\right).$$

Example: For the Poisson point process of intensity λ, we have for all $r > 0$:

$$G(r) = 1 - e^{-\lambda\pi r^2}.$$

Definition 2.18 (J Function [64])**.** *Let ϕ be a realization of a stationary point process. The J function is the ratio for all $r > 0$:*

$$J(r) = \frac{1 - G(r)}{1 - F(r)}$$

Example: For the Poisson point process, the J function is equal to 1 for all $r > 0$, by definition.

Proposition 2.3. *If $J(r) \geq 1$ (resp. $J(r) \leq 1$) for all $r > 0$, then the point process is repulsive (resp. attractive).*

Indeed for a given point process, if J is bigger than 1, then the G function is smaller than the F function. This means that the probability that a point of the point process lies at a distance from a point x smaller than $r > 0$, is smaller when x is part of the process than when x is any point in the plane. Therefore the nearest neighbor is closer if the observer is not in the configuration.

2.3 The β-Ginibre point process

2.3.1 Definition and properties

We now introduce the definition of kernel and determinantal process required to build the β-Ginibre point process.

First, let Λ be a measure on $\mathbb{C}$. Let us consider the square integrable complex functions space $L^2(\mathbb{C}, \Lambda)$, equipped with the Hilbert scalar product defined for any f and g in $L^2(A, \Lambda)$ on a compact set $A \subset \mathbb{C}$:

$$f \cdot g = \int_A f(x)\overline{g(x)}\Lambda(\mathrm{d}x),$$

with $\overline{z}$ being the conjugate complex of $z \in \mathbb{C}$.

A kernel K is a measurable function from $\mathbb{C}^2$ to $\mathbb{C}$.

Definition 2.19 (Locally square integrable kernel)**.** *A kernel K is locally square integrable if for any compact set $A \subset \mathbb{C}$, we have*

$$\int_A |K(x,y)|^2 \Lambda(\mathrm{d}x)\Lambda(\mathrm{d}y) < \infty.$$

Definition 2.20 (Hermitian symmetric kernel)**.** *A kernel K is Hermitian symmetric if*

$$K(x,y) = \overline{K(y,x)}.$$

Theorem 2.3 (Spectral theorem)**.** *If the kernel K is Hermitian symmetric, there exists an orthogonal basis $\left\{\phi_n^K\right\}_{n\in\mathbb{N}}$ on $L^2(A, \Lambda)$, with A compact subset of $\mathbb{C}$, with corresponding eigenvalues $\left\{\lambda_n^K\right\}_{n\in\mathbb{N}}$ such that for all $(x, y) \in A^2$,*

$$K(x,y) = \sum_{n=0}^{\infty} \lambda_n^K \phi_n^K(x)\overline{\phi_n^K(y)}.$$

Definition 2.21 (Trace-class kernel)**.** *A kernel K is trace-class if its eigenvalues verify*

$$K(x,y) = \sum_{n=0}^{\infty} |\lambda_n^K| < \infty.$$

We define the determinantal point process by its correlation functions.

Definition 2.22 (Determinantal point process)**.** *Let K be a bounded, Hermitian symmetric, locally trace-class kernel on $\mathcal{L}^2(A,\Lambda)$, with A compact subset of $\mathbb{C}$, such that its eigenvalues verify $\lambda_n^K < 1$ for all $n \in \mathbb{N}$. For any k-tuple of points $\{x_1,\dots,x_k\} \in A^k$, a determinantal point process is a point process with correlation functions such that:*

$$\rho_k(x_1,\dots,x_k) = \det\left(K(x_i,x_j)_{1\leq i,j\leq k}\right),$$

where $\det\left(K(x_i,x_y)_{1\leq i,j\leq k}\right)$ is the determinant of the matrix of which the element of the i-th row and j-th column is $K(x_i,x_j)$.

Proposition 2.4 (Laplace transform of a determinantal process)**.** *The Laplace transform of a determinantal point process is given for all non negative functions f by*

$$\mathcal{L}_\Phi(f) = \mathrm{Det}(I+K_f),$$

where

$$K_f(x,y) = \left(1-e^{-f(x)}\right)^{1/2} K(x,y) \left(1-e^{-f(y)}\right)^{1/2},$$

and

$$\mathrm{Det}(I+K_f) = \sum_{n=0}^{\infty} \frac{1}{n!} \int_{E^n} \det\left(-K(x_i,x_j)_{1\leq i,j\leq n}\right) \mathrm{d}x_1 \dots \mathrm{d}x_n$$

which is called the Fredholm determinant.

The determinantal point process is a repulsive point process, since its correlation functions verify

$$\rho_k(x_1,\dots x_k) \leq \rho_1(x_1)\dots\rho_k(x_k).$$

Hence, the probability to find k points of the point process in the neighborhood of $\{x_1,\dots,x_k\}$ is smaller than the probability to find a point of the point process near each one of the $\{x_1,\dots,x_k\}$.

There are numerous kernels of determinantal point processes. The β-Ginibre point process is a specific determinantal point process.

Definition 2.23 (β-Ginibre point process)**.** *Let $\lambda > 0$ and $\beta \in]0,1]$. The β-Ginibre point process is the determinantal point process with kernel*

$$K_{\beta,\lambda}(x,y) = \lambda e^{-\frac{\lambda\pi}{2\beta}(|x|^2+|y|^2-2x\overline{y})}, \tag{2.3}$$

λ is then called the intensity of the point process.

If $\beta = 1$, the point process is called the Ginibre point process and has for kernel

$$K_\lambda(x,y) = \lambda e^{-\frac{\lambda\pi}{2}(|x|^2+|y|^2-2x\overline{y})}. \tag{2.4}$$

We introduce now a well-known result.

Lemma 2.1 ([31])**.** *When β goes to zero, the β-Ginibre of intensity λ converges in law to a Poisson point process of the same intensity.*

Proof. We provide here an informal proof, a full proof can be found in [31]. We have that for all $(x, y) \in \mathbb{C}$,

$$\lim_{\beta \to 0} K_{\beta,\lambda}(x, y) = \lambda \delta_x(y).$$

We denote this limit by $K_{0,\lambda}$ and we can see that it is a diagonal matrix with λ as diagonal coefficients. Therefore the Laplace transform of the resulting point process is for any non negative f

$$\begin{aligned}
\mathcal{L}_\Phi(f) &= \sum_{n=0}^{\infty} \frac{1}{n!} \int_{\mathbb{C}^n} \det\left(-(1-e^{-f(x_i)})^{1/2} K_{0,\lambda}(x_i, x_j)(1-e^{-f(x_j)})^{1/2}\right)_{1\le i,j\le n} \mathrm{d}x_1 \dots \mathrm{d}x_n \\
&= \sum_{n=0}^{\infty} \frac{1}{n!} \int_{\mathbb{C}} (1-e^{-f(x)})^n (-\lambda)^n \mathrm{d}x \\
&= e^{-\int_{\mathbb{C}} (1-e^{-f(x)})\lambda \mathrm{d}x}.
\end{aligned}$$

We recognize the Laplace transform of a Poisson point process. □

Therefore, the coefficient β can be seen as a repulsive factor: the greater the coefficient β is , the more repulsive the β-Ginibre point process is. Since the kernel $K_{\beta,\lambda}$ is Hermitian symmetric, the spectral theorem can be applied to any β-Ginibre point process kernels.

Theorem 2.4. *The eigenvalues of the kernel of a β-Ginibre point process restrained on the ball $\mathcal{C} = b(o, R)$, for $R > 0$, is given by*

$$K_{\beta,\lambda}(x, y) = \sum_{n\ge 0} \lambda_n^{\beta,\lambda} \phi_n^{\beta,\lambda}(x) \overline{\phi_n^{\beta,\lambda}(y)},$$

with

$$\lambda_n^{\beta,\lambda} = \beta \frac{\tilde{\gamma}\big(n+1, \lambda\pi R^2/\beta\big)}{n!},$$

and

$$\phi_n^{\beta,\lambda} = \sqrt{\frac{\lambda}{\beta\, \tilde{\gamma}(n+1, \lambda\pi R^2/\beta)}} e^{-\frac{\lambda\pi}{2\beta}|z|^2} \left(\sqrt{\frac{\lambda\pi}{\beta}} z\right)^n,$$

where $\tilde{\gamma}$ is the lower Gamma function defined by for all $z \in \mathbb{C}$ and $a \ge 0$:

$$\tilde{\gamma}(z, a) = \int_0^a e^{-t} t^{z-1} \mathrm{d}t,$$

Proof. Let $(\psi_n^{\beta,\lambda})_{n\in\mathbb{N}}$ be the family on $L^2(\mathbb{C}, \mathrm{d}z)$ such that for all complex $z \in \mathbb{C}$:

$$\psi_n^{\beta,\lambda}(z) = \sqrt{\frac{\lambda}{n!}} e^{-\frac{\lambda\pi}{2\beta}|z|^2} \left(\sqrt{\frac{\lambda\pi}{\beta}} z\right)^n. \tag{2.5}$$

Combining Equation (2.3) and Equation (2.5), the kernel $K_{\beta,\lambda}$ is

$$\begin{aligned} K_{\beta,\lambda}(x,y) &= \lambda e^{-\frac{\lambda\pi}{2\beta}(|x|^2+|y|^2-2x\overline{y})} \\ &= \lambda e^{\frac{\lambda\pi}{\beta}(x\overline{y})} e^{-\frac{\lambda\pi}{2\beta}(|x|^2+|y|^2)} \\ &= \lambda \sum_{n\geq 0} \frac{1}{n!} \left(\frac{\lambda\pi}{\beta} x\overline{y}\right)^n e^{-\frac{\lambda\pi}{2\beta}(x^2+y^2)} \\ &= \sum_{n\geq 0} \psi_n^{\beta,\lambda}(x)\overline{\psi_n^{\beta,\lambda}(y)}. \end{aligned}$$

The family $(\psi_n^{\beta,\lambda})_{n\in\mathbb{N}}$ is an orthogonal family of $L^2(\mathcal{C}, \mathrm{d}z)$. Therefore, each vector has to be normalized to obtain an orthonormal family. The norm of $\psi_n^{\beta,\lambda}$ is :

$$\begin{aligned} \|\psi_n^{\beta,\lambda}\|^2 &= \int_{\mathcal{C}} \psi_n^{\beta,\lambda}(z)\overline{\psi_n^{\beta,\lambda}(z)}\mathrm{d}z \\ &= \int_{\mathcal{C}} \frac{\lambda}{n!} e^{-\frac{\lambda\pi}{\beta}|z|^2} \left(\frac{\lambda\pi}{\beta}\right)^n |z|^{2n}\mathrm{d}z \\ &= \frac{\lambda}{n!}\left(\frac{\lambda\pi}{\beta}\right)^n \left(\int_0^R e^{-\frac{\lambda\pi}{\beta}r^2} r^{2n+1}\mathrm{d}r\right)\left(\int_{-\pi}^{\pi}\mathrm{d}\theta\right) \\ &= \frac{\beta}{n!}\int_0^{\lambda\pi R^2/\beta} e^{-t}t^n\mathrm{d}t \\ &= \beta\frac{\tilde{\gamma}\big(n+1, \lambda\pi R^2/\beta\big)}{n!}. \end{aligned}$$

By identification with the spectral decomposition, we have that for any n in $\mathbb{N}$

$$\phi_n^{\beta,\lambda} = \frac{\psi_n^{\beta,\lambda}}{\|\psi_n^{\beta,\lambda}\|} \quad \text{and} \quad \lambda_n^{\beta,\lambda} = \|\psi_n^{\beta,\lambda}\|^2.$$

□

According to Proposition 2.2, the superposition of independent Poisson point process is Poisson point process. For the superposition of β-Ginibre point processes, we introduce the following theorem :

Theorem 2.5 (β-Ginibre point process superposition convergence theorem [44])**.** *For all $n \in \mathbb{N}^*$, let Φ_n be the superposition of n independent $\beta_{n,i}$-Ginibre point processes $\{\Phi_{n,i}\}$ with intensities $\lambda_{n,i}=\lambda_i/n$ and $\beta_{n,i} \in]0,1]$, for $1 \leq i \leq n$. Let us suppose that:*

(i) the sequence $(\lambda_i)_{i\in\mathbb{N}^*} \subset \mathbb{R}_+^*$ is bounded,

(ii) $\lim\limits_{n\to+\infty} \frac{1}{n}\sum_{i=1}^n \lambda_i = \lambda$.

Then $(\Phi_n)_{n\in\mathbb{N}^*}$ converges in law to a Poisson point process Φ with intensity λ.

Proof. Theorem 2.5 is achieved if all conditions of Theorem 2.6 are satisfied.

Let A be a compact subset of $\mathbb{C}$.

Theorem 2.6. *[Convergence in law theorem [53]] For any A compact subset in $\mathbb{C}$, if the three following properties hold:*

(i) $\lim_{n\to+\infty} \mathbb{P}(\Phi_n(A)=0) = \mathbb{P}(\Phi(A)=0)$

(ii) $\limsup_{n\to+\infty} \mathbb{P}(\Phi_n(A)\leq 1) \geq \mathbb{P}(\Phi(A)\leq 1)$

(iii) $\lim_{t\to+\infty} \limsup_{n\to+\infty} \mathbb{P}(\Phi_n(A)>t) = 0$

Then: $\Phi_n \xrightarrow{n\to\infty} \Phi$.

Proof of Condition (iii) By definition of the expectation,

$$\mathbb{P}(\Phi_n(A)>t) \leq \frac{\mathbb{E}[\Phi_n(A)]}{t}.$$

Since $(\mathbb{E}[\Phi_n(A)])_{n\in\mathbb{N}}$ is bounded, (iii) holds.

Proof of condition (i) and (ii) For a Poisson point process, we know that:

$$\begin{aligned}\mathbb{P}\left(\Phi(A)=0\right) &= e^{-|A|\lambda\pi^{-1}},\\ \mathbb{P}\left(\Phi(A)\leq 1\right) &= e^{-|A|\lambda\pi^{-1}}\left(1+|A|\lambda\pi^{-1}\right).\end{aligned}$$

We have to calculate yet the left-hand side of both inequalities (i) and (ii). Let $\mathcal{K}_{n,i}$ be the kernel of a $\beta_{n,i}$-Ginibre point process. Proposition 3 of Goldman's paper [43] states that:

$$\begin{aligned}\mathbb{P}(\Phi_{n,i}(A)=0) &= 1+\sum_{p\geq 1}\frac{(-1)^p}{p}\int_{A^p}\det[\mathcal{K}_{n,i}](x_1,...,x_p)\mathrm{d}x_1\ldots\mathrm{d}x_n,\\ \mathbb{P}(\Phi_{n,i}(A)=1) &= \mathbb{P}(\Phi_{n,i}(A)=0)\int_A R_{n,i}(z)\mathrm{d}z.\end{aligned}$$

with

$$R_{n,i}(z) = K_{n,i}(z,z)+\sum_{j\geq 2}K_{n,i}^{(j)}(z,z).$$

By hypothesis of Theorem 2.5, $(\lambda_i)_{i\in\mathbb{N}^*}$ is bounded. We also know that $\|K_{n,i}\|_\infty = c_i(n\pi)^{-1}$. We can then prove recursively for all $p\geq 1$, that there exists $M>0$ such that for all $i\in\mathbb{N}^*$,

$$0\leq \det[K_{n,i}](v_1,...,v_p) \leq \|K_{n,i}\|_\infty^p \leq \left(\frac{M}{n\pi}\right)^p.$$

Therefore, the two bounded sequences $(\epsilon_n)_{n\in\mathbb{N}^*}$ and $(\epsilon'_n)_{n\in\mathbb{N}^*}$ independent of i exist and verify:

$$\begin{aligned}\mathbb{P}(\Phi_{n,i}(A)=0) &= 1-\frac{\lambda_i|A|}{n}+n^{-2}\epsilon_n.,\\ \mathbb{P}(\Phi_{n,i}(A)=1) &= \frac{\lambda_i|A|}{n}+n^{-2}\epsilon'_n.\end{aligned}$$

Hence,

$$\mathbb{P}(\Phi_n(A)=0)=e^{O(n^{-2})}e^{-\sum_{i=1}^{n}\frac{\lambda_i|A|}{n}},$$
$$\mathbb{P}(\Phi_n(A)=1)\geq e^{o(\frac{1}{n})}e^{-\sum_{j=1}^{n}\frac{\lambda_j|A|}{n}}\sum_{i=1}^{n}\frac{\lambda_i|A|}{n}+o(1).$$

Therefore,

$$\lim_{n\to\infty}\mathbb{P}(\Phi_n(A)=0)=e^{-|A|\lambda},$$
$$\limsup_{n\to\infty}\mathbb{P}(\Phi_n(A)=1)\geq\lambda|A|e^{-|A|\lambda},$$

consequently (i) and (ii) hold. □

Hypotheses (i) and (ii) of Theorem 2.5 are quite restrictive since the intensities of each β-Ginibre point process are dependent of n. However, here, we mainly work with finite families of β-Ginibre point process. Therefore, we can choose the value of the $(\lambda_i)_{i\in 1\ldots n}$ such that they equal the intensities of the β-Ginibre point processes that are superposed. This result about superposition of the β-Ginibre is completed by the works of Decreusefond et al. [31] that explore in details the asymptotic behavior of point processes superposition.

2.3.2 The F, G and J functions for the β-Ginibre point process

We here give the value of the summary statics functions defined in Paragraph 2.2 for a β-Ginibre point process.

Proposition 2.5 (The F function for the β-Ginibre point process [33])**.** *For all $r>0$, the F function of the β-Ginibre point process is*

$$F(r)=1-\prod_{k=1}^{\infty}\left(1-\beta\frac{\tilde{\gamma}\left(k,\frac{\lambda\pi}{\beta}r^2\right)}{(k-1)!}\right).$$

Proposition 2.6 (The G function for the β-Ginibre point process [33])**.** *For all $r>0$, the G function for the β-Ginibre point process is*

$$G(r)=1-\prod_{k=2}^{\infty}\left(1-\beta\frac{\tilde{\gamma}\left(k,\frac{\lambda\pi}{\beta}r^2\right)}{(k-1)!}\right).$$

Proposition 2.7 (The J function for the β-Ginibre point process[33])**.** *For all $r>0$, the J function for the β-Ginibre point process is*

$$J(r)=\left(1-\beta+\beta e^{-\frac{\lambda\pi}{\beta}r^2}\right)^{-1}.$$

Proofs of these propositions can be found in [33].

2.3.3 Simulation of a β-Ginibre under the Palm measure

The most simple way to simulate a β-Ginibre of intensity λ is the following [42]:

- Draw N^2 i.i.d random complex coefficients $m_{i,j}$ such that $m_{i,j} \sim \mathcal{N}(0,1) + i\mathcal{N}(0,1)$, with $\mathcal{N}(0,1)$ be a normal distributed random value.
- Compute the eigenvalues of $M = (m_{i,j})_{1 \leq i,j \leq N}$.
- Perform an independent thinning of parameter β on the eigenvalues of M. The resulting set is denoted ϕ.
- Perform a scaling of parameter $\sqrt{\lambda\pi\beta}$ on ϕ.

Even if this algorithm is efficient in terms of complexity and time, there are many drawbacks to be considered.

The first one is the fact that this algorithm simulates a β-Ginibre with a truncated kernel defined for all $(x, y) \in \mathbb{C}^2$,

$$K(x,y) = \sum_{n=0}^{N-1} \phi_n^{\beta,\lambda}(x)\overline{\phi_n^{\beta,\lambda}(y)},$$

as showed in [39].

The second drawback comes from the fact that one has no control on the size of the simulation domain.

The third drawback comes from the fact that it is not possible to simulate realizations of a β-Ginibre point process under the Palm measure. For instance, if ϕ is a realization of a point process Φ, and x_1 the point of ϕ that is the nearest to the origin, a naive approach would be to consider the realization $\phi - x_1$, which is the translation of ϕ by a vector x_1. However, this method is not correct. Let us consider the law of the affixes of the points of the realization of a β-Ginibre point process.

Lemma 2.2 ([52, 56]). *Let Φ be a β-Ginibre point process and $\{G_{j,k}\}_{j,k\in\mathbb{N}}$ be i.i.d exponential random variable of parameter one, we define*

$$X_j \overset{law}{=} \sqrt{\frac{\lambda\pi}{\beta}\sum_{k=1}^{i} G_{j,k}}.$$

Then, the law of the affixes of Φ is the same as the law of the set of $\{X_j\}_{j\in\mathbb{N}}$ on which a thinning of probability β has been performed.

Figure 2.2 illustrates the probability law of the event $X_j < X_1$ for $j > 1$, computed for the Ginibre point process. It appears that choosing the point nearest to the origin leads to select a point with an affix following the law of some X_j instead of X_1 with about 50% probability. Therefore, statistical bias is introduced.

As a consequence, in order to simulate a β-Ginibre under the Palm measure, we adapt the framework presented in the works of Flint [39] and Decreusefond et al. [28], that is used to simulate realizations of Ginibre point process. This framework is itself derived from Algorithm 18 of the works of Hough et al.[51], which provides a method to simulate realizations of a determinantal point process provided its kernel eigenvectors and eigenvalues.

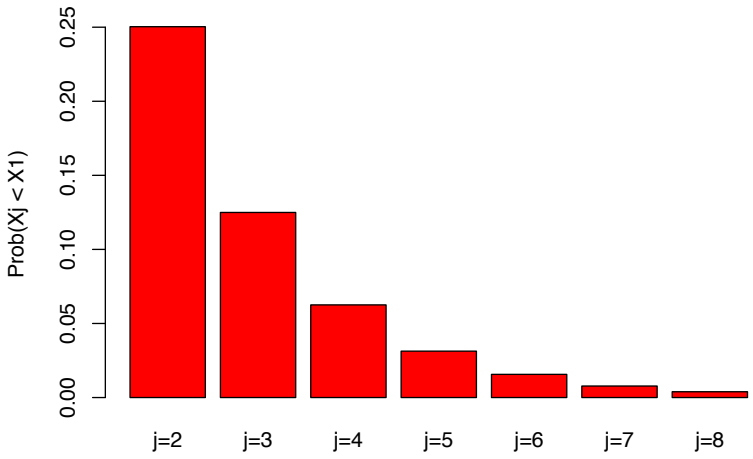

Figure 2.2: Probability $\mathbb{P}(X_j > X_1)$ for a Ginibre point process of intensity λ

The following theorem which can be found in [51], provides us with the first milestone to construct a realization of a β-Ginibre point process. Let us denote by $B(\lambda)$ the 0/1-Bernoulli random variable of parameter λ.

Theorem 2.7 ([51]). *The number of point of a β-Ginibre point process on a ball $\mathcal{C}$ has the the distribution of $\sum_{n=0}^{\infty} B(\lambda_n^{\beta,\lambda})$ where $(B(\lambda_n^{\beta,\lambda}), i \geq 0)$ is a family of independent Bernoulli random variables. In particular,*

$$\mathbb{E}_{\Phi}\left[\phi(\mathcal{C})\right] = \sum_{n=0}^{\infty} \lambda_n^{\beta,\lambda} = \lambda \pi R^2.$$

Moreover, let

$$I = \{n \geq 0, B(\lambda_n^{\beta,\lambda}) = 1\},$$

and

$$K_I^{\beta,\lambda}(x,y) = \sum_{n \in I} \phi_n^{\beta,\lambda}(x)\overline{\phi_n^{\beta,\lambda}(y)}.$$

Then, given I, a realization of Φ on a ball $\mathcal{C}$ has $|I|$ points and the joint distribution of the locations of these points is given by

$$p(X_1 = x_1, \ldots, X_{|I|} = x_{|I|}) = \frac{1}{|I|!} \det\left(K_{\beta,\lambda}^I(x_i, x_j), \quad 1 \leq i, j \leq |I|\right). \tag{2.6}$$

According to Theorem 2.7, a realization of a β-Ginibre of parameter c is build in two times: the first step is to draw the Bernoulli random values in order to get the number of points $|I|$ of the realization and construct the kernel $K_I^{\beta,\lambda}$. Provided these two pieces of information, the second step is to draw the $|I|$ points according to the joint distribution $p(x_1, \ldots, x_{|I|})$.

Let M be the maximum number of points that can be drawn for a given realization of a β-Ginibre point process of parameter λ:

$$M = \sup_n \{n, B(\lambda_n^{\beta,\lambda}) = 1\}.$$

Since the random variables $B(\lambda_n^{\beta,\lambda})$ are independent random variable, the law of M is:

$$\mathbb{P}(M < k) = \prod_{i=k}^{\infty}(1 - \lambda_i^{\beta,\lambda}) \quad \text{and} \quad \mathbb{P}(M = k) = \lambda_k^{\beta,\lambda} \prod_{i=k+1}^{\infty}(1 - \lambda_i^{\beta,\lambda}). \tag{2.7}$$

We also know that since the outcome $M = k$ only depends on the set of random variables $(B(\lambda_i^{\beta,\lambda}), i \leq k)$,

$$\mathbb{P}\left(B(\lambda_i^{\beta,\lambda}) = 1 \;\middle|\; M = k\right) = \lambda_i^{\beta,\lambda}.$$

Algorithm 3 provides the method to draw the number of points M and compute the kernel $K^I_{\beta,\lambda}$.

Data: $(\lambda_n^{\beta,\lambda})$.
Result: $K^I_{\beta,\lambda}$, M.
Let M be drawn according to (2.7);
for n *from* 1 *to* M **do**
  if $B(\lambda_n^{\beta,\lambda}) = 1$ **then**
    $K^I_{\beta,\lambda}(x,y) = K^I_{\beta,\lambda}(x,y) + \phi_n^{\beta,\lambda}(x)\overline{\phi_n^{\beta,\lambda}(y)}$
  end
end

Algorithm 1: Determination of the maximum number of points M and construction of the kernel $K^I_{\beta,\lambda}$.

Once the maximum number of points M fixed and the kernel $K^I_{\beta,\lambda}$ constructed, we can now draw the points in the ball $\mathcal{C}$. Each point of a realization is computed iteratively. Indeed, considering the joint-density $p(x_1, \dots x_{|I|})$ as the product of conditional probabilities:

$$p(X_1 = x_1, \dots, X_{|I|} = x_{|I|}) = p(X_1 = x_1) \dots p(X_{|I|} = x_{|I|} | x_1 \dots X_{|I|-1} = x_{|I|-1}), \tag{2.8}$$

the first point x_1 is placed according to the probability density $p(X_1 = x)$, the second point x_2 is placed according to the probability density $p(X_2 = x | X_1 = x_1)$, etc.

In order to evaluate each conditional probability $p(X_{|I|} = x_{|I|} | x_1 \dots, X_{|I|-1} = x_{|I|-1})$, we first highlight an interesting algebraic property of the kernels with Lemma 2.3.

Lemma 2.3 (Self reproducing property)**.** *For any x_1 and x_2 fixed in $\mathcal{C}$,*

$$K^I_{\beta,\lambda}(x_1, x_2) = \int_{\mathcal{C}} K^I_{\beta,\lambda}(x_1, z)\overline{K^I_{\beta,\lambda}(x_2, z)}\mathrm{d}z = K^I_{\beta,\lambda}(x_1, .) \cdot K^I_{\beta,\lambda}(x_2, .),$$

where $K^I_{\beta,\lambda}(x_1, .) : \; z \mapsto K^I_{\beta,\lambda}(x_1, z)$:

Proof. Since

$$\int_{\mathcal{C}} \phi_n^{\beta,\lambda}(z)\overline{\phi_k^{\beta,\lambda}(z)} = \delta_n(k)$$

we have

$$\begin{aligned}\int_{\mathcal{C}} K^I_{\beta,\lambda}(x_1,z)\ \overline{K^I_{\beta,\lambda}(x_2,z)}dx &= \sum_{n,k\in I} \phi_k^{\beta,\lambda}(x_1)\,\overline{\phi_n^{\beta,\lambda}(x_2)}\ \int_{\mathcal{C}} \overline{\phi_k^{\beta,\lambda}(z)}\,\phi_n^{\beta,\lambda}(z)\mathrm{d}z \\ &= \sum_{n\in I} \phi_n^{\beta,\lambda}(x_1)\overline{\phi_k^{\beta,\lambda}(x_2)} = K^I_{\beta,\lambda}(x_1,x_2).\end{aligned}$$

□

We remark that the joint distribution of the point given in (2.6) can be rewritten as the determinant of a Gram matrix.

Definition 2.24 (Gram matrix)**.** *In an Hilbert space H, let $(y_1,\dots,y_n)$ be a family of elements of H. The Gram matrix of this family is*

$$G(y_1,\dots,y_n) = \left(y_i \cdot y_j, 1\le i,j\le n\right).$$

Hence applying the self reproducing property to the equation (2.6), the joint distribution is given by:

$$p(X_1=x_1,\dots,X_{|I|}=x_{|I|}) = \frac{1}{|I|!}\det\left(K^I_{\beta,\lambda}(x_i,.)\cdot K^I_{\beta,\lambda}(x_j,.),\quad 1\le i,j\le |I|\right). \tag{2.9}$$

We can therefore apply the following lemma to compute the expression of the joint probability.

Lemma 2.4. *(Determinant of Gram-Schmidt matrices) In an Hilbert space H (such as $L^2(\mathcal{C},\mathrm{d}x)$), let $(y_1,\dots,y_n)$ be a family of elements of H. The determinant of the Gram matrix of this family $G(y1,\dots,y_n)$ verifies:*

$$\det\left(G(y_1,\dots,y_n)\right) = \det\left(G(y_1,\dots,y_{n-1})\right)\,\|\,y_n - \mathrm{proj}_{F_{n-1}}y_n\,\|^2,$$

where F_n is the subspace engendered by $(y_1,\dots,y_n)$ and $\mathrm{proj}_{F_n}y$ the orthogonal projection of y on that subspace. By iteration we get:

$$\det\left(G(y_1,\dots,y_n)\right) = \|\,y_1\,\|^2\prod_{j=2}^{n}\left(\|\,y_j\,\|^2 - \|\,\mathrm{proj}_{F_{j-1}}y_j\,\|^2\right),$$

Hence, equation (2.9) becomes

$$p(X_1=x_1,\dots,X_{|I|}=x_{|I|}) = \frac{1}{|I|!}\,\|\,K^I_{\beta,\lambda}(x_1,.)\,\|^2\prod_{j=2}^{M}\left(\|\,K^I_{\beta,\lambda}(x_j,.)\,\|^2 - \|\,\mathrm{proj}_{F_{j-1}}K^I_{\beta,\lambda}(x_j,.)\,\|^2\right).$$

The only remaining quantity to evaluate is $\|\,\mathrm{proj}_{F_{j-1}}K^I_{\beta,\lambda}(x_j,.)\,\|^2$. A method is provided with the Gram-Schmidt orthonormalization process described in Lemma 2.5.

Lemma 2.5 (Gram-Schmidt orthonormalization)**.** *Let $(v_1, \cdots, v_k)$ be k independent vectors in H, an Hilbert space. Set*

$$u_1 = v_1,\ u_{l+1} = v_{l+1} - \sum_{j=1}^{l} \mathrm{proj}_{u_j} v_{l+1} \text{ where } \mathrm{proj}_u v = \frac{u \cdot v}{\|u\|^2}\, u.$$

Let $e_i = u_i/\|u_i\|$. Then $(e_1, \cdots, e_k)$ is an orthonormal basis of $\mathrm{vect}(v_1, \cdots, v_k)$ *and*

$$\mathrm{proj}_{\mathrm{vect}(v_1,\cdots,v_k)} v = \sum_{i=1}^{k} v \cdot e_i\, e_i.$$

Applying Lemma 2.5, on the projection we get that:

$$\mathrm{proj}_{F_{j-1}} K^I_{\beta,\lambda}(x_j, .) = \sum_{i=1}^{j-1} \frac{K^I_{\beta,\lambda}(x_j, .) \cdot K^I_{\beta,\lambda}(x_i, .)}{\|K^I_{\beta,\lambda}(x_i, .)\|^2} K^I_{\beta,\lambda}(x_i, .) \tag{2.10}$$

Furthermore applying the self-reproducing property, we get that

$$\|K^I_{\beta,\lambda}(x_j, .)\|^2 = K^I_{\beta,\lambda}(x_j, .) \cdot K^I_{\beta,\lambda}(x_j, .) = K^I_{\beta,\lambda}(x_j, x_j),$$

and

$$K^I_{\beta,\lambda}(x_j, .) \cdot K^I_{\beta,\lambda}(x_i, .) = K^I_{\beta,\lambda}(x_i, x_j)$$

Equation (2.10) then becomes

$$\mathrm{proj}_{F_{j-1}} K^I_{\beta,\lambda}(x_j, .) = \sum_{i=1}^{j-1} \frac{K^I_{\beta,\lambda}(x_i, x_j)}{K^I_{\beta,\lambda}(x_i, x_i)} K^I_{\beta,\lambda}(x_i, .),$$

and

$$\|\mathrm{proj}_{F_{j-1}} K^I_{\beta,\lambda}(x_j, .)\|^2 = \sum_{i=1}^{j-1} \frac{\|K^I_{\beta,\lambda}(x_i, x_j)\|^2}{K^I_{\beta,\lambda}(x_i, x_i)}.$$

Therefore,

$$\begin{aligned}
\int_{\mathcal{C}} \|K^I_{\beta,\lambda}(x_i, x_j)\|^2 \mathrm{d}x_j &= \int_{\mathcal{C}} K^I_{\beta,\lambda}(x_i, x_j) \cdot \overline{K^I_{\beta,\lambda}(x_i, x_j)} \mathrm{d}x_j \\
&= K^I_{\beta,\lambda}(x_i, .) \cdot K^I_{\beta,\lambda}(x_i, .) \\
&= K^I_{\beta,\lambda}(x_i, x_i),
\end{aligned}$$

we get that:

$$\int_{\mathcal{C}} \|\mathrm{proj}_{F_{j-1}} K^I_{\beta,\lambda}(x_j, .)\|^2 \mathrm{d}x_j = j - 1.$$

We also remark that:

$$\begin{aligned}
\int_{\mathcal{C}} \|K^I_{\beta,\lambda}(x_i, .)\|^2 \mathrm{d}x_i &= \int_{\mathcal{C}} K^I_{\beta,\lambda}(x_i, x_i) \mathrm{d}x_i \\
&= \int_{\mathcal{C}} \sum_{n=0}^{|I|} \phi_n^{\beta,\lambda}(x_i) \overline{\phi_n^{\beta,\lambda}(x_i)} \mathrm{d}x_i \\
&= \sum_{n=1}^{|I|} \|\phi_n^{\beta,\lambda}\|^2 \\
&= |I|.
\end{aligned}$$

Hence we can identify each factor of the conditional probability, such that

$$p(X_1 = x_1) = \frac{1}{|I|}\|K^I_{\beta,\lambda}(x_1, .)\|^2,$$

and for all $2 \leq k \leq |I|$:

$$p(X_k = x_k | X_1 = x_1 \ldots, X_{k-1} = x_{k-1}) = \frac{1}{|I| - k + 1}\left(\|K^I_{\beta,\lambda}(x_k, .)\|^2 - \|\mathrm{proj}_{F_{k-1}} K^I_{\beta,\lambda}(x_k, .)\|^2\right).$$

Knowing this family of probability densities, we are able to derive Algorithm 2 to draw each point x_k, provided the kernel $K^I_{\beta,\lambda}$ and the number of points $|I|$. Note that each point x_k is drawn with the rejection method.

Data: $K^I_{\beta,\lambda}$, $|I|$.
Result: $x_1 \ldots x_{|I|}$.
Draw x_1 with density

$$\frac{1}{|I|}\|K^I_{\beta,\lambda}(x, .)\|^2;$$

Let $e_1 = 1/|I|\ \|K^I_{\beta,\lambda}(x_1, .)\|$;
for *i from* 2 *to* $|I|$ **do**
  Draw x_i with density

$$\frac{1}{|I| - i + 1}\left(\|K^I_{\beta,\lambda}(x, .)\|^2 - \sum_{k=1}^{i-1} |K^I_{\beta,\lambda}(x, .) \cdot e_k|^2\right);$$

  Let $e_i = 1/(|I| - i + 1)\ \left(\|K^I_{\beta,\lambda}(x_i, .)\|^2 - \sum_{k=1}^{i-1} |K^I_{\beta,\lambda}(x_i, .) \cdot e_k|^2\right)$;
end

Algorithm 2: Construction of a realization of a β-Ginibre point process $(x_1, \ldots, x_{|I|})$, provided its number of points and kernel $K^I_{\beta,\lambda}$

With such framework, we are able to simulate any determinantal point process with a kernel which can be decomposed on a orthonormal basis of $L^2(\mathcal{C}, \mathrm{d}x)$. The Palm measure of the β-Ginibre point process falls into this category since its kernel is made explicit by the following theorem.

Theorem 2.8 (Palm measure of a determinantal point process [76])**.** *The Palm measure of a determinantal point process Φ with kernel K is the law of a determinantal point process Φ_0, which kernel is given by*

$$K^{\Phi^0}(x, y) = \frac{K(x, y)K(0, 0) - K(x, 0)K(0, y)}{K(0, 0)}, \quad \forall (x, y) \in \mathbb{C}^2.$$

The Palm measure of the β-Ginibre is then a direct application of Theorem 2.8.

Lemma 2.6 (Palm measure of a β-Ginibre point process)**.** *The Palm measure of a β-Ginibre point process Φ of kernel $K_{\beta,\lambda}$ restrained on a ball $\mathcal{C}$ is the law of a determinantal point process with the kernel defined for all $(x, y) \in \mathbb{C}$*

$$K^{\Phi^0}_{\beta,\lambda}(x, y) = \sum_{n \geq 1} \lambda_n^{\beta,\lambda} \phi_n^{\beta,\lambda}(x) \overline{\phi_n^{\beta,\lambda}(y)}.$$

The kernel $K_{\beta,\lambda}^{\Phi^0}$ is then the same kernel as $K_{\beta,\lambda}$ without the first eigenvector $\phi_0^{\beta,\lambda}$ and its associated eigenvalue $\lambda_0^{\beta,\lambda}$. The remaining eigenvalues and eigenvectors are the ones derived in the Theorem 2.4. A realization of a β-Ginibre point process under the Palm measure is then easily obtained :

1. A realization of a β-Ginibre point process with the kernel $K_{\beta,\lambda}^{\Phi_0}$ is simulated according Algorithms 3 and 2.
2. The origin $(0, 0)$ is added to the realization.

2.4 Conclusion

In this chapter, we have introduced the main mathematical and simulation tools that are used in the next chapters of this thesis. Properties of the Poisson point process and of the β-Ginibre point process have been reviewed. A novel theorem about the superposition of the β-Ginibre point processes is also introduced. Furthermore, we have given a novel simulation scheme to perform simulations of β-Ginibre point processes under the Palm measure.

Chapter 3

Real network fitting

In Chapter 2, we have introduced many theoretical concepts about point processes, and more specifically about the β-Ginibre point processes family. In this chapter, we discuss the relevance of the β-Ginibre point process as a model for cellular wireless networks. Thanks to real data of the location of the base stations, we are able to test the model on a dense urban area, a suburban area and a rural area. For each scenario, we estimate the intensity λ and the parameter β of the underlying β-Ginibre point process. We also link both parameters to qualify the deployment strategy of each french operator.

3.1 Introduction

At the beginning spatial models are based on regular hexagonal lattices, where each base station location has a deterministic location. Simplicity of such models have helped telecommunication operators to efficiently deploy and predict network behavior in the first place. Network performance analysis have been performed on such deployed networks [69]. But, due to local geographical externalities, the reality of a network deployment is of a random nature that deterministic spatial models fail to catch. Furthermore, despite simulations of hexagonal deployed network being straightforward, it lacks mathematical tractability. The bound they provide is optimistic in terms of interference estimation [3].

Stochastic geometry ideas, especially about random point processes were then widely explored in the wireless communication literature. Pioneer work in this field was realized by Baccelli et al. on Poisson point process [6]. Many results such as the coverage probability as a function of the signal quality were then derived. Last developments of Poisson point process models also include modeling of heterogeneous networks [34]. However, positions of the base stations in a Poisson point process deployed network are uncorrelated with one another. Therefore clusters of points may occur. Mean inter-site distance of such configurations is thus smaller than what happens in reality. As a result, Poisson point process models generate more interference than that of a real network. The articles of Andrews et al. [3] and Nakata et al. [68] show that the Poisson point process provides the most pessimistic prediction of outage probability compared with other models.

Spatial correlations between base station locations exist, since they have to be separated from one another to maximize coverage and minimize inter-site interference. To take into account these effects, repulsive or regular models were introduced in the literature. A simple approach is to transform a Poisson point process into a repulsive point process by thinning,

such as Matérn hard-core point processes. Interference for such deployed networks was investigated [48] but hard-core models proved to be difficult to manipulate since the outage probability can not be analytically deduced. Soft-core processes then rose the community's interest. Among them, the Ginibre point process and the β-Ginibre point process were investigated in the wireless communication field. They were at first introduced by Shirai et al. [76] in quantum physics to model fermion interactions. Then works of Miyoshi et al. [63] and Deng et al. [33] have derived coverage probability in respect of the SINR for both Ginibre point process and β-Ginibre point process models.

In this chapter, we show that the base stations distribution for an operator and for a technology can be fitted with a β-Ginibre point process distribution in several parts of France and that the distribution of all base stations of all operators can be fitted with a Poisson point process. This phenomenon is justified by the theorem stating that the superposition of different β-Ginibre point processes converges in distribution to a Poisson point process [44]. Finally we draw conclusions on the coverage-capacity trade-off made by different operators. Qualitative results are derived from the model fitting.

Other existing works on antenna deployment models mainly consider the computation of the SINR and coverage probability for a wide set of point processes. We are instead interested in validating the β-Ginibre point process model and the Poisson point process superposition model with real data on a dense urban area. Such a case study is made possible because the French frequency regulator (ANFR) provides location in an open access database [4].

In the first part of this chapter, we give the method to fit the β-Ginibre point process model. We consider three scenarios: an urban dense area, a suburban area and a rural area. A qualitative interpretation of the deployment strategies is then provided. In the last part of this chapter, we explore the superposition of β-Ginibre point process realizations, and shows that the overall realization converges to the realization of a Poisson point process.

3.2 Point processes and real deployment

3.2.1 Fitting method

The very first step before performing fitting on a real network, is to consider a region in the plane where the density of the points formed by the antennas is globally spatially homogeneous. This is a reasonable choice since that local homogeneity of the density of antennas is closely linked to the underlying geographical and sociological area. For instance, a densely and homogeneously distributed configuration of antennas might only be found in a densely populated urban area, with high traffic needs. The second step is to derive the intensity of the point process, which is done by counting the antennas in the window considered. The third step is determining the value of the parameter β, which proves to be more difficult. Since the law of the number of points is not accessible, it is not possible to deduce factor β from the number of points in a subset of compacts. Model fitting is realized using the statistic functions J, since for a β-Ginibre, this function is a tractable analytical expression of the coefficient β. This summary statistic can be applied because we assume the stationarity of the properties of the realization observed.

We recall that for the β-Ginibre, the J function is given in 2 by

$$\forall r \in \mathbb{R}_+^*,\ J(r) = \left(1 - \beta + \beta e^{-\frac{\lambda\pi}{\beta} r^2}\right)^{-1} \tag{3.1}$$

Finding the β parameter becomes then a matter of curve fitting. Given a sample of the locations of the base stations, we first consider a window embracing 60% of the surface of the convex hull formed by the sample. The J function estimate is derived for the points inside the window thanks to the function `Jest` of the R package `spatstat` [7]. Then the minimum mean square error method is used to fit the theoretical J function onto the estimated J function. Once fitting is performed, the parameter β is derived.

3.2.2 Dataset

Real exact data about the locations of every radio emitter in France is available to anyone in an open access database, thanks to the French frequency regulator (ANFR). Operators are obliged by the law to provide accurate information about the location of any of their base stations, which ensures the quality and the accuracy of the data. This database contains the GPS coordinates of each cell, associated with its operator, the technology implemented (2G, 3G, 4G) and the part of the spectrum on which it operates. The β-Ginibre point process model is fitted for each scenario, for different technologies and bands.

3.2.3 A detailed analysis on Paris networks

We focus on Paris networks and detail results for each technology and each band. Results in Table 4.1.

Table 3.1: Numerical values of β and λ (base station per km^2) per technology and operator

		Orange	SFR	Bouygues	Free
GSM 900	β	0.9	0.6	0.7	NA
	λ	3.67	4.03	4.0	NA
GSM 1800	β	0.9	0.7	0.7	NA
	λ	4.71	3.64	5.50	NA
UMTS 900	β	NA	1.0	0.6	1.0
	λ	NA	2.92	3.72	1.60
UMTS 2100	β	1.0	0.6	0.8	1.0
	λ	4.99	5.27	6.17	1.60
LTE 800	β	1.0	1.0	0.55	NA
	λ	1.03	2.52	2.88	NA
LTE 1800	β	NA	NA	0.75	NA
	λ	NA	NA	5.30	NA
LTE 2600	β	0.9	0.64	0.6	1.0
	λ	4.23	4.18	3.73	1.60

Among the four operators, Free is the one without a 2G network, since it is a new comer in the market and has only deployed its own 3G and 4G antennas. Furthermore, most operators

does not operate in every band. For instance Orange has not deployed UMTS 900MHz, nor LTE 1800MHz base stations.

From the point of view of a user, a device can potentially be attached to any of the antennas of an operator's network. Therefore, we provide the aggregated results for each operator in Table 5.1. The total density of the base stations is not the sum of the densities of the base stations of each technology. This is due to the fact that most of the sites provide coverage from 2G to 4G. Finding a new implantation has become complex in a busy city such as Paris, since deployment is bound to many externalities -i.e. public awareness of the potential toxicity of radio waves, cost of the rent, municipal laws, etc. With site sharing, the parameter β also remains stable per operator.

Table 3.2: Numerical values of β and λ (base station per km^2) per operator and for the superposition of all the sites.

	Orange	SFR	Bouygues	Free	**Superposition**
β	1.0	0.5	0.8	1.0	**0.11**
λ	5.29	5.60	6.44	1.60	**15.65**
Number of sites	185	197	225	56	**547**

When considering the superposition of every network, the number of sites is smaller than expected since about 20% of the sites are also shared between operators in order to reduce costs. However as for the 80% of the remaining sites, operator have chosen sites independently from one another. The superposition of all four networks is significantly small with $\beta = 0.2$. This result is expected and validates with the experience the superposition theorem of Chapter 2.

3.3 Influence of the geographical context

A network can not be considered without its geographical context. In that matter, we consider three fitting scenarios: a dense and homogeneous urban area, a suburban area and a rural area. Each scenario is coherent in terms of traffic homogeneity and interference context. A given deployment is indeed an engineering response to the challenge of satisfying traffic demand. The first scenario corresponds to the one of a busy city where inter-site interference mitigation and user demand satisfaction are the two antagonist forces that drive deployment strategy. However in rural areas, coverage is a major concern and cells are placed in a fashion that maximizes their footprint.

In this cross-comparison, we focus only on 3G and 4G networks for each operator, since Free has not deployed a 2G network. Furthermore, we consider each network generation as a whole since from the point of view of the user, it is the generation of the network that matters and not the band itself.

3.3.1 Model fitting on a dense populated area: Paris

There is only one densely homogeneous urban city in France large enough for the fitting process: Paris. The development of the capital has been shaped by two thousand years of history. Being the political and economic center of France, Paris has grown evenly among the last five

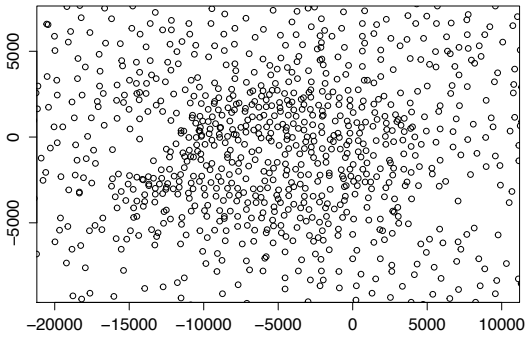

(a) Orange 3G

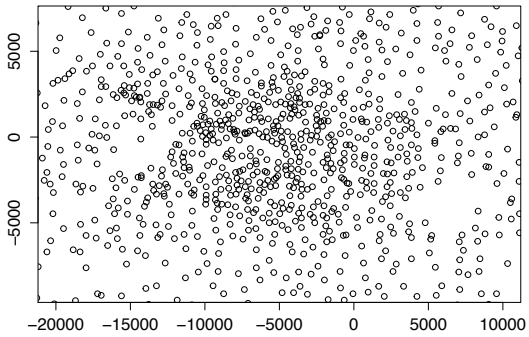

(b) SFR 3G

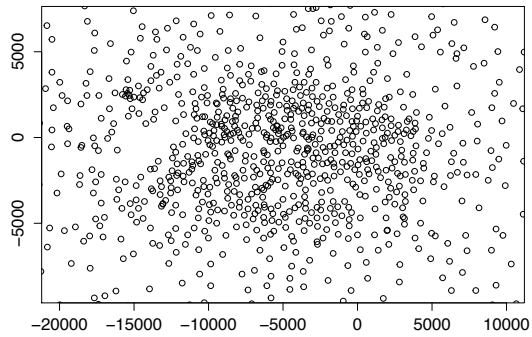

(c) Bouygues Télécom 3G

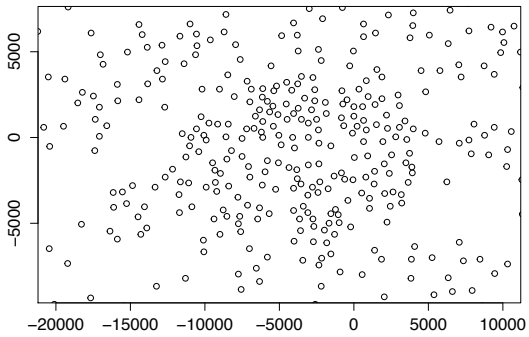

(d) Free 3G

Figure 3.1: 3G networks for the four operators in Paris and its region in January 2015 (distances in meters).

centuries. After the industrial revolution, Paris reached its current size and population: 2 million inhabitants are spread among 105 km^2 with a mean density of 21,000 inhabitants per square kilometer. Today's urban tissue is inherited from the transformation that happened during the middle of the 19th century, instigated by Baron Haussmann. The city is organized along large boulevards that connect on star-shaped intersections. This backbone is completed by smaller streets that spread deeper in the city, like the veins of a leaf. Urban parks (the Luxembourg garden, the Buttes de Chaumont park, the Tuileries garden...) and the Seine river provide open spaces in such busy urban space. Paris also has major hot-spots such as the Gare du Nord and the Gare Saint Lazare railway stations that are respectively the first and second European train stations in terms of passenger traffic, but also tourism attractions and large shopping malls (the Grands Magasins). Such characteristics are difficult to match in other French cities, whose urban development have happened later in time (mostly after the 1960's). Figure 3.1 plots the locations of the 3G base stations for each operator in Paris and its surroundings. Cold spots and hot spots are visible to the naked eye. The limits of

the city can be clearly identified, since population density is significantly lower in the suburbs than in the city.

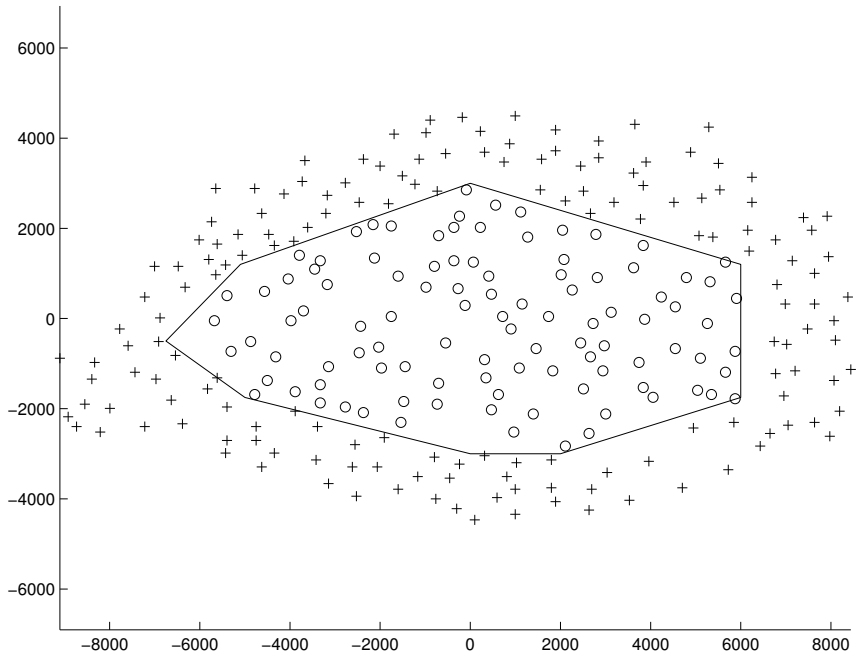

Figure 3.2: SFR UMTS 900 MHz deployment over Paris (distances in meters).

When computing the J function estimate on a finite set of antennas, edge-effect might appear. We then have to define a subset of the data to perform the estimation. Figure 3.2 gives the window we considered for extracting data in Paris. It covers about 60% of the city and its shape matches the geographical borders. The values of the J function estimate are computed for $r \leq 600\ m$. Above $600\ m$, the estimation is not relevant due to the edge-effect. J is then directly fitted on the estimate and the parameter β is deduced. An example of fitting is given in Figure 3.3. The empirical J is always bigger than one of the three curves, which means that the point processes formed by the base stations locations is repulsive. The empirical J curves fit also well the theoretical J curves derived from the β-Ginibre point process model and outfit the Poisson point process model.

Table 3.3: Fitting results for Paris 3G and 4G networks

	LTE				UMTS			
	Orange	SFR	Bouygues	Free	Orange	SFR	Bouygues	Free
β	0.9	0.6	0.8	1.0	1	0.6	0.8	1.0
λ	4.23	4.17	5.44	1.60	4.99	5.27	6.19	1.60
N. ant.	149	147	189	56	174	185	216	56

For each operator, numerical values of β and λ (base station per km^2) obtained from the fitting are given in Table 3.3. The fitting was performed in January 2015. Antenna

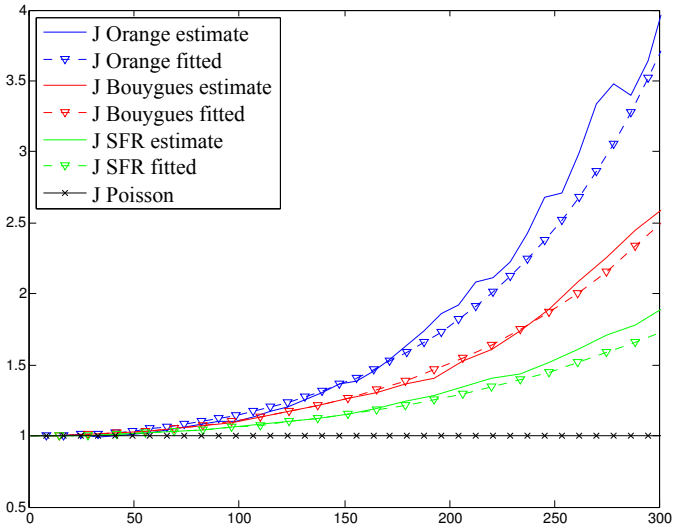

Figure 3.3: Example of J function fitting for Orange, SFR and Bouygues on the 3G 2100 MHz band. As a comparison, $J(r) = 1$ for all r in the Poisson point process case.

density is very high in Paris (up to 6.2 antennas per square kilometer). Repartition of the antennas follows the main boulevards. Density of the antennas locally increases where density of the population or the flow of people is high. Values of β and λ provide insights about the deployment strategy of each cellular network operators, especially about the coverage-capacity trade-off. Orange's high values of β and λ suggest that this operator (as the historic, previously state-owned operator) deployed a network that fulfill an optimal coverage and an optimal traffic capacity, that is a densely deployed network. Free, as a newcomer 3G and 4G operator, was still deploying its network in 2015, therefore its antennas are fewer than the ones of the other operators (small λ) and are more regularly spread over the city to ensure signal coverage (high β). The results suggest that SFR and Bouygues first deployed a network with a minimum number of antennas in order to abide by the coverage requirement of the regulator and then gradually increased traffic capacity on hot-spots by increasing locally the number of antennas. This involves adding more antennas on sites that are already covered, thus creating clusters and decreasing the value of β and increasing the value of λ. The French telecommunication regulator authority (ARCEP) published yearly reports [5] that suggest such evolution.

3.3.2 Model fitting on a suburban area: Bordeaux

Contrary to Paris, main urban areas in the country side have developed after World War II, and have not gone through the urban transformation that the capital underwent in the 19th century. Downtown areas have kept their Middle Ages shape: a densely populated area organized around a church or a belfry. Later urban development (especially beginning from the 1960's) has seen the growing of residential areas or blocks of buildings. Newly developed zones were less dense as distances shrunk with the car becoming the standard way of transportation. On Figure 3.4, the repartition of the antennas is also the result of this historical reality. Antennas are densely deployed in the center of the town and then spread along the major roads. In order to fit the β-Ginibre model, a window centered on the town

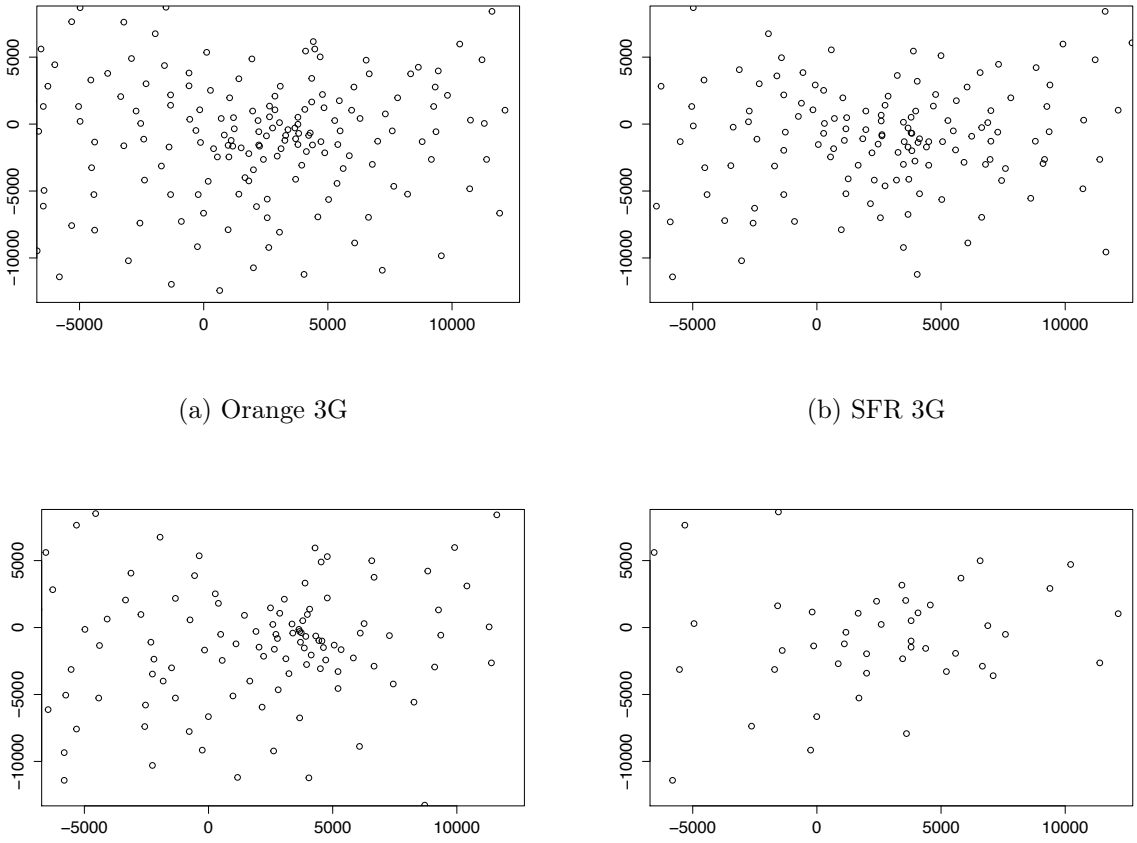

(a) Orange 3G

(b) SFR 3G

(c) Bouygues Télécom 3G

(d) Free 3G

Figure 3.4: 3G deployement for each operator on Bordeaux and its surroundings (distances are in meter).

center has been selected. Results of the fitting are given in Table 3.4.

Table 3.4: Fitting results on Bordeaux

	LTE				UMTS			
	Orange	SFR	Bouygues	Free	Orange	SFR	Bouygues	Free
β	1.0	1.0	0.4	0.8	0.7	0.8	0.4	0.8
λ	2.16	1.67	1.76	0.73	2.44	2.02	1.76	0.77
N. ant.	48	37	39	16	54	45	39	17

The density of antennas is about half of the one of Paris. However, the following observations are made:

- Orange and SFR have deployed a dense (highest λ) and regular network (highest β);

- Free, the new comer, has deployed fewer antennas than its competitors (lowest λ), but has placed them regularly (high value of β) maximizing each cell footprint.
- Bouygues has also deployed a dense network, but is the least regular one (lower β).

More fitting results on other french cites are found in Appendix A.

3.3.3 Model fitting on a rural area

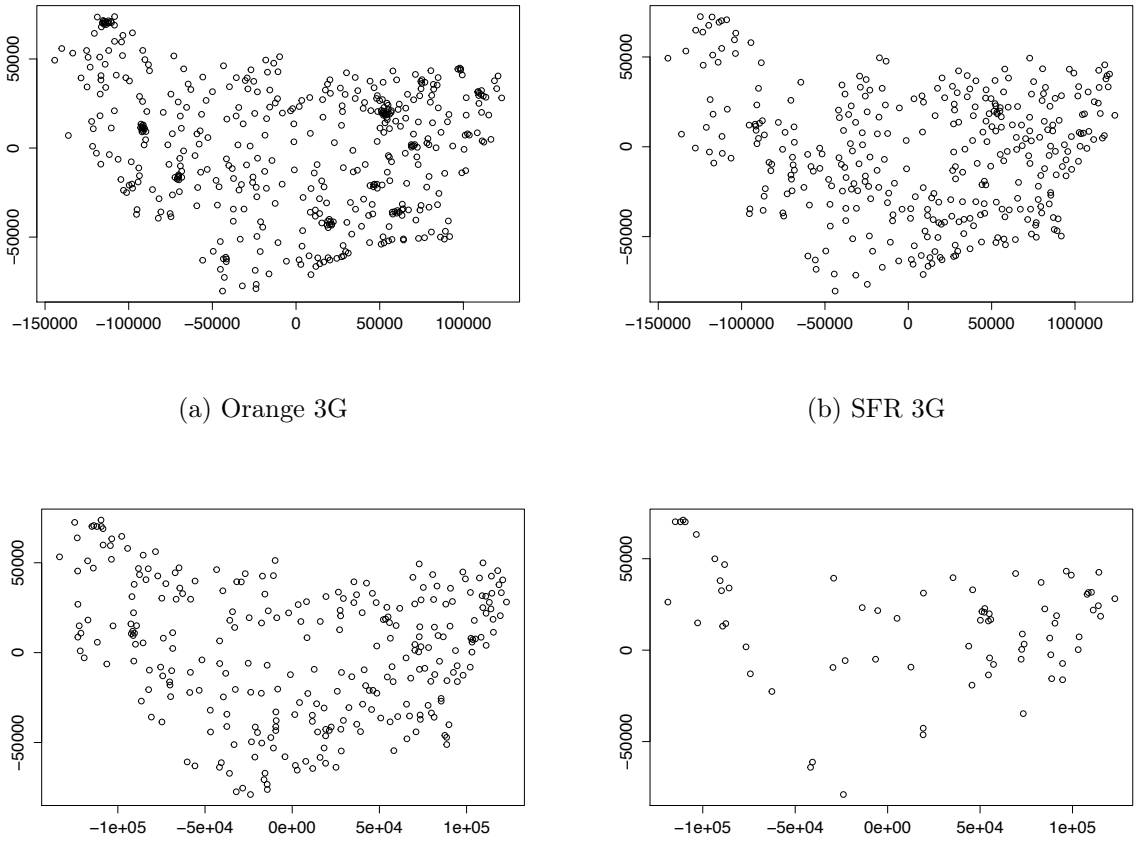

(a) Orange 3G

(b) SFR 3G

(c) Bouygues 3G

(d) Free 3G

Figure 3.5: 3G deployment for rural areas for the Haute-Saône, la Haute-Marne and Vosges perfectures (distance are in meter).

At the rural level, the territory is organized along attractive spots, such as towns and cities holding local government institutions, roads and valleys. Antennas are therefore placed along highways and main roads and in main cities. Figure 3.5 plots the antenna repartition on a region of 20,000 km^2. The fitting window has been chosen in order to contain *empty* areas and avoid attraction spots.

In 2015, 4G was still under nationwide deployment. Therefore, there was no 4G coverage outside main towns and cities. 3G on the contrary was mature for Orange, SFR and Bouygues.

Table 3.5: Fitting results for the Vosges, Haute-Saône, Haute-Marne departments

	LTE				UMTS			
	Orange	SFR	Bouygues	Free	Orange	SFR	Bouygues	Free
β	NA	NA	NA	NA	1.0	0.4	0.7	1.0
λ (10^{-3} ant/km^2)	0.63	0	1.56	1.56	16.7	16.7	10.7	2.50
N. ant.	2	0	5	6	53	57	34	8

The disparity between 3G and 4G networks exists since operators are obliged by law to ensure minimum coverage in rural areas for 3G networks.

The following observations are made on the results Table 3.5:

- Orange has deployed a dense (highest λ) and regular network (highest β);
- Free, the new comer, has deployed fewer antennas than its competitors (lowest λ), but has placed them regularly (high value of β) maximizing each cell footprint.
- Bouygues and SFR have also deployed a dense network, but less regularly than Orange.

More fitting results on other French rural area are found in Appendix A.

3.4 Conclusion

The β-Ginibre model has been successfully fitted on three environments: a dense urban area, a suburban area and a rural area. Each network is characterized by the couple parameters λ and β. The intensity λ describes the overall density of antennas and is strongly linked to the underlaying traffic. The parameter β describes the *uniformity* or *regularity* of a network, and characterizes the repulsiveness strength that exists between base stations.

Observing the relative values of the couples (λ, β), two different deployment strategies arise from these results:

- The first strategy consists in fulfilling both coverage and optimal traffic capacity at once: values of λ ranging between 2.5 and 3.5 antenna per square kilometer for an urban dense area, and β ranging between 0.8 and 1.
- The second strategy is to deploy a network that complies to the coverage requirements in the first stage: values of λ ranging between 1 and 2 antennas per square kilometer and β ranging between 0.8 and 1. Then in the second stage, the number of antennas is increased on hot-spots in order to improve the traffic capacity : values of λ ranging between 2.5 and 3.5 antenna per square kilometer and β ranging between 0.5 and 0.8.

Considering the aggregated networks on Paris of each operator, the overall deployment strategy is aimed at maximizing the coverage (β between 0.7 and 1), while providing a dense enough network to fulfill traffic. Sites are most of the time shared between technologies and sometimes among operators. Considering the superposition of the realizations of β-Ginibre point process, we have proved theoretically, as well as practically that the Poisson Point process model still holds for an aggregate of networks independently deployed.

Chapter 4

Point processes and network performance

Network performance assessment are often considered through the prism of point-to-point link capacity. The well known Shannon's law, indeed links the capacity C, the bandwidth W and the Signal to Interference and Noise ratio (*SINR*) of the link such that:

$$C = W \log_2(1 + SINR)\,.$$

The *SINR* includes the inter-cell interference. It is often considered for hexagonal deployed networks [37]. However, as described in Chapter 3, networks are of random nature and are characterized by the couple (β, λ). Therefore, the spatial properties of the deployment are not fully taken into account in the assessment of network performance. For instance, if clusters of antennas are likely to exist in a network, especially in urban area, one can understand that the inter-cell interference are likely to degrade the overall signal quality, resulting in sub-optimal resource allocation. In this chapter, we introduce a multi-cell framework in order to theoretically and numerically analyze the downlink performance and dimensioning for OFDMA networks. Performance metrics are introduced and theoretical results are derived for interference-limited networks deployed under a Poisson point process. Numerical analysis is also performed for β-Ginibre point processes deployed networks in order to highlight the influence of the repulsive factor β.

4.1 Network and user model

The performance of the downlink channel of LTE networks is considered. Networks are deployed according to a Poisson point process or a β-Ginibre point process. The worst case scenario in terms of interference is assumed: each antenna uses the same frequency band as its neighbors. Furthermore, since we study an LTE system, the downlink channel of each antenna is sliced in a grid of resource blocks, which are 180kHz - 0.5 millisecond frequency-time blocks. We consider the system during a snapshot of 1 millisecond. During this snapshot, each antenna disposes of N_{avail} resource blocks. These resource blocks are then allocated to active users, which positions are drawn according to a Poisson point process. Antennas do not cooperate with one another and are considered identical and omni-directional.

We aim at highlighting the role of the quality of deployment represented by the repulsive factor β on the performance of the network and especially its impact on bandwidth allocation.

Many studies already link the *SIR* with β. We first recall their conclusions below under the unified formalism introduced in Chapter 2.

Let Φ_u be a Poisson point process of intensity λ_u, that represents the active users' positions in the plane. Let Φ_b be a point process of intensity λ_b, that represents the base stations. Let ϕ_u, respectively ϕ_b , be one of the realizations of Φ_u, respectively Φ_b. Let $x \in \phi_u$ and $y \in \phi_b$. We denote by $(G_{xy})_{(x,y)\in\phi_u\times\phi_b}$ the family of i.i.d random values following an exponential law of parameter 1. It models the channel fading between the base station y and the position x. Therefore, we have the following channel model.

Definition 4.1 (Channel model)**.** *The power received at a position $x \in \phi_u$ from a base station $y \in \phi_b$ is*

$$P(x, y) = P_t G_{xy} \, \| x - y \|^{-\gamma}, \tag{4.1}$$

where the constant P_t is the transmission power of all the base stations and γ is the path-loss exponent.

Equation (4.1) explicits the power that is received by a user placed at a position x in the plane from a base station placed at a position y. In this model, we only consider fading and path-loss.

A user is attached to the base station with the strongest signal. Therefore, the signal quality or the *SIR* that it enjoys, is given by the following definition.

Definition 4.2 (*SIR*)**.** *The downlink SIR is given by for all $(x, \phi_b) \in E \times \mathfrak{N}_E$*

$$SIR(x, \phi_b) = \max_{y_0\in\phi_b} \frac{P(x, y_0)}{\sum_{y\in\phi_b} P(x, y) - P(x, y_0)}.$$

Blaszczyszyn et al. [13] and Natakta et al. [68] have analytically characterized the signal quality of networks deployed respectively as a Poisson point process and as a β-Ginibre point process thanks to the concept of coverage probability.

Definition 4.3 (Coverage probability)**.** *For all $\theta \geq 0$, and a stationary point process Φ_b the coverage probability $\mathbb{P}(SIR \geq \theta)$ is given by*

$$\mathbb{P}(SIR(\Phi_b) \geq \theta) = \int_{\mathfrak{N}_E} \mathbb{1}_{[-\infty,\theta]} \left(SIR(o, \phi_b)\right) \mathrm{d}\mathbb{P}_{\Phi_b}(\phi_b),$$

where $\mathbb{1}$ is the indicator function.

The coverage probability represents the proportion of the network that enjoys at least a given *SIR*. Such interpretation is reasonable, since we consider Φ_b is either a homogeneous Poisson point process or a β-Ginibre point process and therefore both stationary [6, 43]. We now provide analytical expressions of the coverage probability for both Poisson and β-Ginibre point processes.

Proposition 4.1 (Poisson Point process coverage probability [13])**.** *For all $\theta \geq 1$ and $\gamma > 2$ the SIR coverage probability for networks deployed under Poisson point process is expressed as:*

$$\mathbb{P}(SIR \geq \theta) = \frac{\gamma \sin(2\pi/\gamma)}{2\pi} \theta^{-2/\gamma}.$$

Proposition 4.2 (β-Ginibre point process coverage probability [68]). *For all $\theta > 0$ and $\gamma > 2$ the SIR coverage probability for a β-Ginibre network is expressed as:*

$$\mathbb{P}(SIR \geq \theta) = \beta \int_0^\infty e^{-s} \mathcal{M}(s,\theta) S(s,\theta)\ ds$$
$$\text{where } \mathcal{M}(s,\theta) = \prod_{j=0}^{\infty} \left(1 - \beta + \frac{\beta}{j!} \int_s^\infty \frac{t^j e^{-t}}{1+\theta(s/t)^{\gamma/2}}\ dt\right)$$
$$\text{and } S(s,\theta) = \sum_{i=0}^{\infty} s^i \left((1-\beta)i! + \beta \int_s^\infty \frac{t^i e^{-t}}{1+\theta(s/t)^{\gamma/2}}\ dt\right)^{-1}.$$

Both Propositions 4.1 and 4.2 show that the coverage probability does not depend on the density of points λ_b. However, these formula have several drawbacks, when it comes to implementation. The coverage probability model of the Poisson point process network is indeed only valid for *SIR* bigger than 0dB as shown in Figure 4.1. The one of the β-Ginibre is also numerically too complex to compute accurately since one has to deal with infinity sums and quotients of factorials.

In Figure 4.2, the simulated coverage probability is plotted for a network deployed according to an hexagonal grid, three β-Ginibre point processes and a Poisson point process, with independent fading and a path-loss exponent of 4. For the hexagonal deployed network, the empirical coverage probability is assessed by taking the values of the *SIR* at each point of the network. For the Poisson point process, numerous networks are simulated and the empirical coverage probability is derived at the origin of the plane. For the β-Ginibre point process, a efficient way to obtain the empirical coverage probability, we first recall Lemma 2.2 of Chapter 1 :

Lemma ([52, 56]). *Let Φ be a β-Ginibre point process and $\{G_{j,k}\}_{j,k\in\mathbb{N}}$ be i.i.d exponential random variable of parameter one, we define*

$$X_j \overset{law}{=} \sqrt{\frac{\lambda\pi}{\beta} \sum_{k=1}^{i} G_{j,k}}.$$

Then, the law of the affixes of Φ is the same as the law of the set of $\{X_j\}_{j\in\mathbb{N}}$ on which a thinning of probability β has been performed.

From this lemma, it is possible to efficiently simulate the *SIR* at the origin of the plane and therefore deduce the coverage probability.

Figure 4.2 also shows that there is a strong correlation between the spatial properties of the network and the mean signal quality in the network. As a result, for a given coverage probability, there is up to 2dB difference between the most *uniform* point process and the most *regular* point process. The repulsive factor β, that characterize the *regularity* of a category of networks, thus has a dramatic influence on signal quality and is assessed in Section 4.3.

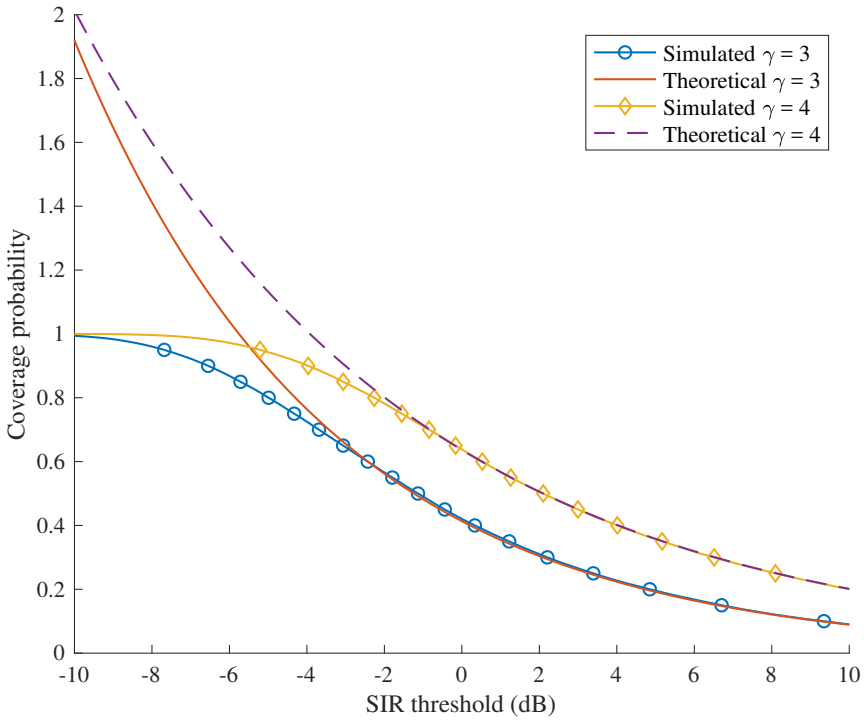

Figure 4.1: Theoretical and simulated coverage probability $\mathbb{P}(SIR > \theta)$ for a Poisson point process

Thanks to Shannon's formula, three variables are linked together: the channel capacity, the bandwidth and the signal quality. Considering that the channel capacity is given by users demand, we are able to derive the influence of signal quality on bandwidth, and more precisely on resource block allocation.

Definition 4.4 (Potential number of resource blocks)**.** *The potential number of resource blocks that might be allocated to a user placed at a position x in the plane to fulfill its capacity requirement C is given for all $(x, \phi_b) \in E \times \mathfrak{N}_E$:*

$$n_r(x, \phi_b) = \min\left(\left\lceil \frac{C}{W_{rb} \log_2(1 + SIR(x, \phi_b))} \right\rceil, l_m\right), \tag{4.2}$$

with W_{rb} being the bandwidth of a resource block. The quantity l_m is the maximum number of resource blocks that can be allocated to one user.

Hence for any realization of active users ϕ_u, the total number of resource blocks that must be allocated in the network ϕ_b to fulfill users's demand in a compact $A \in E$ is given by

$$n_{tot}(\phi_u, \phi_b) = \int_{x \in A} n_r(x, \phi_b) \phi_u(\mathrm{d}x). \tag{4.3}$$

There is, however, another way to obtain the quantity $n_{tot}(\phi_u, \phi_b)$. We consider the family of functions $(a_l)_{1 \le l \le l_m}$, such that for each integer l and any compact subset $A \subset E$,

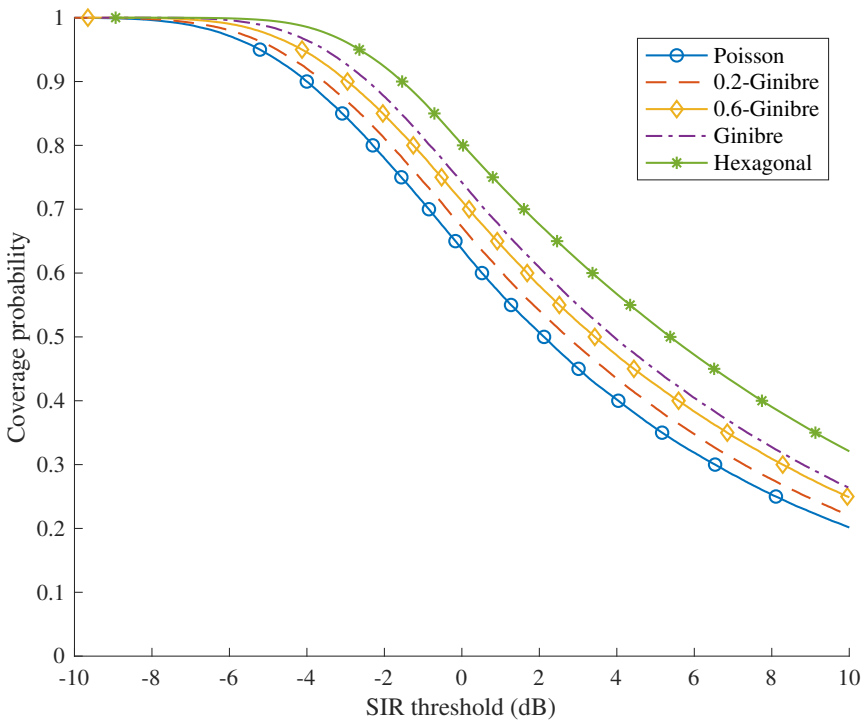

Figure 4.2: Coverage probability $\mathbb{P}(SIR > \theta)$, for $\gamma = 4$ and independent fading.

$a_l : A \times \mathfrak{N}_E \to [0,1]$,

$$a_l(x,\phi_b) = \begin{cases} \mathbb{1}_{[t_1,+\infty[}\left(SIR(x,\phi_b)\right) & \text{if } l = 1, \\ \mathbb{1}_{[0,t_{l_m-1}]}\left(SIR(x,\phi_b)\right) & \text{if } l = l_m, \\ \mathbb{1}_{[t_l,t_{l-1}]}\left(SIR(x,\phi_b)\right) & \text{otherwise,} \end{cases}$$

where t_l is the required SIR to allocate l resource blocks. According to Shannon's formula:

$$t_l = 2^{C/lW_{rb}} - 1.$$

Therefore, the number of resource blocks that are requested by the users can also be written as

$$n_{tot}(\phi_u,\phi_b) = \sum_{l=1}^{l_m} l \int_{x\in A} a_l(x,\phi_b)\phi_u(\mathrm{d}x).$$

The quantity $n_{tot}(\phi_u,\phi_b)$ is computed for one given network ϕ_b and one realization of users ϕ_u. We can consider the random variable $n_{tot}(\Phi_u,\Phi_b)$ that depends on both the point process of the base stations and the users. Since we wish to characterize the number of resource blocks in function of the point process of the network, we consider the expectation of $n_{tot}(\Phi_u,\Phi_b)$ over all the configuration of networks, in respect to a given measure $\mathrm{d}\mathbb{P}_{\Phi_b}$.

Definition 4.5 ($N_{tot}(\Phi_u)$)**.** *The random variable $N_{tot}(\Phi_u)$ is the conditional expectation in*

respect to the point process Φ_b. If ϕ_u is a given realization of Φ_u, we have

$$\begin{aligned} N_{tot}(\phi_u) &= \mathbb{E}_{\Phi_b}[n_{tot}(\Phi_u, \phi_b)|\Phi_u = \phi_u], \\ &= \sum_{l=1}^{l_m} l \iint_{(x,\phi_b)\in A\times\mathfrak{N}_E} a_l(x,\phi_b)\mathrm{d}\mathbb{P}_{\Phi_b}(\phi_b)\phi_u(\mathrm{d}x). \end{aligned}$$

The random variable $N_{tot}(\Phi_u)$ is a cornerstone concept. It is the mean number of resource blocks required by users in function of a given point process Φ_b of base stations and for a random configuration of users Φ_u in the network.

We now characterize the law of $N_{tot}(\Phi_u)$. Let the family $(\alpha_l)_{1\leq l\leq l_m}$ be

$$\alpha_l = \begin{cases} \mathbb{P}(t_1 < \mathit{SIR}(0,\Phi_b)) & \text{if } l = 1, \\ \mathbb{P}\big(t_{l_{m-1}} \geq \mathit{SIR}(0,\Phi_b)\big) & \text{if } l = l_m, \\ \mathbb{P}(t_l \leq \mathit{SIR}(0,\Phi_b) < t_{l-1}) & \text{otherwise.} \end{cases}$$

Proposition 4.3. *For a stationary point process Φ_b and users distributed according to a Poisson point process Φ_u with parameter λ_u, the random variable $N_{tot}(\Phi_u)$ observed on a compact $A \subset E$ is a compound Poisson process given by*

$$N_{tot}(\Phi_u) = \sum_{l=1}^{l_m} l M_l,$$

where each M_l follows a Poisson law of intensity $\lambda_u \alpha_l |A|$.

Proof. Let $(A_l(\phi_b))_{1\leq l\leq l_m}$, the family of compacts defined for all l and ϕ_b by :

$$|A_l(\phi_b)| = \int_{x\in A} a_l(x,\phi_b)\mathrm{d}x.$$

Each compact A_l corresponds to a subset of the compact A where a user demands l resource blocks. An example of the family $(A_l(\phi_b))_{1\leq l\leq l_m}$ is given in Figure 4.3. The darker the surface, the less the demand in resource blocks. Furthermore, with γ increasing, the surfaces with potentially a high number of resource block required are decreasing. This effect is studied in details in Section 4.2. From the definition of $N_{tot}(\Phi_u)$, we have

$$\begin{aligned} N_{tot}(\Phi_u) &= \sum_{l=1}^{l_m} l \iint_{(x,\phi_b)\in A\times\mathfrak{N}_E} a_l(x,\phi_b)\mathrm{d}\mathbb{P}_{\Phi_b}(\phi_b)\Phi_u(\mathrm{d}x) \\ &= \sum_{l=1}^{l_m} l \int_{\phi_b\in\mathfrak{N}_E} \int_{x\in A_l(\phi_b)} \Phi_u(\mathrm{d}x)\mathrm{d}\mathbb{P}_{\Phi_b}(\phi_b). \end{aligned}$$

Since the point process Φ_b is stationary, we have:

$$\int_{\phi_b\in\mathfrak{N}_E} a_l(x,\phi_b)\mathrm{d}\mathbb{P}_{\Phi_b}(\phi_b) = \int_{\phi_b\in\mathfrak{N}_E} a_l(o,\phi_b)\mathrm{d}\mathbb{P}_{\Phi_b}(\phi_b).$$

From Definition 4.3 of the coverage probability, we get that

$$\int_{\phi_b\in\mathfrak{N}_E} a_l(o,\phi_b)\mathrm{d}\mathbb{P}_{\Phi_b}(\phi_b) = \alpha_l. \tag{4.4}$$

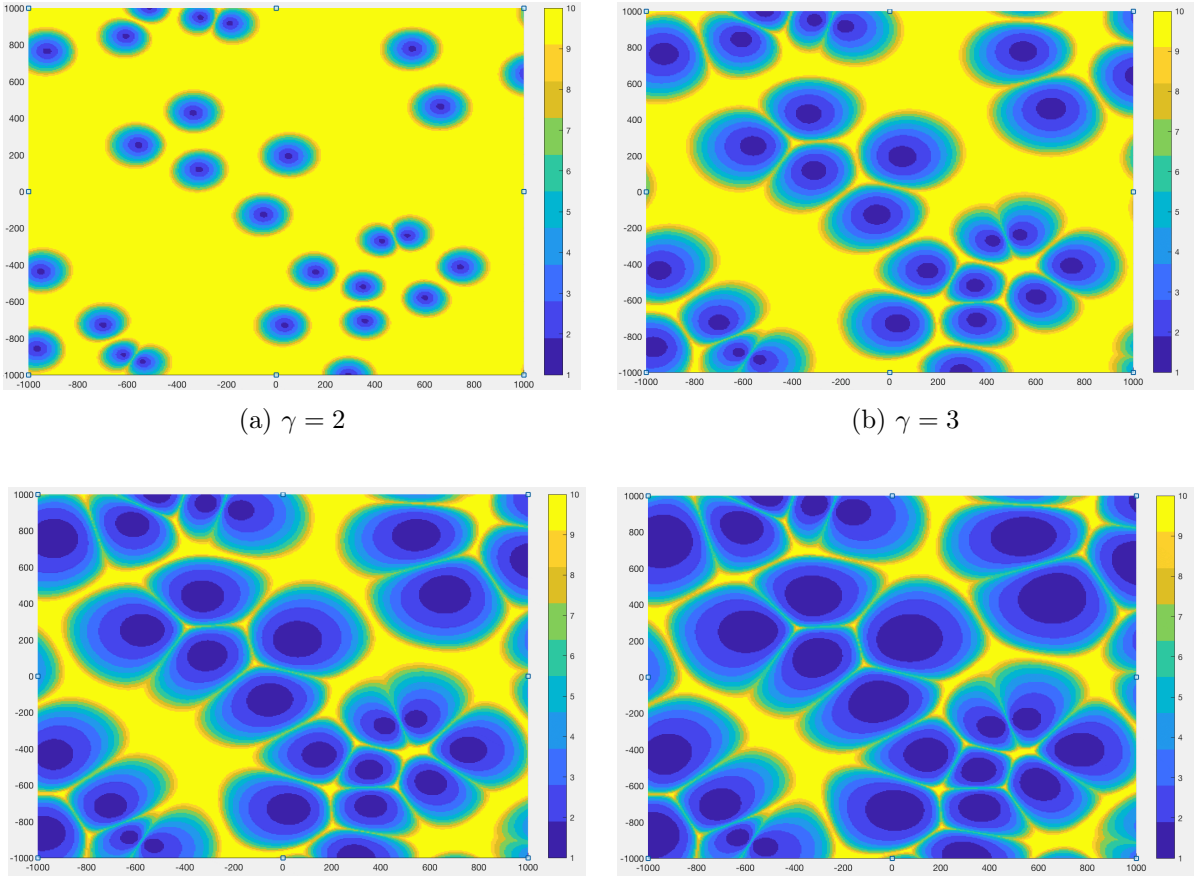

(a) $\gamma = 2$ (b) $\gamma = 3$

(c) $\gamma = 4$ (d) $\gamma = 5$

Figure 4.3: Evolution of the familly $(A_l(\phi_b))_{1\leq l\leq l_m}$ with γ for a realization of a Poisson point process of parameter $\lambda_b = 6$ ant.km^{-2}, $C/W_{rb} = 5.5$ and $l_m = 10$ without any fadding and noise. Axes are in metres.

Thanks to the Fubini theorem we get:

$$\begin{aligned}\int_{\phi_b\in\mathfrak{N}_E} |A_l(\phi_b)|\mathrm{d}\mathbb{P}_{\Phi_b}(\phi_b) &= \int_{x\in A}\int_{\phi_b\in\mathfrak{N}_E} a_l(x,\phi_b)\mathrm{d}\mathbb{P}_{\Phi_b}(\phi_b)\mathrm{d}x \\ &= \alpha_l|A|.\end{aligned}$$

Let $(\tilde{A}_l)_{1\leq l\leq l_m}$ be a family defining a partition of A such that for all $1 \leq l \leq l_m$

$$\tilde{A}_l = \alpha_l|A|, \quad \bigcup_{l=1}^{l_m} \tilde{A}_l = A, \quad \forall i \neq j,\ \tilde{A}_i \bigcap \tilde{A}_j = \emptyset.$$

Hence, we have

$$N_{tot}(\Phi_u) = \sum_{l=1}^{l_m} l \int_{x \in \tilde{A}_l} \Phi_u(\mathrm{d}x) \tag{4.5}$$

$$= \sum_{l=1}^{l_m} l \Phi_u(\tilde{A}_l). \tag{4.6}$$

Since the point process Φ_u is a Poisson point process, $\Phi_u(\tilde{A}_l)$ follows a Poisson law of parameter $\alpha_l \lambda_u |A|$. □

Since the characteristic function of each M_l is given by

$$\forall t \in \mathbb{R}, \quad \Psi_l(t) = \exp\left(\alpha_l \lambda_u |A| \left(e^{it} - 1\right)\right),$$

the characteristic function of $N_{tot}(\Phi_u)$ is derived below:

Proposition 4.4 (Characteristic function of $N_{tot}(\Phi_u)$)**.** *The characteristic function Ψ of $N_{tot}(\Phi_u)$ is given by:*

$$\forall t \in \mathbb{R}, \quad \Psi(t) = \prod_{l=1}^{l_m} \Psi_l(lt). \tag{4.7}$$

Following Equation (4.7), the distribution of $N_{tot}(\Phi_u)$, as well as its cumulative distribution is computed by discrete convolution of the probability densities of each term lM_l:

$$\mathbb{P}(lM_l = \omega) = \begin{cases} 0 & \text{if } \omega \neq 0 \bmod l, \\ \exp\left(-m_l\right) m_l^q / q! & \text{if } \exists q \in \mathbb{N},\ \omega = ql, \end{cases}$$

where $m_l = \lambda_u \alpha_l |A|$. On the practical side, while computing the convolutions to access the distribution of $N_{tot}(\Phi_u)$, one needs to truncate the sum of each term of the convolution. Thanks to large derivations theory [32], for any real number $a > 0$,

$$\mathbb{P}(M_l \geq a\, m_l) \leq \exp(-m_l(a \ln a + 1 - a)).$$

Therefore, since the Poisson distribution vanishes exponentially at infinity, it is possible to wisely chose the parameter a to achieve the desired threshold. In practice, truncating at $a = 3$ leads to an error smaller than 10^{-3}.

4.2 Characterization of $N_{tot}(\Phi_u)$ under a Poisson point process

In this section, we characterize the random variable $N_{tot}(\Phi_u)$ as well as the outage probability for networks deployed under a Poisson point process in respect to the path-loss γ. An application to dimensioning is proposed to determine the number of resource blocks N_{avail} that should be given to each base station to fulfill active users requirement.

4.2.1 Influence of the path-loss on the expectation of the random variable $N_{tot}(\Phi_u)$

For $2 \leq l_m \leq \lfloor C/W_{rb} \rfloor$, in a Poisson point process deployed network, $\mathbb{E}_{\Phi_u}[N_{tot}(\Phi_u)]$ decreases as γ increases.

According to Equation (4.6), the expectation $\mathbb{E}_{\Phi_u}[N_{tot}(\Phi_u)]$ is given by

$$\mathbb{E}_{\Phi_u}[N_{tot}(\Phi_u)] = \sum_{l=1}^{l_m} l\lambda_u \alpha_l |A|.$$

Hence the expectation depends on the linear combination of the family $(\alpha_1, \ldots, \alpha_{l_m})$.

For γ large enough, the following conditions are verified:

1. $\lim_{\gamma\to\infty} \alpha_1 = 1$,
2. $\lim_{\gamma\to\infty} \alpha_l = 0$, with $l \neq 1$,
3. For $3 \leq l_m \leq \lfloor C/W_{rb} \rfloor$, $\alpha_1 \geq \ldots \geq \alpha_{l_{m-1}}$.

According to their definition by the Equation (4.1), each α_l depends on γ. The expression of the *SIR* is provided in Proposition 4.1.

- Proof of (1) and (2):

Since the limits

$$\lim_{\gamma\to\infty} \gamma \frac{\sin(2\pi/\gamma)}{2\pi} = 1,$$

and

$$\forall 1 \leq l \leq l_m, \quad \lim_{\gamma\to\infty} t_l^{-2/\gamma} = 1,$$

converge to 1, conditions (1) and (2) are verified.
When $\lfloor C/W_{rb} \rfloor = 2$, the critical γ is reached when

$$\frac{\gamma \sin(2\pi/\gamma)}{2\pi} t_1^{-2/\gamma} = \frac{1}{2}$$

- Proof of (3):

When $\lfloor C/W_{rb} \rfloor \geq 3$, $\alpha_1 \leq \alpha_2$ is realized when

$$\gamma \geq 2\frac{\ln(t_1) - \ln(t_2)}{\ln(2)}.$$

For all $1 < l < l_m - 1$, let us consider the difference $\alpha_{l+1} - \alpha_l$,

$$\alpha_{l+1} - \alpha_l = \frac{\gamma \sin(2\pi/\gamma)}{2\pi} \left((t_{l+1}^{-2/\gamma} - t_l^{-2/\gamma}) - (t_l^{-2/\gamma} - t_{l-1}^{-2/\gamma}) \right).$$

The first factor $\frac{\gamma \sin(2\pi/\gamma)}{2\pi}$ is always positive. Therefore in order to ensure that $\alpha_{l+1} - \alpha_l$ is negative, the second factor must verify

$$(t_{l+1}^{-2/\gamma} - t_l^{-2/\gamma}) - (t_l^{-2/\gamma} - t_{l-1}^{-2/\gamma}) \leq 0 \tag{4.8}$$

Let $f : \mathbb{R}^+ \to \mathbb{R}$,

$$f(x) = (2^{C/xW_{rb}} - 1)^{-2/\gamma}.$$

Equation 4.8 is true on the domain on which f is concave, and therefore on which $\frac{\mathrm{d}^2 f}{\mathrm{d}x^2}(x) \leq 0$. The first and second derivatives of f for all $x > 0$ are

$$\frac{\mathrm{d}f}{\mathrm{d}x}(x) = \frac{C\ln(2)2^{\frac{C}{xW_{rb}}+1}\left(2^{\frac{C}{xW_{rb}}} - 1\right)^{-\frac{\gamma+2}{\gamma}}}{x^2\gamma W_{rb}},$$

$$\frac{\mathrm{d}^2 f}{\mathrm{d}x^2}(x) = \frac{C\ln(2)2^{\frac{C}{xW_{rb}}+1}\left(2^{\frac{C}{xW_{rb}}} - 1\right)^{-\frac{\gamma+2}{\gamma}} g(x)}{x^4\gamma^2 W_{rb}^2},$$

where $g : \mathbb{R}^+ \to \mathbb{R}$ is such that:

$$g(x) = \left(\gamma C\ln(2) - \gamma x W_{rb}2^{\frac{C}{xW_{rb}}+1} + C\ln(2)2^{\frac{C}{xW_{rb}}+1} + 2\gamma x W_{rb}\right).$$

An asymptotic study of g gives that

$$\lim_{x\to 0} g(x) = \lim_{x\to 0} C2\ln(2)2^{\frac{C}{xW_{rb}}} = +\infty$$

and

$$\lim_{x\to+\infty} g(x) = (2-\gamma)C\ln(2) < 0$$

Therefore, there is a root of g denoted x_r such that for all $x > x_r$, $g(x) < 0$. Numerical analysis shows that g has only one root $x_r \in \mathbb{R}^+$ and $x_r \leq 2$ for $\gamma > 2.5$ and $C/W_{rb} = 6$. Figure 4.4 gives an example of the evolution of the family $(\alpha_1, \ldots, \alpha_{l_m})$ in function of γ for $l_m = 6$.

These conditions shows that the coefficients α_l for small l become preponderant in the weight sums with an increasing γ. In other terms, the surface areas covered with low *SIR* are becoming smaller as the radio conditions become harsher. Such result holds for interference limited networks, because the interference is mitigated by the difficult propagation environment. However, in real networks, under harsh conditions, the received power of the base station signal might drop to the magnitude of the noise floor, which may degrade performance. As a consequence, the *SINR* is also considered in our numerical analysis.

4.2.2 Application to dimensioning

We now introduce the metrics to evaluate the performance of a given network.

Definition 4.6 (Outage probability)**.** *The outage probability associated to networks deployed under a stationary point process Φ_b and users deployed under a Poisson point process Φ_u on a compact $A \subset E$ is*

$$\mathbb{P}_{\Phi_u,\Phi_b}(n_{tot}(\Phi_u,\Phi_b) > N_{avail}\Phi_b(A)).$$

Such definition of the outage probability depends on two random point processes which are the ones of the base stations and of the users. Since we wish to characterize networks according to the quality of their deployment, we prefer the mean outage probability defined below.

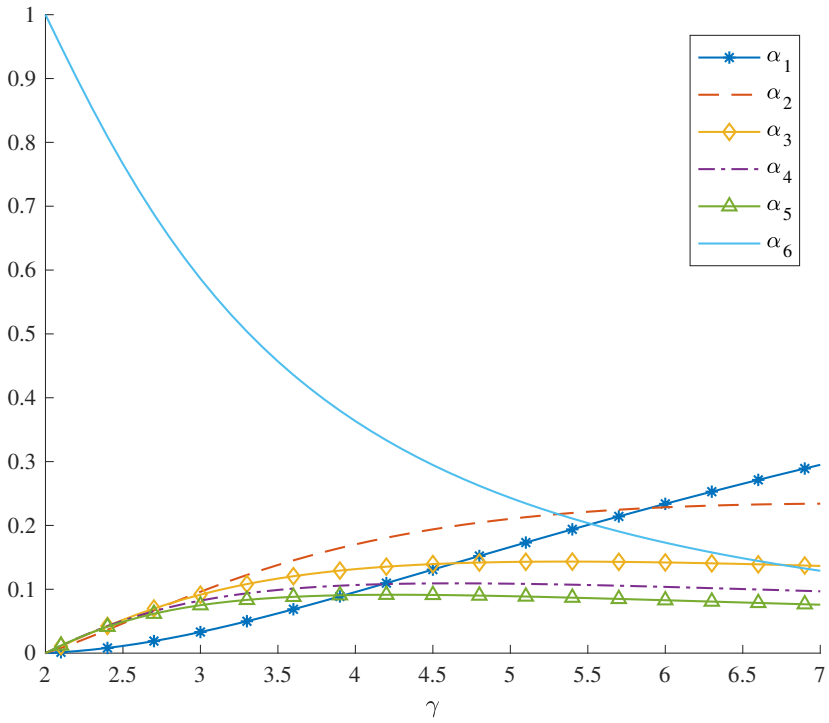

Figure 4.4: Family $(\alpha_1, \ldots, \alpha_{l_m})$ for $C/W_{rb} = 6$ and $l_m = 6$

Definition 4.7 (Mean outage probability)**.** *The mean outage probability associated to networks deployed under a β-Ginibre point process or a Poisson point process Φ_b and users deployed under a Poisson point process Φ_u on a compact $A \subset E$ is*

$$\mathbb{P}_{\Phi_u}(N_{tot}(\Phi_u) > N_{avail}\lambda_b|A|)\,.$$

This definition of the outage probability only depends on the point process of the users, and especially on $N_{tot}(\Phi_u)$. It characterizes the performance of networks deployed under a given β-Ginibre point process.

Since the probability density of $N_{tot}(\Phi_u)$ is fully defined by its characteristic function, we now introduce a method to dimension the number of resources per antenna N_{avail}, provided a constraint on outage probability. Formally,

$$\mathbb{P}_{\Phi_u}(N_{tot}(\Phi_u) > N_{avail}\lambda_b|A|) \leq \epsilon,$$

with $\epsilon > 0$ being the desired threshold. The outage probability is computable thanks to Proposition 4.4. However, Decreusefond et al.[27] have shown that computing the convolutions involves a memory size that is proportional to $\max_l(m_l^2)$. Therefore, for a given small desired threshold, computation might be memory and time consuming. Thanks to the concentration inequality applied on $N_{tot}(\Phi_u)$, an upper bound is derived for engineering purposes.

Theorem 4.1 (Concentration inequality [27])**.** *For any non-negative f bounded by M, any compact A and a realization ϕ of a Poisson point process Φ with intensity measure λ, we have*

$$\mathbb{P}_\Phi\left(\int_A f(x)\phi(\mathrm{d}x) \geq \int_A f(x)\lambda(\mathrm{d}x) + a\right) \leq \exp\left(-\frac{\int_A f^2(x)\lambda(\mathrm{d}x)}{M^2}\,\mathrm{g}\left(\frac{a\,M}{\int_A f^2(x)\lambda(\mathrm{d}x)}\right)\right),$$

where $g(\theta) = (1+\theta)\ln(1+\theta) - \theta$ *for all* $\theta > 0$.

Theorem 4.1 is an application of Chernoff's bound.
In order to apply the concentration inequality to $N_{tot}(\Phi_u)$, we introduce the function n_r such that for all $x \in A$:

$$n_r(x) = \sum_{l=1}^{l_m} l \mathbb{1}_{x \in \tilde{A}_l}(x).$$

According to Equation (4.6),

$$\begin{aligned} N_{tot}(\Phi_u) &= \sum_{l=1}^{l_m} l \int_{x \in \tilde{A}_l} \Phi_u(\mathrm{d}x) \\ &= \int_{x \in A} n_r(x) \Phi_u(\mathrm{d}x). \end{aligned}$$

By the definition of the indicator function and the fact that the family $(\tilde{A}_l)_{1 \leq l \leq l_m}$ is a partition of A, for all $p > 0$,

$$\begin{aligned} \int_{x \in A} n_r^p(x) \lambda_u \mathrm{d}x &= \sum_{l=1}^{l_m} l^p \int_{x \in A} \lambda_u \mathbb{1}_{x \in \tilde{A}_l}(x) \mathrm{d}x \\ &= \sum_{l=1}^{l_m} l^p \lambda_u \alpha_l |A|. \end{aligned}$$

For $p = 1$, we get

$$\begin{aligned} \int_{x \in A} n_r(x) \lambda_u \mathrm{d}x &= \sum_{l=1}^{l_m} l \lambda_u \alpha_l |A| \\ &= \mathbb{E}_{\Phi_u}[N_{tot}(\Phi_u)] \end{aligned}$$

Since n_r is a non-negative function bounded by l_m, Theorem 4.1 can be applied.

Theorem 4.2. *For any real number* $a > 0$*, an upper bound is given by:*

$$\mathbb{P}_{\Phi_u}(N_{tot}(\Phi_u) \geq \mathbb{E}_{\Phi_u}[N_{tot}(\Phi_u)] + a) \leq \exp\left(-\frac{\int_A n_r^2(x) \lambda_u \mathrm{d}x}{l_m^2} \, \mathrm{g}\left(\frac{a \, l_m}{\int_A n_r^2(x) \lambda_u \mathrm{d}x} \right) \right),$$

where $g(\theta) = (1+\theta)\ln(1+\theta) - \theta$ *for all* $\theta > 0$.

Since the number of resource blocks l is a positive integer with maximum l_m, the concentration inequality is applied on $N_{tot}(\Phi_u)$ to derive Theorem 4.2. Hence, an upper bound of $\hat{N}_{avail}$ is given by the expression:

$$\hat{N}_{avail} = \mathbb{E}_{\Phi_u}[N_{tot}(\Phi_u)] + a,$$

where a is the solution of:

$$\mathrm{g}\left(\frac{a \, l_m^2}{\int_A n_r^2(x) \lambda_u \mathrm{d}x} \right) = -\frac{\ln(\epsilon) \, l_m}{\int_A n_r^2(x) \lambda_u \mathrm{d}x}.$$

4.3 Numerical analysis

Numerical analysis is performed on networks that are generated according to a Poisson and five types of β-Ginibre point processes. In order to provide consistent and statistically coherent data, performance analysis is computed with a reference cell placed at the origin of the plane, which means that the simulations must be performed under the Palm measure. A powerful simulation scheme have been introduced in Chapter 2 to obtain realizations of the β-Ginibre point process under Palm. Three scenarios are explored:

- for a given outage probability ϵ, the number of resource blocks N_{avail}, is derived in function of the path-loss γ,
- for a given outage probability ϵ, the upper bound $\hat{N}_{avail}$ provided by Theorem 4.2 is derived in function of the path-loss γ,
- for a given N_{avail}, the outage probability is derived in function of the path-loss γ.

Simulations are performed in two sets: the first considering the *SIR*, and the second considering the *SINR*. For both sets of simulations, the influence of the regularity of the deployment, through the parameter β is derived. Cross comparison between both sets reveals the range of the path-loss exponent γ where the approximation of interference limited networks applies.

4.3.1 Numerical results considering the *SIR*

Table 4.1: Simulation parameters

P	1 W
λ_b	3.0 per km^2
λ_u	40 per km^2
l_m	10
C	1 Mb/s
W_{rb}	180 kHz
Path-loss exponent	from 2 to 5
Network radius	1.8 km

Simulation parameters are summarized in Table 4.1. The values λ_n and λ_u are chosen to match a busy urban environment. Users are assumed to be identical and each of them asks for a download throughput of 1 Mb/s.

Figure 4.5 illustrates that the mean number of resource blocks required to fulfill an outage probability of 10^{-2} decreases dramatically of 30% with the path-loss exponent γ ranging from 2 to 5. Such results are coherent with the fact that these results focus on interference limited systems. Since radio propagation conditions become harsher with a high value of γ, interfering signals are weaker compared to the main signal, granting more surface of the cell with a higher *SIR*. Likewise, Figure 4.7 shows that for a fixed number of resource blocks per cell, the outage probability decreases with γ. Figure 4.6 shows that the approximation given by the inequality concentration stated in Theorem 4.2 is as expected pessimistic and

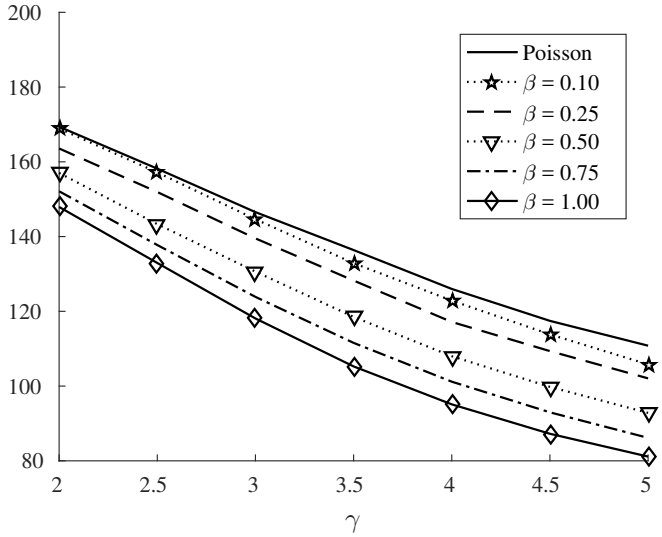

Figure 4.5: Number of resource blocks N_{avail} in function of the path loss exponent γ required to achieve a outage probability of $\epsilon = 10^{-2}$, in respect to the *SIR*

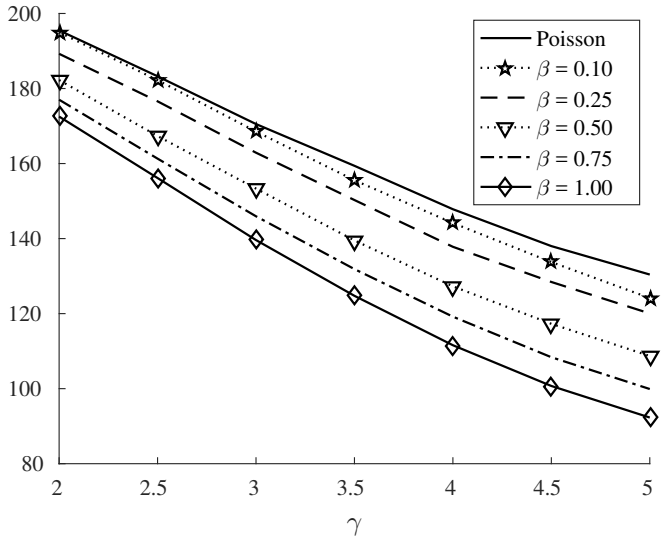

Figure 4.6: Upper bound $\hat{N}_{avail}$ in function of the path loss exponent γ required to achieve a outage probability of $\epsilon = 10^{-2}$, in respect to the *SIR*

over estimate the exact result by 10%. For each figure, the worst case scenario is held by the Poisson point process whereas the best case scenario is given by the 1-Ginibre point process. The overall *SIR* is indeed improved in the network with β going to 1 as shown in Figure 4.2. Figure 4.5 and Figure 4.6 show that the improvement between Poisson point process and Ginibre point process varies between 12% and 26% depending on the value of γ. Likewise, the outage probability is improved up to a factor of 4 between the Poisson point process and the Ginibre point process.

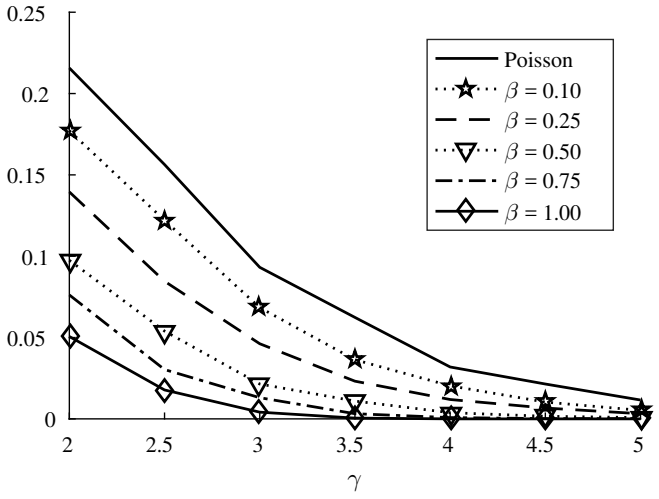

Figure 4.7: Outage probability for $N_{avail} = 100$ in function of the path loss exponent γ, in respect to the *SIR*

4.3.2 Numerical results considering the *SINR*

The derivations about the characterization of $N_{tot}(\Phi_u)$ are derived by replacing the expression of the *SIR* by the one of the *SINR*.

Definition 4.8. *Let ϕ_b a realization of the point process Φ_b of the base stations and $x \in E$. Let N_0 be the noise floor power. The SINR is given by*

$$SINR(x, \phi_b) = \max_{y_0 \in \phi_b} \frac{P(x, y_0)}{\sum_{y \in \phi_b} P(x, y) - P(x, y_0) + N_0 W_{rb}}.$$

Figures 4.8, 4.9 and 4.10 are derived for a noise power of $10^{-14.4}$ W/Hz. Each figure shows that two working regimes exist and depend on the path-loss exponent γ for a wireless network. The first working regime is valid for γ between 2 and 3.5. In that range, interference is predominant over the noise. Therefore, results are analog to the one of Figures 4.5, 4.6 and 4.7: the number of resource blocks that are required to fulfill traffic demand decreases with the path-loss, as well as the loss probability. The second working regime happens for γ bigger than 3.5. In that region, radio conditions are so harsh that interference is mitigated by the noise floor. Hence, performance of the network declines with γ.

Even if a noise floor is considered, the performance of the network is still dramatically influenced by the coefficient β. Especially in the second regime, β has an even higher impact on network performance, especially under difficult conditions. Finally, there is an optimal radio condition between 3 and 3.5 where the *SINR* is of the same magnitude of the noise floor. This is of a particular importance when deploying networks: in order to reach the best performance, an operator should choose a band that must have a path loss between 3 and 3.5. Conditions are severe enough to mitigate interference, but signal quality is good enough to compensate the noise.

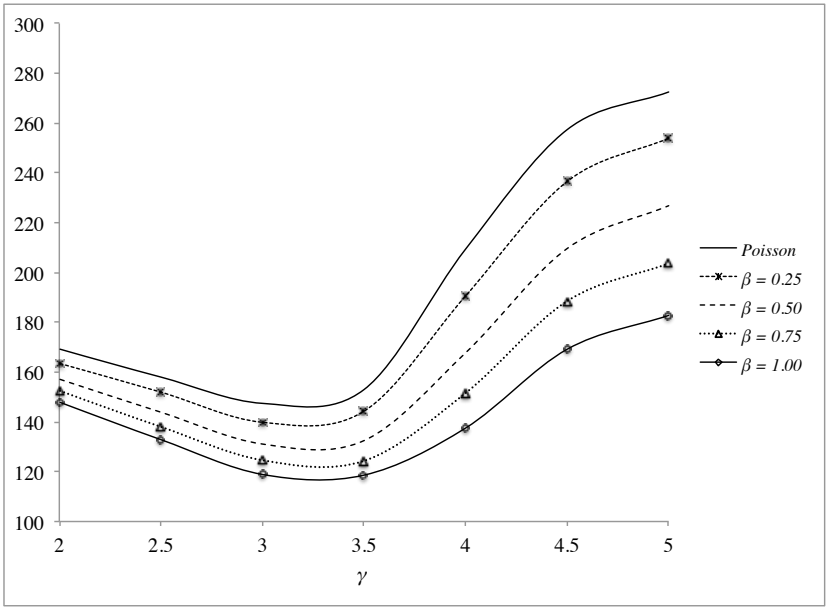

Figure 4.8: Number of resource blocks N_{avail} in function of the path loss exponent γ required to achieve a loss-probability of $\epsilon = 10^{-2}$, in respect to the *SINR*

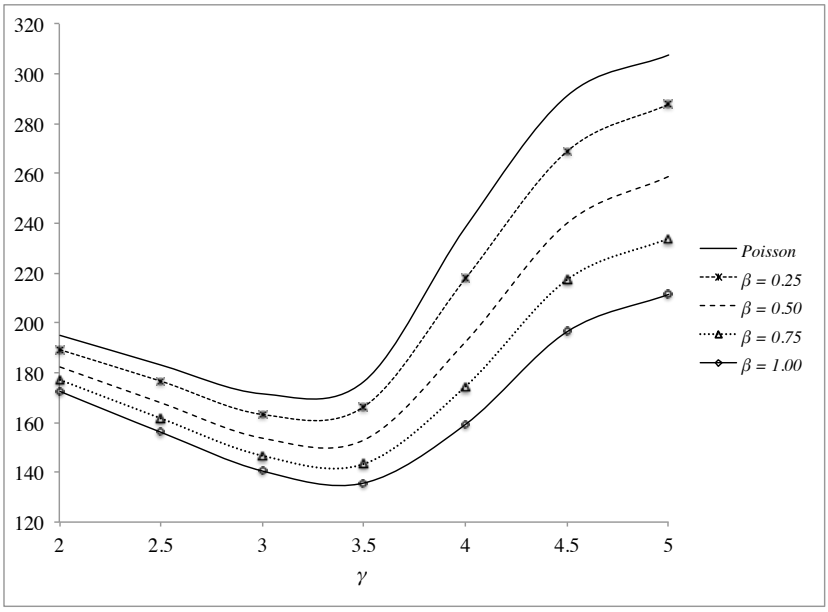

Figure 4.9: Upper bound $\hat{N}_{avail}$ in function of the path loss exponent γ required to achieve a loss-probability of $\epsilon = 10^{-2}$, in respect to the *SINR*

4.4 Conclusion

In this chapter, a new multi-cell framework based on point processes have been introduced. Analytical results on performance and dimensioning have been derived for interference limited networks deployed under Poisson point processes. Numerical analysis extends these theoretical

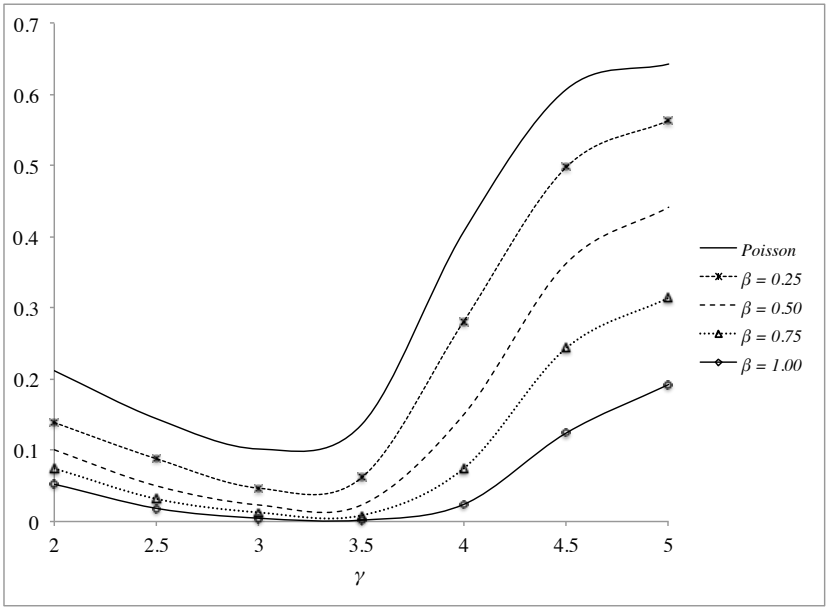

Figure 4.10: Loss-probability for $N_{avail} = 100$ in function of the path loss exponent γ, in respect to the *SINR*

results to networks deployed under five types of β-Ginibre point processes. Results show that the repulsive factor β have a significant impact on network performance. The more *regular* the network is, the more optimal the spectrum is used. The Poisson point process provides however a good engineering pessimistic bound. The influence of the noise floor is also considered. Two regimes are observed: an interference limited regime and a noise limited regime. We show that for all simulated point processes, there is a range of optimal radio conditions where network performance is maximum.

Chapter 5

New paradigms for OFDMA network resource allocation

In Chapter 4, we have linked the outage probability of OFDMA cellular networks with the parameter β and the path-loss γ. In this chapter, we consider the problem of resource allocation on downlink, under base station cooperation. Thanks to optimal transport and Cournot-Nash equilibria, we tackle the challenge of resource dimensioning in case of network outage. We also provide an approximate resource allocation framework that is a good compromise between computation complexity and accuracy.

5.1 Introduction

Many models based on dynamic resource allocation have been introduced in cellular networks. Strategies based on Markov processes [22, 61, 59], queuing theory [36, 26, 30], graph theory [18, 38, 83] or game theory [50, 49, 45] are used to finely tune bandwidth and power allocation. Nash bargaining theory has been used in this matter [2, 82, 84], assimilating the optimal resource allocation as a Nash equilibrium.

Other examples of resource allocation algorithms based on optimization have been described [60]. One example is the α-fair resource allocation [1] that gives a unified framework for optimization solution. Going one step further, optimal transport theory has been introduced [77, 67]. This theory is used to shape cell boundaries and efficiently allocate power. Silvia et al. [77] introduces a congestion term, in order to modify the optimized solution, using the Wardrop equilibrium. Unlike pure optimization problems, optimal transport based framework provides many mathematical tools to characterize optima. However, pure optimal transport frameworks suffer from the fact that users' resources requirements have to be known in order to compute the solution. Authors also limit their analysis to power allocation.

Resource allocation algorithms mostly focus on frameworks where one user receives resource blocks from a unique base station. However, to increase the downlink throughput of users, cooperation between base stations can be introduced. In the case of an OFDMA network, a user can then receive resource blocks from multiple base stations. One has then to know which resource block is allocated to which user from which base station. That is what we call the routing problem.

This chapter focuses on a novel approach that jointly optimizes bandwidth allocation and resource routing in OFDMA networks. In the downlink scenario, base stations are deployed

according to a Poisson point process or a β-Ginibre point process. The *SINR* between each user and each base station is the only known information. Under these rough assumptions, we are able to solve the user bandwidth allocation and find the optimal policy to route resources from base stations to users, thanks to the Cournot-Nash equilibria. Theses equilibria were defined by Antoine Augustin Cournot in 1838 and were reformulated by Mas-Colell [62] in probabilistic terms. Blanchet et al. were able to characterize existence and uniqueness of such equilibria [11] by taking advantage of properties of probability spaces and optimal transport theory exposed in the book of Villani [80].

We show that the optimal policies of the joint routing-allocation problem correspond to the Cournot-Nash equilibria. We also show the link between Cournot-Nash equilibria and optimal transport theory and give a tractable mathematical formulation of the problem. A low complexity approximate optimal solution is also provided and characterized. Simulations reveal that there is an optimal working point of the network, where the user satisfaction ratio and the network occupancy are equal. We finally numerically compare the impact of the spatial deployment of the base stations, assuming that they are localized according to a β-Ginibre point process.

5.2 System model and problem formulation

As in Chapter 4, we consider a cellular wireless network composed of omnidirectional identical base stations drawn in the plane according to a point process Φ_b (Poisson or β-Ginibre point process) of intensity λ_b. Each base station disposes of N_{avail} resource blocks. Users are drawn according to a Poisson point process Φ_u of intensity λ_u. We denote by n, the number of base stations and m, the number of users in a compact $A \subset E$. Realizations of the base stations and users in the compact A are respectively the sets of points $\phi_b = \{y_i\}_{1\leq i\leq n}$ and $\phi_u = \{x_j\}_{1\leq j\leq m}$. We denote by N_j the number of resource blocks that a user x_j requires to fulfill its desired capacity C, based on the best *SINR* :

$$N_j = n_r(x_j, \phi_b) = \min\left(\left\lceil \frac{C}{W_{rb}\log_2(1+SINR(x_j,\phi_b))}\right\rceil, l_m\right).$$

Hence, the total demand of resources is given by

$$n_{tot}(\phi_u, \phi_b) = \sum_{j=1}^{m} N_j.$$

There are two case scenarios:

1. The network is in outage : $n_{tot}(\phi_u, \phi_b) \geq N_{avail}\phi_b(A)$.
2. The network is not in outage : $n_{tot}(\phi_u, \phi_b) \leq N_{avail}\phi_b(A)$.

From now on, we consider the network in outage. In that situation, it is the network resources that limits the number of resource blocks to be allocated to users. Therefore, we consider that all the resource blocks available in the network are used.

Definition 5.1. *Let μ_i be the fraction of the resources of the network that is available at a base station y_i:*

$$\mu_i = \frac{1}{n}.$$

Definition 5.2. *Let ν_j^f be the fraction of the required resources by a user x_j:*

$$\nu_j^f = \frac{N_j}{n_{tot}(\phi_u, \phi_b)}.$$

Definition 5.3. *Let ν_j be the fraction of the total network resources allocated to a user x_j, such that:*

$$\nu_j = \frac{n_j^a}{N_{avail}\phi_b(A)},$$

where n_j^a is the number of resource blocks allocated to a user x_j.

Definition 5.4. *Let π_{ij} be the proportion of the total number of resource blocks that are taken from the base station y_i to the user x_j. The quantity π_{ij} verifies:*

$$\sum_{i=1}^{n} \pi_{ij} = \nu_j,$$

and

$$\sum_{j=1}^{m} \pi_{ij} = \mu_i.$$

These equations translates the fact that from the point of view of a user, the total number of resource blocks allocated to this user is equal to the sum of the resources blocks coming from each base stations. Likewise, the total number of resource blocks of one base station is equal to the resource blocks allocated to its users.

Let $\mathcal{P}([1,n])$ be the set of the probability measures on the integer interval $[1,n]$. The quantities $\boldsymbol{\mu} = (\mu_1, \ldots, \mu_n)$, $\boldsymbol{\nu} = (\nu_1, \ldots, \nu_m)$ and $\boldsymbol{\pi} = (\pi_{1,1}, \ldots \pi_{nm})$ are discrete probability measures. The probability measure $\boldsymbol{\mu}$ (respectively $\boldsymbol{\nu}$) belongs to $\mathcal{P}([1,n])$ (respectively $\mathcal{P}([1,m])$. The probability $\boldsymbol{\pi}$ belong to the set of measures on $[1,n] \times [1,m]$ with first (respectively second) marginal equal to $\boldsymbol{\mu}$ (respectively $\boldsymbol{\nu}$), denoted by $\Sigma(\boldsymbol{\mu}, \boldsymbol{\nu})$.

Since the network needs to dimension the resources that are allocated to each user, one must introduce a metric to characterize the difference between the number of resources allocated to a user and the resources requested by each user. This metric must also capture the global fairness of the allocation policy on a network level. We therefore introduce the following fairness function.

Definition 5.5 (Fairness function)**.** *The fairness function is given by*

$$s(\boldsymbol{\nu}) = {}^t(\boldsymbol{\nu} - \boldsymbol{\nu}^f)(\boldsymbol{\nu} - \boldsymbol{\nu}^f),$$

where $\boldsymbol{\nu}^f = \left(\nu_1^f, \ldots, \nu_m^f\right)$ and ${}^t\boldsymbol{\nu}$ is the transposition of $\boldsymbol{\nu}$.

The fairness function represents the quadratic distance between the requested and the allocated proportion of resources. Fairness among users is ensured since the proportion of resources rather than the absolute number of resources is considered. The choice of a quadratic function also gives good optimization properties, since it is intrinsically convex on $\mathbb{R}^n$.

Let c_{ij} be the cost of transmitting a resource block between the base station y_i and the user x_i such that

$$c_{ij} = \frac{\sum_{k=1}^{n} P(x_j, y_k) - P(x_j, y_i) + N_0 W_{rb}}{P(x_j, y_i)}.$$

The cost c_{ij} is the inverse of the *SINR* in respect to the base station y_i at a user x_j.

Definition 5.6 (Cost function)**.** *For a probability measure $\boldsymbol{\pi} \in \Sigma(\boldsymbol{\mu}, \boldsymbol{\nu})$, the overall cost of routing resources from the base stations to the users is given by*

$$W_c(\boldsymbol{\pi}) = \sum_{(i,j)} c_{ij}\, \pi_{ij}.$$

Definition 5.7 (Joint routing-allocation problem)**.** *The joint resource allocation problem is the optimal optimization problem such that:*

$$\boldsymbol{\pi}^* = \underset{\pi \in \Sigma(\boldsymbol{\mu}, \boldsymbol{\nu})}{\operatorname{argmin}} W_c(\boldsymbol{\pi}) + s(\boldsymbol{\nu}),$$

where the optimum $\boldsymbol{\pi}^*$ verifies:

$$\begin{aligned}
&\forall 1 \leq i \leq n,\ \sum_{j=1}^{m} \pi_{ij}^* = \mu_i, \\
&\forall 1 \leq j \leq m,\ \sum_{i=1}^{n} \pi_{ij}^* = \nu_j \leq \nu_j^f, \\
&\forall (i,j),\ \pi_{ij} \geq 0.
\end{aligned}$$

This optimization problem aims at jointly minimize the cost function and the fairness function. Along the fairness term, the cost function provides the routing of the resources under full cooperation. This means that any base station can provide resource blocks to any user. However, it is unlikely that resource blocks are transfered from base stations that are far away from a given user. The cost indeed increases with distance and interferences, which is an incentive to prevent such behavior. The three constraint sets of the optimization problem are relative to the displacement of resource blocks between base stations and users. If we consider the network in a congested state: the constraint on the family $(\mu_i)_{1 \leq i \leq n}$ is saturated which means that every resource block from every antenna is dispatched to users. The second constraint is not saturated, which means that the demand of each user might not be fully satisfied.

In order to characterize the solutions of the joint routing-allocation problem, we introduce Optimal transport theory and the Cournot-Nash equilibria.

5.3 Optimal Transport and Cournot-Nash equilibira

5.3.1 Optimal transport

In 1781, Monge first described the optimal transport problem. One has to transfer sand from a pile to a hole in the ground. Knowing the shape of the pile and of the hole, what are the paths taken by each grain of sand that minimizes the energy used to transfer the pile to the hole? This problem is known as the Monge-Kantorovitch transport problem. Let X and Y be two subsets of $\mathbb{R}^n$. The pile of sand is represented by a measure μ on the space X and the hole in the ground by a measure ν on Y. Let $T(X, Y)$ be the set of bijections between the spaces X and Y. Each element of $T(X, Y)$ denoted Tr represents the path followed by each point from the subset X to the subset Y. Hence, on a Newtonian physics point of view, minimizing the energy to move a grain of sand from its position x in X to some position $Tr(x)$ in Y is

equivalent to find the path and the arrival point in Y that minimizes the distance along the chosen path and arrival point $Tr(x)$. Since this operation has to be repeated for each point in X, this problem is equivalent to finding the mapping Tr between X and Y such that

$$Tr^* = \underset{T(X,Y)}{\operatorname{argmin}} \left(\int_{x \in X} \| x - Tr(x) \| \, \mathrm{d}x \right),$$

under the condition that

$$Tr^* \left[\mu(X) \right] = \nu(Y)$$

This is a non-linear problem which explains why it was still unsolved until 1945. Kantorovich made the key step by reformulating the Monge problem in terms of measures:

$$\min_{\pi \in \Sigma(\mu,\nu)} \int_{X \times Y} \| x - y \| \, \mathrm{d}\pi(x, y). \tag{5.1}$$

where $\Sigma(\mu, \nu)$ is the set of measures on $X \times Y$ with first (respectively second) marginal equal to μ (respectively ν). Kantorovich have shown that if we minimize the quantity

$$\min_{\pi \in \Sigma(\mu,\nu)} \int_{X \times Y} \| x - y \|^2 \, \mathrm{d}\pi(x, y),$$

instead of Equation (5.1), and if μ is absolutely continuous in respect to the Lebesgue measure, then there exists a unique function Tr such that

$$\min_{\pi \in \Sigma(\mu,\nu)} \int_{X \times Y} \| x - y \|^2 \, \mathrm{d}\pi(x, y) = \left(\int_{x \in X} \| x - Tr(x) \| \, \mathrm{d}x \right).$$

and $y = Tr(x)$, π almost surely [16, 17].

The optimal transport problem has been generalized to characterize solutions for continuous cost functions $c : \mathbb{R}^n \times \mathbb{R}^n \to \mathbb{R}_+$:

$$\pi = \underset{\Sigma(\mu,\nu)}{\operatorname{argmin}} \left(\int_{(x,y) \in X \times Y} c(x, y) \mathrm{d}\pi(x, y) \right), \tag{5.2}$$

However, optimal transport implies the knowledge of both measures μ and ν to be computed. From the analogy of the Monge problem, this means that both pile and hole should be the same volume. In our case, however, the resources available in the network might not be enough to fulfill users demand or the contrary. This corresponds to the situation where the hole is bigger that the pile. On a probabilistic point of view this means that the measure ν must be defined or characterized and the Cournot-Nash equilibrium provides the mathematical tools to overcome this problem.

5.3.2 Cournot-Nash equilibium

Let us consider a cost function $\zeta : X \times Y \times \mathcal{P}(Y) \to \mathbb{R}$.

Definition 5.8 (Cournot-Nash equilibrium [11])**.** *A Cournot-Nash equilibrium is a joint probability density measure $\pi \in \mathcal{P}(X \times Y)$ such that*

$$\pi \left(\left\{ (x, y) \in X \times Y \, : \, \zeta(x, y, \nu) = \min_{z \in Y} \zeta(x, z, \nu) \right\} \right) = 1.$$

Existence and uniqueness of Cournot-Nash equilibrium are not guaranteed in every case. However, if the cost function is of the form

$$\zeta(x, y, \nu) = c(x, y) + s(\nu(y)),$$

where c and s are continuous functions on their respective space, Theorem 4.2 [11], states that the Cournot-Nash equilibrium exists and is unique. With such formulation of the cost function, finding the Cournot-Nash equilibrium is equivalent to solve

$$\begin{aligned}\pi &= \text{argmin}_{\pi\in\Sigma(\mu,\nu)} \iint_{X\times Y} (c(x, y) + s(y))\, \mathrm{d}\pi(x, y),\\ &= \text{argmin}_{\pi\in\Sigma(\mu,\nu)} \iint_{X\times Y} c(x, y)\mathrm{d}\pi(x, y) + \int_Y s(y)\mathrm{d}\nu(y).\end{aligned}$$

With such formulation, there is a clear link with the optimal transport theory, since the first term is the same as Equation (5.2). It is by partly taking advantage of the properties optimal transport theory that Blanchet et al. were able to derive their results. Under the light of the Monge-Kantorovich problem, the measures μ and ν embody the shape of respectively the pile and the hole and the solution of optimal transport does not affect either of the measures. However, under the Cournot-Nash framework, each displacement of a grain of sand will affect the shape of the hole, by an effect that is quantified by the function s. Such property is very interesting for resource allocation, since when displacing resources from base stations to users, only the information about user demand is known. Resource allocation itself involves that the traffic requirement of some users might not be fully satisfied. The term s therefore embodies the impact of a resource allocation policy on each user.

5.4 Characterization of the joint routing-allocation problem

The joint routing-allocation problem as defined in Definition 5.7 complies with the definition of the Cournot-Nash problem. Since the cost function is also a linear combination of a cost term W_c and a fairness term s, the joint routing-allocation problem is similar to the case that has been exposed in the works of Blanchet et al.[11]. However, the measures $\boldsymbol{\mu}$ and $\boldsymbol{\nu}$ are not continuous in respect to the Lebesgue measure. Therefore, results of Blanchet et al. does not apply to this optimization problem. Hence, the solutions of the joint routing-allocation problem must be characterized.

5.4.1 Exact resolution

Lemma 5.1. *The joint routing-allocation problem is the following quadratic optimization problem:*

$$\boldsymbol{\pi}^* = \underset{\boldsymbol{\pi}}{\text{argmin}}\, {}^t\boldsymbol{\pi} H \boldsymbol{\pi} + {}^t\mathbf{L}\boldsymbol{\pi},$$

such that:

$$\begin{aligned}&T_n\boldsymbol{\pi} = \boldsymbol{\mu},\\ &T_m\boldsymbol{\pi} \leq \boldsymbol{\nu}^f,\\ &\forall 1 \leq l \leq nm,\ \pi_l \geq 0,\end{aligned}$$

where:

$$\begin{aligned} T_n &= \mathbf{1}_{1,m} \otimes \mathbf{Id}_n, \\ T_m &= \mathbf{Id}_m \otimes \mathbf{1}_{1,n}, \\ H &= {}^tT_m T_m = \mathbf{Id_m} \otimes \mathbf{1}_{n,n}, \\ \mathbf{L} &= \mathbf{c} - 2T_m \boldsymbol{\nu}^f. \end{aligned}$$

The operand $\otimes$ is the Kronecker product. The matrix $\mathbf{Id_m}$ corresponds to the identity matrix of dimension m and the matrix $\mathbf{1}_{m,n}$ is the matrix of ones with m lines and n columns.

This lemma is the vectorial reformulation of Definition 5.7. Since H is a positive semi-definite matrix and $\boldsymbol{\pi}^*$ is a probability measure, the boundedness of the optimization domain is ensured. The existence of a solution is hence guaranteed. Such formulation is implementable in a quadratic common solver. However, the matrix H not being full rank, the solution is not necessarily unique and finding such solution might be NP-hard [74]. In the next paragraph, we introduce an approximate Cournot-Nash equilibria, that provides a solution in polynomial time.

5.4.2 Approximate Cournot-Nash equilibria

The Lemma 5.1 highlights the algebraic structure of the optimization problem: the coupling induced by the fact that there exists a mapping between the probabilities $\boldsymbol{\mu}$ and $\boldsymbol{\nu}$, defines the matrix H. The representation of H as a Kroneker product ($H = \mathbf{Id_m} \otimes \mathbf{1}_{n,n}$) shows the underlying superposition of the user allocation problem and the resource routing problem. The $\mathbf{Id_m}$ factor stands for the allocation of resources and the $\mathbf{1}_{n,n}$ factor represents the optimal resource transfer for each user. The quadratic formalization however cannot be fully separated due to the cost term $\mathbf{c}$ that uniquely characterizes the quality of the signal between a base station and a user. Considering that most of the resources are allocated on the link of the minimal cost c_j^{min}, defined by $c_j^{min} = \min_i c_{ij}$, the following simplified strategy is applied:

- first, we solve the resource allocation problem with the cost expressed as a vector $\mathbf{c}^{min}$ of coefficients c_j^{min},
- second, we route the allocated resources among cooperating base stations to attain the final user with the regular cost function.

In order to solve the resource allocation problem, the cost matrix is replaced by the cost vector $\mathbf{c}^{min}$. Hence, for each user, derivations are done as if every resource blocks were delivered only from the best signal quality base station. The resolution of the resource allocation problem is then only considered from the user's point of view, which is equivalent to find the measure $\boldsymbol{\nu}$ that satisfies the quadratic optimization problem independently to the measure $\boldsymbol{\mu}$.

Definition 5.9. *The simplified allocation problem is given by:*

$$\boldsymbol{\nu}^* = \underset{\boldsymbol{\nu}}{\operatorname{argmin}} \, {}^t\boldsymbol{\nu} H \boldsymbol{\nu} + {}^t\tilde{\mathbf{L}}\boldsymbol{\nu},$$

such that:

$${}^t\mathbf{1}_{1,m} \cdot \boldsymbol{\nu} = 1 \text{ and } \nu_j \geq 0,$$

with:

$$H = \mathbf{Id}_m, \text{ and } \tilde{\mathbf{L}} = \mathbf{c}^{min} - 2\boldsymbol{\nu}^f.$$

Lemma 5.2. *The utility function of the simplified optimization problem is equivalent to a hypersphere equation.*

Proof. The simplified optimization problem can be written in the following form:

$$\boldsymbol{\nu}^* = \underset{\boldsymbol{\nu}}{\operatorname{argmin}} {}^t\boldsymbol{\nu} H \boldsymbol{\nu} + {}^t\tilde{\mathbf{L}}\boldsymbol{\nu} + \frac{1}{4}{}^t\tilde{\mathbf{L}}\tilde{\mathbf{L}},$$

such that:

$${}^t\mathbf{1}_{1,m} \cdot \boldsymbol{\nu} = 1 \text{ and } \nu_j \geq 0,$$

We denote by $\mathcal{C}$, the convex hull defined by the constraints of this optimization problem. The added constant does not modify the optima and therefore this problem is equivalent to the simplified optimization problem. Furthermore, the utility function is the equation of an hypersphere of center $\boldsymbol{\nu}^0 = -\tilde{\mathbf{L}}/2$ and the objective value is its radius. □

Theorem 5.1. *The solution $\boldsymbol{\nu}^*$ of the is unique and is of the form:*

$$\boldsymbol{\nu}^* = \boldsymbol{\nu}^0 - \frac{{}^t\mathbf{u}(\boldsymbol{\nu}^0 - \mathbf{M})}{(m-k)}\mathbf{u},$$

where k is the number of zero coordinates of $\boldsymbol{\nu}^*$, $\mathbf{u} = \mathbf{1}_{m-k,1}$, $\boldsymbol{\nu}^0 = -\tilde{\mathbf{L}}/2$ and $\mathbf{M} = \mathbf{u}/(m-k)$.

Proof. Thanks to Lemma 5.2, the optimum $\boldsymbol{\nu}^*$ is given by the intersection of the minimal radius hypersphere of center $\boldsymbol{\nu}^0 = -\tilde{\mathbf{L}}/2$ and of $\mathcal{C}$. Let $\mathcal{H}$ be the hyperplane defined by:

$$\mathcal{H} = \left\{ \mathbf{x} \in \mathbb{R}^m \mid {}^t\mathbf{1}_{m,1}\mathbf{x} = 1 \right\}.$$

The convex hull $\mathcal{C}$ is included in the hyperplane $\mathcal{H}$. Let $\boldsymbol{\nu}^*$ be the orthogonal projection of $\boldsymbol{\nu}^0$ on $\mathcal{H}$. Two cases can be distinguished:

1. $\boldsymbol{\nu}^*$ has no strictly negative coordinates.
2. $\boldsymbol{\nu}^*$ has some strictly negative coordinates.

In the first case, $\boldsymbol{\nu}^*$ is the tangent point between $\mathcal{C}$ and the hypersphere. Since $\boldsymbol{\nu}^*$ is the orthogonal projection of $\boldsymbol{\nu}^0$ on $\mathcal{C}$, it also minimizes the radius of the hypersphere that intersect $\mathcal{C}$. The optimum is given by:

$$\boldsymbol{\nu}^* = \boldsymbol{\nu}^0 - \frac{{}^t\mathbf{u}(\boldsymbol{\nu}^0 - \mathbf{M})}{m}\mathbf{u},$$

where $\mathbf{M} = \mathbf{1}_{m,1}/m$ and $\mathbf{u} = \mathbf{1}_{m,1}$. If all coordinates are positive, then the optimum has been reached.
In the second case (indexing from 1 to $m-k$ the strictly positive coordinates, where k is the number of negative coordinates), the positivity constraints $m-k+1$ to m are saturated. $\boldsymbol{\nu}^*$ is in $\mathcal{H}$ but outside $\mathcal{C}$. Therefore, $\nu^*_{m-k+1} \dots \nu^*_m$ are set to zero and $\nu^*_1 \dots \nu^*_{m-k}$ have to be computed. $\mathbf{M}, \mathbf{u}$ and $\boldsymbol{\nu}^0$ are first projected on the non-null subspace:

$$\begin{aligned}
&\forall 1 \leq j \leq m-k,\ \mathrm{M}_j = 1/(m-k),\\
&\forall m-k+1 \leq j \leq m,\ \nu^0_j = 0, \mathrm{M}_j = 0, \mathrm{u}_j = 0.
\end{aligned}$$

Then the optimum is calculated in the non-null subspace:

$$\boldsymbol{\nu}^* = \boldsymbol{\nu}^0 - \frac{{}^t\mathbf{u}(\boldsymbol{\nu}^0 - \mathbf{M})}{(m-k)}\mathbf{u}.$$

In this case, the previous operations must be repeated until all coordinates are positive. Uniqueness of the solution is ensured by the fact that the optimal solution is the orthogonal projection of the center of an hypersphere. □

Once resource allocation is made and the measure $\boldsymbol{\nu}$ is fully defined, the coupling $\boldsymbol{\pi}$ is derived from the optimal transport problem:

$$\boldsymbol{\pi}^* = \underset{\boldsymbol{\pi}}{\operatorname{argmin}}\, {}^t\mathbf{c} \cdot \boldsymbol{\pi},$$

such that:

$$T_n\boldsymbol{\pi} = \boldsymbol{\mu},$$
$$T_m\boldsymbol{\pi} = \boldsymbol{\nu}^*.$$

The optimal coupling $\boldsymbol{\pi}^*$ is a solution of a linear optimization problem and provides the optimal number of resources that are transfered from each base station i to each user j.

Algorithm 3 computes the approximate Cournot-Nash equilibrium. The optimal allocation $\boldsymbol{\nu}^*$ is first computed, thanks to the constructive proof of Theorem .3, then the optimal transport $\boldsymbol{\pi}^*$ between the two discrete probability measures $\boldsymbol{\mu}$ and $\boldsymbol{\nu}^*$ is derived by linear programming. The algorithm is centralized and iterative. The while-loop converges as the dimensions of the projective space is strictly decreasing and bounded by one.

Data: $\mathbf{c}, \mathbf{c_{min}}, \boldsymbol{\nu}^f, T_m, T_n$.
Result: $\boldsymbol{\pi}^*$.
Initalize (k, $\boldsymbol{\nu}^0$, $\mathbf{M}$, $\mathbf{u}$, $\boldsymbol{\nu}^*$);
while $\exists \nu_j^* < 0$ **do**
  Project ($\boldsymbol{\nu}^0$, $\mathbf{M}$, $\mathbf{u}$, $\boldsymbol{\nu}^*$) on the space of strictly positive coordinates of $\boldsymbol{\nu}^*$;
  Let k be the number of negative coordinates of $\boldsymbol{\nu}^*$;
  Project $\boldsymbol{\nu}^*$ on the new hyperplane defined by (k, $\boldsymbol{\nu}^0$, $\mathbf{M}$, $\mathbf{u}$, $\boldsymbol{\nu}^*$);
end
$\boldsymbol{\pi}^* = \text{LinearProg}(\boldsymbol{\mu}, \boldsymbol{\nu}^*, \mathbf{c}, T_n, T_m)$;

Algorithm 3: Approximate solution algorithm

Theorem 5.2. *An approximate optimum can be found in polynomial time.*

Proof. In order to compute approximate Cournot-Nash equilibria, one must first solve the allocation problem and then the optimal transport problem. Since the allocation problem involves at most m projections, its complexity is in $\mathcal{O}(m^2)$. The optimal transport part is a linear programming optimization problem and is known to be solved in polynomial time. □

5.4.3 Case without network outage

When the network is not in outage, there are too many resource blocks to fulfill users demand. Therefore the roles of μ_i, ν_j and ν_j^f are inverted. Therefore, μ_i becomes the fraction of the resources of the network that is required by a user x_i:

$$\mu_i = \frac{N_i}{n_{tot}(\phi_u, \phi_b)}.$$

The fraction ν_i^f becomes the fraction of the resources that is available at a base station y_j:

$$\nu_j^f = \frac{1}{n}.$$

and the fraction ν_j becomes the fraction of the total network resources used at a base station y_j, such that:

$$\nu_j = \frac{n_j^u}{N_{avail}},$$

where n_j^u is the number of resource blocks used at a base station y_j.

For both cases, the fractions μ_i, ν_j and ν_j^f plays the same role: μ_i is the fraction of resource of the limiting entity, ν_j^f is the fraction of resource that must be dimensioned and ν_j is the actual fraction of resource that is allocated to this entity.

5.5 Numerical analysis

On a system level, three indicators are analyzed in function of the number of users in the network.

- The user satisfaction ratio is
$$r_u = \frac{1}{m}\sum_{j=1}^{m}\frac{n_j^a}{N_j},$$
in case of network outage. It is the mean of the ratio between the number of resource blocks allocated by the network to each user and the number of resources requested by each user. If the network is not in outage,
$$r_u = 1.$$

- The network occupancy is
$$r_n = 1.$$
when the network is in outage. If the network is not in outage,
$$r_n = \frac{1}{n}\sum_{j=1}^{n}\frac{n_j^u}{N_{avail}}.$$
It is the proportion of total available resources used in the network.

- The cooperation proportion given by

$$r_c = \frac{1}{m}\sum_{j=1}^{m} \mathbb{1}_{\left[\left[\sum_{i=1}^{n} \mathbb{1}_{[\pi_{ij}\neq 0]}\right]>1\right]},$$

  is the proportion of users that receive resource blocks from multiple base stations.

We define the optimum network working point as the intersection of user satisfaction curve and the network occupancy curve. In the next section, this point is identified for both the exact and the approximate Cournot-Nash solutions. Its relative position is investigated under several network deployment schemes.

Table 5.1: Simulation parameters

P	1 Watt
λ_b	10 antennas per km^2
λ_u	10 to 500 users per km^2
l_m	10
C	500 kb/s
W_{rb}	180 kHz
N_{avail}	100
Path-loss exponent γ	3
Shadowing	10 dB
Network radius	1.8 km

Simulation parameters are summarized in Table 5.1. Curves derived in Figures 5.1, 5.2a and 5.2b are the expectancy of each indicator in respect to the point processes of the base stations Φ_b and of the users Φ_u.

5.5.1 Exact vs. approximate Cournot-Nash solution

In Figure 5.1, r_n, r_u and r_c are plotted for the exact Cournot-Nash equilibria in function of the density ratio λ_u/λ_b in solid lines. Using Matlab `quadprog` function, an iteration for the maximum number of users takes about 3 seconds to compute on a late 2014, 8 cores CPU laptop computer. This figure was produced with 500 iterations. The optimum working point of the network is reached for a density ratio of 21 and for a user satisfaction ratio (or a network occupancy) of 89%. The cooperation proportion reaches a minimum in the neighborhood of the optimum working point, with about 10% of the users under base station cooperation. The u-shape of the cooperation curve also highlights a shift from a network with a low probability of outage to a network with a high probability of outage. From the point of view of the current framework, small network load and high network load are identical situations: there is a great imbalance between the quantity of resource blocks available to move and the quantity of resource blocks that can be moved. Therefore, the minimum cooperation proportion is reached when the active users density is between 5 to 15 times the base station density, which

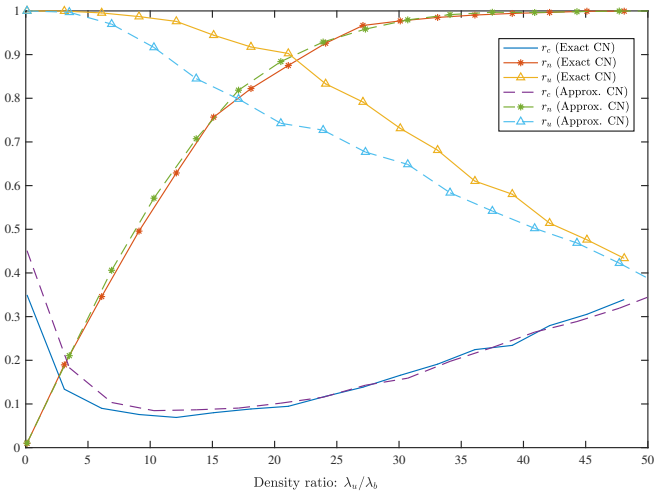

Figure 5.1: Exact Cournot-Nash vs. approximate Cournot-Nash for a 1/4-Ginibre point process.

is the area where the probability of outage is of the same magnitude of the probability of not being in outage.

A comparison between the approximate solutions and the exact solutions is also given in Figure 5.1. The optimal transport was solved with the `intlinprog` function. One iteration for a density of 500 users and 10 base stations per unit square is computed in about 350 ms. The network optimum working point is reached for a density ratio of 17 and for a user satisfaction ratio (or a network occupancy) of 80%. The approximate algorithm thus proves to be a pessimistic bound of the exact Cournot-Nash solution, that can be used for an underestimate of the network performance. It is a good trade-off between computational complexity and precision, since computation is about ten times faster than the exact algorithm whereas the error made is less than of 5% on the cooperation and the network occupancy indicators. The cooperation proportion and the network occupancy behaviors are similar to the exact curves.

5.5.2 Impact of network deployment on the optimum network working point

We consider networks composed of antennas drawn according to a β-Ginibre or Poisson point process with the same intensity λ_b.

In Figures 5.2a and 5.2b, the impact of regularity is studied. Curves for Poisson and β-Ginibre point processes are plotted for the exact and the approximate Cournot-Nash equilibria. Four β-Ginibre point processes are considered with four values of β: 0.25, 0.50, 0.75 and 1. Results are given in Table 5.2.

For both exact and approximate Cournot-Nash equilibria, the density ratio and the user satisfaction of the optimum working point jointly increase with the value of the parameter β. This can be explained by the fact that the overall *SINR* quality in the network increases with the regularity of the deployment as seen in Chapter 4.

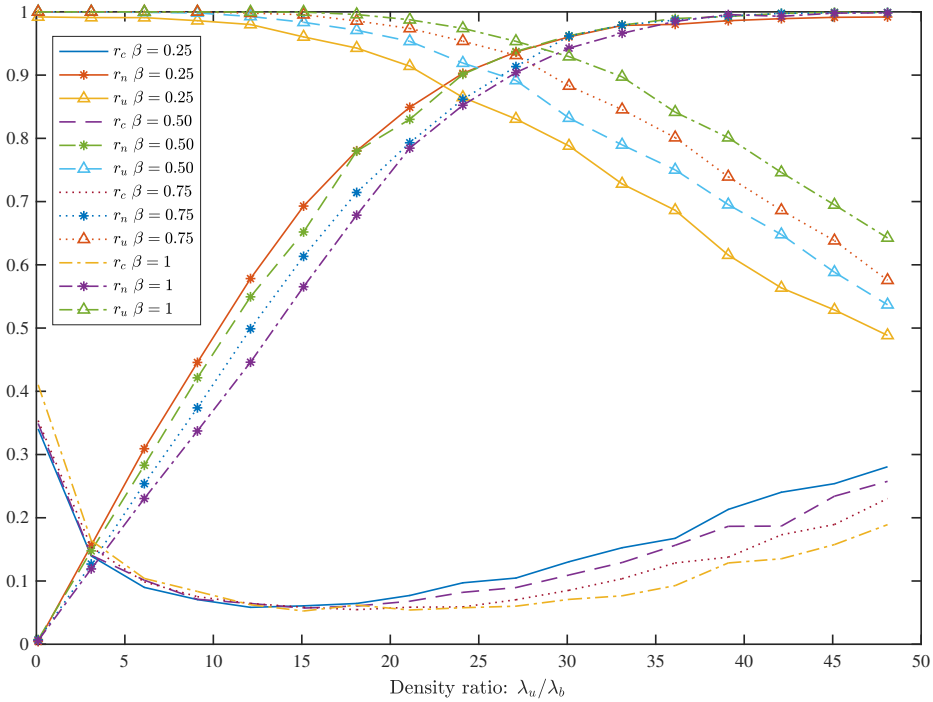

(a) Exact Cournot-Nash

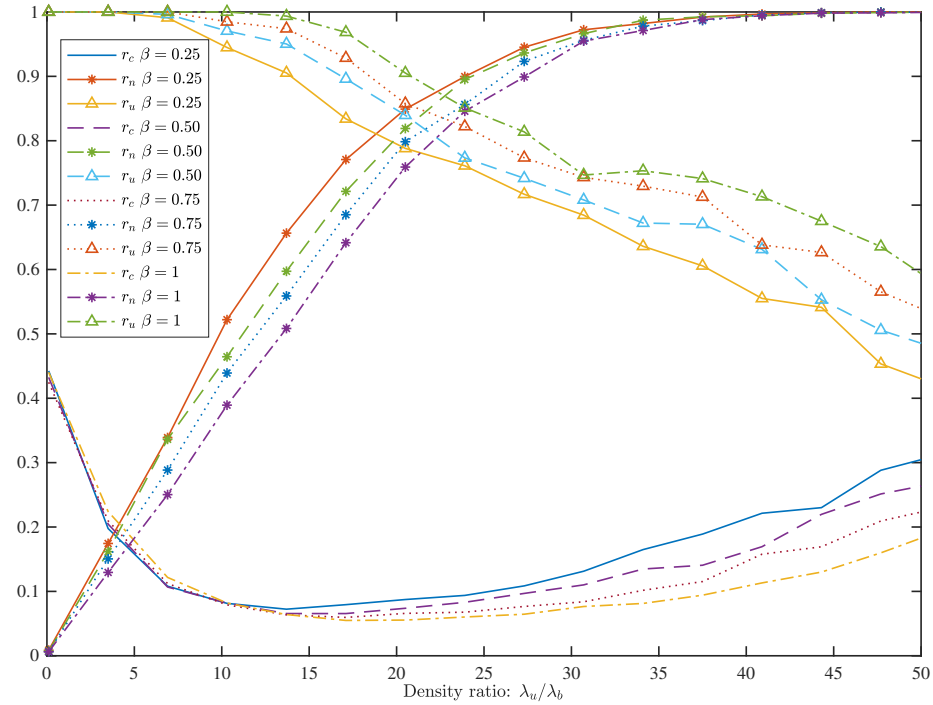

(b) Approximate Cournot-Nash

Figure 5.2: Equilibria obtained for β =0.25, 0.50, 0.75 and 1

Table 5.2: Optimum network working points in function of the repulsive factor β.

	Exact CN		Approx. CN	
Point Process	λ_u/λ_b	r_u or r_n	λ_u/λ_b	r_u or r_n
Poisson	21	88%	17	80%
$\beta = 0.25$	22.5	88%	19	82%
$\beta = 0.50$	25	90%	21	84%
$\beta = 0.75$	27.5	92%	22.5	85%
$\beta = 1$	29	94%	24	87%

5.6 Conclusion

Thanks to the concept of Cournot-Nash equilibria, a novel network performance analysis framework has been introduced. It only requires rough assumptions about the *SINR* and is capable of handling cooperation between base stations. The Cournot-Nash scheme reinterprets resource allocation and routing, as a coupling between two probability measures that characterize network traffic capabilities and traffic demand. The optimal coupling between these two probability measures provide the resource allocation and routing strategy. An exact as well as an approximate fast computable solution have been provided. Numerical analysis has shown the existence of an optimum network working point, where network occupancy and user satisfaction ratio are jointly maximized. The cooperation proportion, is minimum in the neighborhood of the optimum working point. The impact of the network deployment has been analyzed with simulated networks deployed as Poisson point processes and β-Ginibre point processes. Results are coherent with Chapter 4, with a working point reached for a higher user density and a higher network occupancy when repulsive factor β is close to one.

Chapter 6

Conclusion and future work

6.1 Conclusion

In this dissertation, we have adopted the β-Ginibre model to analyze cellular network performance. Networks of antennas are modeled as point processes, that are objects of stochastic geometry. Early stochastic models for antenna locations are based on the Poisson point process and already provides a abundant literature. Beyond the Poisson point process, the β-Ginibre point process is an interesting class of point process in order to model antenna positions. The Poisson point process is indeed unable to grasp the fact that positions of the base stations tend to exclude one another. On the contrary, the β-Ginibre introduces repulsiveness between points of a realization.

The β-Ginibre point process has been theoretically explored in Chapter 2. A novel theorem on the superposition of realizations of the β-Ginibre point process was introduced. A simulation method based to provide realizations of the β-Ginibre under the Palm measure has been proposed.

In Chapter 3, thanks to open data provided by the French frequency regulator, the suitability of the β-Ginibre point process has been successfully fitted on real data segmented under three scenarios: urban, suburban and rural areas. Each network of each operator is characterized by a couple (λ, β), with λ being the density of the network, while the parameter β characterizes the repulsiveness of the network. Clear deployment strategies emerge from such characterization. The first deployment strategy consists in deploying an efficient network all at once, with base stations regularly spread on the plane. The second deployment strategy is incremental: first, the network is regularly deployed but with just enough base stations to fulfill minimum coverage, then the number of base stations is increased around hot spots (tourist attractions, transportation nodes, etc).

Since the density of the network is a constraint imposed by traffic demand, only the repulsive factor β is controlled by the deployment strategies. Qualitatively, the mean signal quality of the network is influenced by β. Placing cells in a more regular manner, with a higher value of β, limits inter-cell interference. In order to evaluate quantitatively the effects of β on the number of simultaneous active users that a given network can handle, Chapter 5 introduces a theoretical and numerical model to evaluate the performance of an interference limited network. The metric that qualifies the performance is the outage probability. Thanks to the fact that users are modeled according to a marked Poisson point process, we are able to quantify the outage probability of a reference cell, given the density of the users. Numerical

analysis shows that there is a significant increase of performance (up to 4 times between a Poisson network and a Ginibre network) for high values of β.

In order to generalize the previous analysis to the network level and to any *SINR* distribution, we introduce a powerful analytical model that is based on Cournot-Nash equilibria. Traffic demand and offer is modeled as a discrete probability measure. We also consider that base stations are under cooperation. With the Cournot-Nash framework, two challenges are tackled simultaneously: resources must be first allocated to each user (the network decides the quantity of resources that is provided to a user provided its traffic requirement), then resources must be routed from base stations to the users. The Cournot-Nash problem is formulated as a quadratic optimization problem, whose exact solutions are complex to qualify and whose complexity is yet to characterize. However the algebraic structure of the Cournot-Nash problem enables us to separate the general quadratic optimization problem into two sub-optimization problems at the cost of an approximation. An algorithm is derived. Its polynomial complexity makes it suitable for engineering application. Numerical analysis is performed for Poisson and β-Ginibre networks. For each network, an optimal working point is highlighted, where network occupancy and user satisfaction are equal.

6.2 Future work

The β-Ginibre point processes provide many insights on network performance and deployment strategies. In that matter, we have precisely characterized the performance of the network for the downlink. Limitations of the β-Ginibre point process model is partly due to the fact that the part of the network, we wish to characterize, must have homogeneous spatial properties (such as density). On regional of country level, other point process can be studied. Furthermore, since the β-Ginibre is a determinantal point process, some of the derivations in this document (such as the simulation scheme for the β) can be generalized to particular kernels. Because the β-Ginibre point process is a repulsive one, it fails to model the users, since users mostly tends to group themselves in particular area (buildings, streets, parks). As for performance analysis, queuing theory might be introduced to characterize the link between user density and antenna density. Other parameters such as modulation, relaying are also at the reach of the Cournot-Nash framework, deepening the engineering applications of such theory.

Bibliography

[1] Eitan Altman, Konstantin Avrachenkov, and Andrey Garnaev, *Generalized α-fair resource allocation in wireless networks*, Decision and Control, 2008. CDC 2008. 47th IEEE Conference on, IEEE, 2008, pp. 2414–2419.

[2] Luca Anchora, Leonardo Badia, and Michele Zorzi, *A Framework for Scheduling and Resource Allocation in LTE Downlink Using Nash Bargaining Theory.*

[3] J.G. Andrews, F. Baccelli, and R.K. Ganti, *A Tractable Approach to Coverage and Rate in Cellular Networks*, Communications, IEEE Transactions on **59** (2011), no. 11, 3122–3134.

[4] ANFR, *Cartoradio*, 2014.

[5] ARCEP, *La qualité des services mobiles (only available in french language)*, (2014).

[6] François Baccelli and Bartlomiej Blaszczyszyn, *Stochastic Geometry and Wireless Networks, Volume I - Theory*, Foundations and Trends in Networking Vol. 3: No 3-4, pp 249-449, vol. 1, NoW Publishers, 2009.

[7] Adrian Baddeley and Rolf Turner, *Spatstat: an R package for analyzing spatial point patterns*, Journal of statistical software **12** (2005), no. 6, 1–42.

[8] Adrien Blanchet and Guillaume Carlier, *Optimal transport and Cournot-Nash equilibria*, arXiv preprint arXiv:1206.6571 (2012).

[9] ———, *From Nash to Cournot–Nash equilibria via the Monge–Kantorovich problem*, Phil. Trans. R. Soc. A **372** (2014), no. 2028, 20130398.

[10] ———, *Remarks on existence and uniqueness of Cournot-Nash equilibria in the non-potential case*, Mathematics and Financial Economics **8** (2014), no. 4, 417–433.

[11] ———, *Optimal transport and Cournot-Nash equilibria*, Mathematics of Operations Research (2015).

[12] Adrien Blanchet, Guillaume Carlier, and Luca Nenna, *Computation of Cournot-Nash equilibria by entropic regularization*, arXiv preprint arXiv:1609.02814 (2016).

[13] Bartłomiej Błaszczyszyn, Mohamed Kadhem Karray, and Holger Paul Keeler, *Using Poisson processes to model lattice cellular networks*, INFOCOM, 2013 Proceedings IEEE, IEEE, 2013, pp. 773–781.

[14] Alexei Borodin, *Determinantal point processes*, arXiv preprint arXiv:0911.1153 (2009).

[15] Alexei Borodin and Grigori Olshanski, *Harmonic analysis on the infinite-dimensional unitary group and determinantal point processes*, Annals of mathematics (2005), 1319–1422.

[16] Yann Brenier, *Décomposition polaire et réarrangement monotone des champs de vecteurs*, CR Acad. Sci. Paris Sér. I Math **305** (1987), no. 19, 805–808.

[17] Haim Brezis, *Functional analysis, Sobolev spaces and partial differential equations*, Springer Science & Business Media, 2010.

[18] Lijun Chen, Steven H Low, and John C Doyle, *Joint congestion control and media access control design for ad hoc wireless networks*, INFOCOM 2005. 24th Annual Joint Conference of the IEEE Computer and Communications Societies. Proceedings IEEE, vol. 3, IEEE, 2005, pp. 2212–2222.

[19] Luca Chiaraviglio, Francesca Cuomo, Andrea Gigli, Maurizio Maisto, Yifan Zhou, Zhifeng Zhao, and Honggang Zhang, *A reality check of base station spatial distribution in mobile networks*, Computer Communications Workshops (INFOCOM WKSHPS), 2016 IEEE Conference on, IEEE, 2016, pp. 1065–1066.

[20] Luca Chiaraviglio, Francesca Cuomo, Maurizio Maisto, Andrea Gigli, Josip Lorincz, Yifan Zhou, Zhifeng Zhao, Chen Qi, and Honggang Zhang, *What is the best spatial distribution to model base station density? a deep dive into two european mobile networks*, IEEE Access **4** (2016), 1434–1443.

[21] Jean-François Coeurjolly, Jesper Møller, and Rasmus Waagepetersen, *A tutorial on Palm distributions for spatial point processes*, (2016).

[22] R. Combes, Z. Altman, and E. Altman, *Self-Organizing Relays: Dimensioning, Self-Optimization, and Learning*, IEEE Transactions on Network and Service Management **9** (2012), no. 4, 487–500.

[23] Antoine-Augustin Cournot, *Recherches sur les principes mathématiques de la théorie des richesses par Augustin Cournot*, chez L. Hachette, 1838.

[24] Daryl J Daley and David Vere-Jones, *An introduction to the theory of point processes: volume II: general theory and structure*, Springer Science & Business Media, 2007.

[25] L Decreusefond, *Wasserstein distance on configuration space*, Potential Analysis **28** (2008), no. 3, 283–300.

[26] Laurent Decreusefond, Eduardo Ferraz, and Philippe Martins, *Upper Bound of Loss probability for the dimensioning of OFDMA systems with multi class randomly located users*, Proc. WiOpt, 2009, pp. 1–6.

[27] Laurent Decreusefond, Eduardo Ferraz, Philippe Martins, and Than-Tung Vu, *Robust methods for LTE and WiMAX dimensioning*, Performance Evaluation Methodologies and Tools (VALUETOOLS), 2012 6th International Conference on, IEEE, 2012, pp. 74–82.

[28] Laurent Decreusefond, Ian Flint, and Anais Vergne, *A note on the simulation of the Ginibre point process*, Journal of Applied Probability **52** (2015), no. 04, 1003–1012.

[29] Laurent Decreusefond, Ian Flint, Anais Vergne, et al., *A note on the simulation of the Ginibre point process*, Journal of Applied Probability **52** (2015), no. 4, 1003–1012.

[30] Laurent Decreusefond and Pascal Moyal, *Stochastic Modeling and Analysis of Telecoms Networks*, John Wiley & Sons, 2012.

[31] Laurent Decreusefond and Aurélien Vasseur, *Asymptotics of superposition of point processes*, GSI'15 (2015).

[32] Amir Dembo and Ofer Zeitouni, *Large Deviations Techniques and Applications (1998)*.

[33] Na Deng, Wuyang Zhou, and Martin Haenggi, *The Ginibre point process as a model for wireless networks with repulsion*, IEEE Transactions on Wireless Communications **14** (2015), no. 1, 107–121.

[34] Harpreet S Dhillon, Radha Krishna Ganti, François Baccelli, and Jeffrey G Andrews, *Modeling and analysis of K-tier downlink heterogeneous cellular networks*, Selected Areas in Communications, IEEE Journal on **30** (2012), no. 3, 550–560.

[35] Arnaud Doucet, *Fast computation of Wasserstein barycenters*, (2014).

[36] A. A. El-Sherif and A. Mohamed, *Joint Routing and Resource Allocation for Delay Minimization in Cognitive Radio Based Mesh Networks*, IEEE Transactions on Wireless Communications **13** (2014), no. 1, 186–197.

[37] TR ETSI, *136 942,«*, LTE; Evolved Universal Terrestrial Radio Access (E-UTRA); Radio Frequency (RF) system scenarios (3GPP TR 36.942 version 10.2. 0 Release 10) **10** (2011), 0.

[38] Zuyuan Fang and Brahim Bensaou, *Fair bandwidth sharing algorithms based on game theory frameworks for wireless ad-hoc networks*, INFOCOM 2004. Twenty-third AnnualJoint Conference of the IEEE Computer and Communications Societies, vol. 2, IEEE, 2004, pp. 1284–1295.

[39] Ian Flint, *Stochastic analysis of point processes : beyond the Poisson process*, Ph.D. thesis, Paris, Télécom ParisTech, 2013.

[40] Radha Krishna Ganti and Martin Haenggi, *Asymptotics and approximation of the SIR distribution in general cellular networks*, IEEE Transactions on Wireless Communications **15** (2016), no. 3, 2130–2143.

[41] Hans-Otto Georgii and Hyun Jae Yoo, *Conditional intensity and Gibbsianness of determinantal point processes*, Journal of Statistical Physics **118** (2005), no. 1-2, 55–84.

[42] Jean Ginibre, *Statistical ensembles of complex, quaternion, and real matrices*, Journal of Mathematical Physics **6** (1965), no. 3, 440–449.

[43] André Goldman et al., *The Palm measure and the Voronoi tessellation for the Ginibre process*, The Annals of Applied Probability **20** (2010), no. 1, 90–128.

[44] J.S. Gomez, A. Vasseur, A. Vergne, P. Martins, L. Decreusefond, and Wei Chen, *A Case Study on Regularity in Cellular Network Deployment*, Wireless Communications Letters, IEEE **4** (2015), no. 4, 421–424.

[45] Mohsen Guizani, *Game theory for wireless communications and networking*, CRC press, 2011.

[46] Anjin Guo and Martin Haenggi, *Asymptotic deployment gain: A simple approach to characterize the SINR distribution in general cellular networks*, IEEE Transactions on Communications **63** (2015), no. 3, 962–976.

[47] Martin Haenggi, *Mean interference in hard-core wireless networks*, IEEE Communications Letters **15** (2011), no. 8, 792–794.

[48] _____, *Mean interference in hard-core wireless networks*, Communications Letters, IEEE **15** (2011), no. 8, 792–794.

[49] Zhu Han, *Game theory in wireless and communication networks: theory, models, and applications*, Cambridge University Press, 2012.

[50] Zhu Han, Zhu Ji, and K. J. R. Liu, *Fair Multiuser Channel Allocation for OFDMA Networks Using Nash Bargaining Solutions and Coalitions*, IEEE Transactions on Communications **53** (2005), no. 8, 1366–1376.

[51] J Ben Hough, Manjunath Krishnapur, Yuval Peres, Bálint Virág, et al., *Determinantal processes and independence*, Probability surveys **3** (2006), no. 206-229, 9.

[52] John Ben Hough, Manjunath Krishnapur, Yuval Peres, and Bálint Virág, *Zeros of Gaussian analytic functions and determinantal point processes*, vol. 51, American Mathematical Society Providence, RI, 2009.

[53] Olav Kallenberg, *Random measures*, 3rd ed., Akademie-Verlag Berlin, 1983.

[54] Leonid Kantorovitch, *On the translocation of masses*, Management Science **5** (1958), no. 1, 1–4.

[55] Allen Knutson and Terence Tao, *The honeycomb model of GL_ {n}(C) tensor products I: Proof of the saturation conjecture*, Journal of the American Mathematical Society **12** (1999), no. 4, 1055–1090.

[56] Eric Kostlan, *On the spectra of Gaussian matrices*, Linear algebra and its applications **162** (1992), 385–388.

[57] Alex Kulesza and Ben Taskar, *Structured determinantal point processes*, Advances in neural information processing systems, 2010, pp. 1171–1179.

[58] Christian Léonard, *A saddle-point approach to the Monge-Kantorovich optimal transport problem*, ESAIM: Control, Optimisation and Calculus of Variations **17** (2011), no. 3, 682–704.

[59] Lin Li, Long Zhao, Hang Long, Xiaoyu Wang, and Kan Zheng, *Traffic-aware resource allocation schemes for HetNet based on CDSA*, IET Communications (2017).

[60] Xiaojun Lin, N. B. Shroff, and R. Srikant, *A tutorial on cross-layer optimization in wireless networks*, IEEE Journal on Selected Areas in Communications **24** (2006), no. 8, 1452–1463.

[61] Ruofei Ma, Hsiao-Hwa Chen, and Weixiao Meng, *Dynamic Spectrum Sharing for the Coexistence of Smart Utility Networks and WLANs in Smart Grid Communications*, IEEE Network **31** (2017), no. 1, 88–96.

[62] Andreu Mas-Colell, *On a theorem of Schmeidler*, Journal of Mathematical Economics **13** (1984), no. 3, 201–206.

[63] Naoto Miyoshi, Tomoyuki Shirai, et al., *A cellular network model with Ginibre configured base stations*, Advances in Applied Probability **46** (2014), no. 3, 832–845.

[64] Jesper Moller and Rasmus Plenge Waagepetersen, *Statistical inference and simulation for spatial point processes*, CRC Press, 2004.

[65] G Monge, *Mémoire sur la théorie des déblais et des remblais: Histoire de 1'AcademieRoyale des Sciences*, (1781).

[66] Clarence C Morrison, *Cournot, Bertrand, and modern game theory*, Atlantic Economic Journal **26** (1998), no. 2, 172–174.

[67] Mohammad Mozaffari, Walid Saad, Mehdi Bennis, and Mérouane Debbah, *Optimal Transport Theory for Power-Efficient Deployment of Unmanned Aerial Vehicles*, arXiv preprint arXiv:1602.01532 (2016).

[68] Itaru Nakata and Naoto Miyoshi, *Spatial stochastic models for analysis of heterogeneous cellular networks with repulsively deployed base stations*, Performance Evaluation **78** (2014), no. 0, 7 – 17.

[69] Ridha Nasri and Aymen Jaziri, *Analytical tractability of hexagonal network model with random user location*, IEEE Transactions on Wireless Communications **15** (2016), no. 5, 3768–3780.

[70] Jacques Neveu, *Processus ponctuels*, Ecole d'Eté de Probabilités de Saint-Flour VI-1976, Springer, 1977, pp. 249–445.

[71] Kangyu Ni, Xavier Bresson, Tony Chan, and Selim Esedoglu, *Local histogram based segmentation using the Wasserstein distance*, International journal of computer vision **84** (2009), no. 1, 97–111.

[72] Gabriel Peyré, Jalal Fadili, and Julien Rabin, *Wasserstein active contours*, Image Processing (ICIP), 2012 19th IEEE International Conference on, IEEE, 2012, pp. 2541–2544.

[73] Julien Rabin, Gabriel Peyré, Julie Delon, and Marc Bernot, *Wasserstein barycenter and its application to texture mixing*, International Conference on Scale Space and Variational Methods in Computer Vision, Springer, 2011, pp. 435–446.

[74] Sartaj Sahni, *Computationally related problems*, SIAM Journal on Computing **3** (1974), no. 4, 262–279.

[75] Antonello Scardicchio, Chase E Zachary, and Salvatore Torquato, *Statistical properties of determinantal point processes in high-dimensional Euclidean spaces*, Physical Review E **79** (2009), no. 4, 041108.

[76] Tomoyuki Shirai and Yoichiro Takahashi, *Random point fields associated with certain Fredholm determinants I: fermion, Poisson and boson point processes*, Journal of Functional Analysis **205** (2003), no. 2, 414 – 463.

[77] Alonso Silva, Hamidou Tembine, Eitan Altman, and Mérouane Debbah, *Optimum and equilibrium in assignment problems with congestion: mobile terminals association to base stations*, Automatic Control, IEEE Transactions on **58** (2013), no. 8, 2018–2031.

[78] Alexander Soshnikov, *Determinantal random point fields*, Russian Mathematical Surveys **55** (2000), no. 5, 923–975.

[79] Hal R Varian and Jack Repcheck, *Intermediate microeconomics: a modern approach*, vol. 6, WW Norton & Company New York, 2010.

[80] Cédric Villani, *Optimal transport: old and new*, vol. 338, Springer Science & Business Media, 2008.

[81] Micah Warren, *On solutions to Cournot–Nash equilibria equations on the sphere*, Pacific Journal of Mathematics **272** (2014), no. 2, 423–437.

[82] Yang Yan, Jianwei Huang, and Jing Wang, *Dynamic bargaining for relay-based cooperative spectrum sharing*, IEEE Journal on Selected Areas in Communications **31** (2013), no. 8, 1480–1493.

[83] C David Young, *USAP multiple access: dynamic resource allocation for mobile multihop multichannel wireless networking*, Military Communications Conference Proceedings, 1999. MILCOM 1999. IEEE, vol. 1, IEEE, 1999, pp. 271–275.

[84] Zijie Zheng, Lingyang Song, Dusit Niyato, and Zhu Han, *Resource Allocation in Wireless Powered Relay Networks: A Bargaining Game Approach*, IEEE Transactions on Vehicular Technology (2016).

[85] Yifan Zhou, Rongpeng Li, Zhifeng Zhao, Xuan Zhou, and Honggang Zhang, *On the α-Stable Distribution of Base Stations in Cellular Networks*, IEEE Communications Letters **19** (2015), no. 10, 1750–1753.

[86] Yifan Zhou, Zhifeng Zhao, Yves Louët, Qianlan Ying, Rongpeng Li, Xuan Zhou, Xianfu Chen, and Honggang Zhang, *Large-scale spatial distribution identification of base stations in cellular networks*, IEEE access **3** (2015), 2987–2999.

Appendix A: Complete list of studied sites

We provide the complete list of investigated sites and their fitting results for the β-Ginibre model. Each site is typical of the deployment environments that can be found in France.

Suburban area

Table 1: Toulouse

	LTE				UMTS			
	Orange	SFR	Bouygues	Free	Orange	SFR	Bouygues	Free
β	0.5	0.9	0.5	0.9	0.5	0.9	0.5	0.9
λ	3.11	2.09	1.48	0.71	3.11	2.19	1.48	0.71
N. ant.	61	41	29	14	61	43	29	14

Table 2: Lyon, Villeurbanne, Bron

	LTE				UMTS			
	Orange	SFR	Bouygues	Free	Orange	SFR	Bouygues	Free
β	1.0	1.0	1.0	NA	1.0	0.5	1.0	NA
λ	3.73	5.07	2.80	0.20	4.43	5.60	2.80	0.20
N. ant.	28	38	21	7	34	42	21	7

Table 3: Marseille

	LTE				UMTS			
	Orange	SFR	Bouygues	Free	Orange	SFR	Bouygues	Free
β	0.9	0.2	1.0	1.0	0.9	0.5	1.0	1.0
λ	2.93	7.70	2.49	1.32	2,93	10.9	2.93	1.32
N. ant.	20	43	17	9	20	74	20	9

For suburban area, the results for each cities are consistent with the ones presented in Chapter 3. For each of these cities, the Orange network deployment is dense and regular

(high values of λ and β). Whereas for SFR and Bouygues Telecom networks, deployment has followed a densification process that lead to a high value of λ and low value of β. As for Free, its network is still under deployment (low values of λ, high values of β). In terms of performance, the SFR network seems to provide the lowest signal quality. However, the network capacity of Free is up to 10 times less than the one of its competitors.

Rural areas

Table 4: Cantal, Haute-Loire, Lozère, Aveyron

	LTE				UMTS			
	Orange	SFR	Bouygues	Free	Orange	SFR	Bouygues	Free
β	NA	NA	NA	NA	0,62	0,81	0,59	NA
λ	7,30 10^{-4}	0	0	3,65 10^{-4}	1,02 10^{-2}	6,93 10^{-3}	7,66 10^{-3}	7,30 10^{-4}
N. ant.	2	0	0	1	28	19	21	2

Table 5: Jura, Doubs

	LTE				UMTS			
	Orange	SFR	Bouygues	Free	Orange	SFR	Bouygues	Free
β	NA	NA	NA	NA	0.6	1.0	0.7	NA
λ	0	0	0	0	7.26 10^{-3}	1.24 10^{-2}	6.22 10^{-3}	1.0 10^{-3}
N. ant.	0	0	0	0	7	12	6	1

Table 6: Drôme, Vaucluse, Alpes-de-Haute-Provence, Hautes-Alpes

	LTE				UMTS			
	Orange	SFR	Bouygues	Free	Orange	SFR	Bouygues	Free
β	NA	NA	NA	NA	0.14	1.0	1.0	0.2
λ	0	0	0	1.00 10^{-3}	3.01 10^{-3}	4.82 10^{-3}	5.22 10^{-3}	1.20 10^{-3}
N. ant.	0	0	0	5	15	24	26	6

For rural areas, the results are consistent with the one presented in Chapter 3. For each of these cities, the Orange network deployment is dense and regular (high values of λ and β). Whereas for SFR and Bouygues Telecom networks, deployment has followed a densification process that lead to a high value of λ and low value of β. As for Free, its network is still under deployment (λ faible, β élevé). In terms of performance, the SFR network seems to provide the lowest signal quality. However, for the 4G networks, coverage is still under deployment.

GPS coordinates of each region considered

Paris Coordinates of the polygonal window over Paris

- (2.33660, 48.88713)
- (2.29073, 48.87095)
- (2.27589, 48.85566)
- (2.29163, 48.84442)
- (2.33660, 48.83318)
- (2.35458, 48.83318)
- (2.39056, 48.84442)
- (2.39056, 48.87095)

Toulouse Coordinates of the diagonal of the rectangular window:

- (1.42282, 43.58188)
- (1.46689, 43.61786)

Lyon, Villeurbanne, Bron Coordinates of the diagonal of the rectangular window:

- (4.84562, 45.74854)
- (4.86810, 45.77552)

Marseille Coordinates of the diagonal of the rectangular window:

- (5.37338, 43.27919)
- (5.39791, 43.30168)

Bordeaux Coordinates of the diagonal of the rectangular window:

- (-0.60801; 44.81227)
- (-0.55405; 44.86173)

Vosges, Haute-Saône, Haute-Marne Coordinates of the diagonal of the rectangular window:

- (5.51532; 47.78211)
- (6.36968; 48.23177)

Cantal, Haute-Loire, Lozère, Aveyron Coordinates of the diagonal of the rectangular window:

- (2.70704, 44.7220)
- (3.415533, 45.03503)

Jura et Doubs Coordinates of the diagonal of the rectangular window:

- (5.63864, 46.42444)
- (5.86347, 46.77131)

Drôme, Vaucluse, Alpes-de-Haute-Provence, Hautes-Alpes Coordinates of the diagonal of the rectangular window:

- (5.22847, 43.95498)
- (5.91796, 44.53954)

Appendix B

.1 Introduction

Avec l'explosion des solutions nomades autour de l'Internet des objets, les systèmes et réseaux sans-fils se doivent de supporter le développement exponentiel d'un éco-système numérique. En particulier, le développement des services intelligents de supervision et d'optimisation des infrastructures doivent allier à la fois fiabilité et faible consommation pour des débits faibles. Ceci est en particulier critique pour les réseaux électriques et de distribution d'eau qui s'appuient sur les données de milliers de capteurs pour détecter les avaries, mais aussi la supervision et l'anticipation des besoins des utilisateurs finaux. Les récents développement des réseaux LTE notamment le NB-IoT et le LTE-M apportent une réponse à ces nouveaux usages. Les réseaux mobiles de cinquième génération (5G), intégreront ces solutions.

Les communications machine à machine génèrent ainsi un volume de données important et en croissance. Cependant le haut débit mobile à disposition des utilisateurs a permis à l'Internet de revêtir un caractère immanent en proposant des services toujours plus personnalisés et immédiats. Ceux-ci nécessitent une infrastructure permettant une connexion avec une très faible latence, et avec des débits toujours plus importants. Ces limites inhérentes au traitement du trafic par une série de machines physiques sont en passe d'être levées grâce aux technologies de virtualisations. En effet, il est possible de réduire un cœur de réseau dans un serveur classique. Du point de vue de la gestion du medium, la radio logicielle délocalise le traitement du signal réalisé par un équipement spécifique déployé sur site vers un centre de données. Ces techniques sont au centre du Cloud-RAN ainsi que du Massive MIMO, véritables révolutions quant à gestion et à l'optimisation du lien radio.

Ainsi, l'évaluation et l'optimisation des performances radio de tels systèmes, véritable colonne vertébrale du monde des objets connectés, revêtent un caractère crucial. En effet, l'évaluation des performances des réseaux et plus spécifiquement des réseaux radio-mobiles est en général vu sous l'angle de la capacité du canal. Grâce à la géométrie stochastique, l'influence du facteur spatial, c'est à dire l'influence de la position des interféreurs, est prise en compte. Dans cette thèse, nous utiliserons le processus ponctuel β-Ginibre pour modéliser la position des stations de base dans le plan. Le β-Ginibre est un processus ponctuel répulsif, dont la répulsion est contrôlée par le coefficient β. Lorsque β tend vers 0, le processus ponctuel converge en loi vers un processus ponctuel de Poisson. Si β est égal à 1, alors c'est un processus ponctuel de Ginibre. L'analyse numérique des données réelles collectées en France montrent que la position des stations de base peut être modélisée par un processus de β-Ginibre. De plus, il est prouvé que la superposition de processus ponctuels de β-Ginibre tend vers un processus de Poisson, comme il est observé sur les données réelles. Une interprétation qualitative de la qualité du déploiement du réseau peut aussi être déduite de cette analyse.

Le paramètre β, représentant la stratégie de déploiement d'un opérateur, est aussi un

indicateur de la qualité globale du signal : plus le déploiement est régulier, meilleure sera la qualité du signal. Le gain de performance induit par un β plus proche de 1 est quantifié dans le cadre d'un réseau mobile uniquement limité par les interférences et l'affaiblissement.

Afin de généraliser l'évaluation des performances réseau, nous proposons une nouvelle méthode d'allocation et de dimensionnement des ressources dans les réseaux 4G, basée sur les équilibres de Cournot-Nash. Pour cette méthode, seule la qualité du signal entre les équipements communicants est nécessaire pour déterminer la stratégie d'allocation des ressources. La fourniture des ressources ainsi que les besoins en trafic sont modélisés par des mesures de probabilité. C'est le couplage entre ces deux mesures qui permet de déduire une stratégie d'allocation de ressources optimale, par minimisation d'une fonction de coût quadratique. L'analyse numérique révèle qu'il existe un point de fonctionnement optimal, où la satisfaction des utilisateurs est égale à la part d'occupation du réseau.

Dans un premier temps, nous présenterons les processus ponctuels et notamment du β-Ginibre d'un point de vue mathématique. Dans un second temps, nous appliquerons ces principes à la caractérisation du déploiement des réseaux mobiles des différents opérateurs grâce au couple (β, λ). Dans une troisième partie nous quantifierons l'effet du paramètre β sur les performance des réseaux mobile. Enfin dans la dernière partie, nous proposerons un nouvel algorithme d'allocation de ressource basé sur les équilibre de Counot-Nash, et montrerons qu'il existe un point de fonctionnement optimal pour un réseau mobile.

.2 Processus ponctuels

Trois processus ponctuels sont présentés: le processus ponctuel de Poisson homogène, le Ginibre et le β-Ginibre.

.2.1 Processus ponctuel de Poisson homogène

Le processus ponctuel de Poisson a été le premier processus ponctuel utilisé pour étudier la répartition des stations de base. Ses propriétés mathématiques relativement simples lui ont permis d'être plébiscité dans la communauté. Les premiers travaux sur le processus ponctuel de Poisson ont été réalisés par François Baccelli et al. [6]. Considérons l'espace euclidien $\mathbb{R}^2$. Soit λ un réel strictement positif, c'est l'intensité du processus de Poisson (on peut comprendre cette valeur physiquement comme la densité moyenne du nombre de points par unité de surface) et soit Φ une réalisation du processus de Poisson d'intensité λ. Pour tout compact A de $\mathbb{R}^2$, on note par $\Phi(A)$ le nombre de points dans ce compact et par $|A|$, l'aire de ce compact.

Définition .1 (Processus ponctuel de Poisson)**.** *Soit n, un entier naturel.*

$$\forall A \,\text{compact} \in \mathbb{R}^2,\ \mathbb{P}\left(\Phi(A) = n\right) = \frac{(\lambda|A|)^n}{n!} e^{-\lambda|A|}.$$

Le processus de Poisson est défini par la probabilité du nombre de points dans un compact donné. De plus, cette variable aléatoire suit une loi de Poisson de paramètre $\lambda|A|$.
Quelques propriétés du processus de Poisson homogène:

Proposition .1.

- *pour tout compact A, l'espérance de $\Phi(A)$ est telle que $\mathbb{E}\left[\Phi(A)\right] = \lambda|A|$;*

- *une superposition de plusieurs processus de Poisson est un processus de Poisson dont l'intensité est la somme des intensités des processus sous-jacents;*

- *un processus de Poisson homogène est isotrope et stationnaire;*

- *le processus résultant d'un amincissement ou d'une homothétie d'un processus de Poisson, est un processus de Poisson;*

- *soit deux compacts disjoints, alors le nombre de points dans chacun des deux compacts est indépendant.*

Une réalisation d'un processus de Poisson de paramètre λ se construit simplement dans un compact A: on tire un entier n selon une loi de Poisson de paramètre $\lambda|A|$. On tire n points successivement et indépendamment dans le compact A selon une loi uniforme. La Figure 1

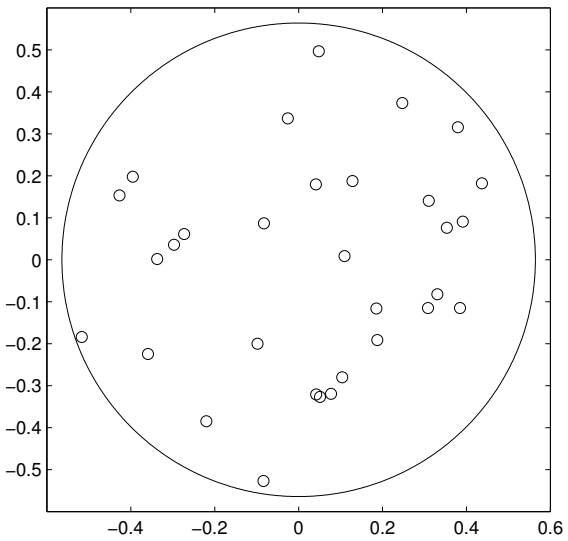

Figure 1: Réalisation d'un processus ponctuel de Poisson d'intensité $\lambda = 30$ dans une boule de surface unité.

nous donne un exemple d'une réalisation d'un processus ponctuel de Poisson. Ce processus sera dit *uniforme*, c'est à dire que la position de chaque point est indépendante des points qui l'entoure. Ainsi, il peut se former des zones où les points peuvent s'amasser. Ce phénomène est assez visible dans la Figure 1 et nuit à la bonne modélisation d'un réseau d'antennes. La distance moyenne (égale à $0.5\lambda^{-0.5}$) entre les antennes étant plus faible qu'en réalité, les interférences sont plus importantes dans un réseau poissonien que dans un réseau réel [3].

Pour inclure le fait qu'il existe une zone d'exclusion à l'échelle locale entre les stations de base, nous discuterons des propriétés des processus de Ginibre et de β-Ginibre dans les paragraphes suivants.

.2.2 Le processus ponctuel de Ginibre

Le processus de Ginibre fait partie des processus determinantaux, étudiés par Shirai et al. [76] dans le contexte de la mécanique quantique pour modéliser la répartition des particules chargées dans un plan. Le Ginibre est le cas particulier où ces particules ont toutes une charge égale de même signe et se repoussent les unes les autres. Soit Φ, une réalisation d'un processus déterminantal dans $\mathbb{C}$. Alors, un processus déterminantal se définit comme suit:

Définition .2 (Processus déterminantal)**.** *Les densités jointes d'un processus déterminantal sont telles que, pour tous les k-plets* $(x_1, x_2, ..., x_k) \in \mathbb{C}^k$ *deux à deux distincts,*

$$\rho^{(k)}(x_1, \ldots, x_k) = \det\left(K(x_i, x_j), 1 \leq i, j \leq k\right),$$

où K est un noyau (nous ne rentrerons pas ici dans les propriétés d'un tel objet mathématique).

Il est aisé de constater que si deux points x_i et x_j différents sont proches l'un de l'autre, les densités jointes tendront vers zéro à cause du déterminant. Par conséquent, les amas de points ne peuvent exister qu'avec une faible probabilité. Ceci donne le caractère répulsif de tels processus ponctuels.

Définition .3 (Ginibre)**.** *Un processus de Ginibre d'intensité* λ *est un processus déterminantal dont le noyau est de la forme, pour tout* $(x, y) \in \mathbb{C}$

$$K(x, y) = \lambda e^{-\frac{\lambda\pi}{2}\left(|x|^2+|y|^2\right)+2x\bar{y}}.$$

Le lecteur pourra se référer aux travaux d'André Goldman et al. [43] pour une description plus détaillée du Ginibre, ainsi qu'aux travaux de Laurent Decreusefond et al. [29] pour simuler un Ginibre. Comme les amas de points ne peuvent exister qu'avec faible probabilité

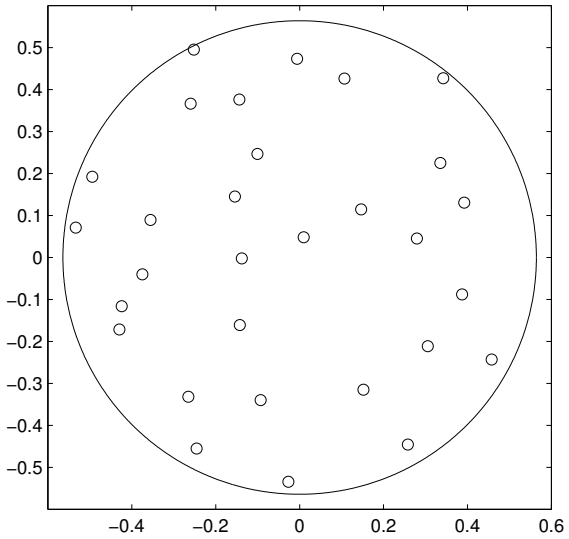

Figure 2: Réalisation d'un processus ponctuel de Ginibre d'intensité $\lambda = 30$, dans une boule de surface unité.

(cf. Figure 2), la répartition des points d'une réalisation d'un Ginibre sera dite *régulière* (à opposer à *uniforme*, voir sous-section précédente). Cependant, le Ginibre est un processus trop régulier pour modéliser la réalité. Le β-Ginibre que nous détaillons dans la prochaine partie est un intermédiaire entre l'uniformité du Poisson et la régularité du Ginibre.

.2.3 Le processus ponctuel de β-Ginibre

Le β-Ginibre est, comme le Ginibre, un processus déterminantal. β est un paramètre réel tel que: $0 < \beta \leq 1$.

Définition .4 (β-Ginibre)**.** *Le noyau $K_{\beta,\lambda}$ d'un β-Ginibre est de la forme*

$$K_{\beta,\lambda}(x,y) = \lambda e^{-\frac{\lambda\pi}{2\beta}(|x|^2+|y|^2-2x\overline{y})}.$$

Outre cette définition théorique, une réalisation d'un β-Ginibre d'intensité λ peut se simuler de la manière suivante:

- à partir d'une réalisation d'un Ginibre d'intensité λ, on réalise un amincissement selon cette règle: chaque point est gardé avec une probabilité β, et ce de manière indépendante pour chaque point;
- une homothétie de paramètre $\sqrt{\beta}$ est appliquée à la réalisation obtenue (ce qui a pour effet de conserver l'intensité).

A partir de cette description, il est aisé de constater que si:

- $\beta = 1$ alors on a un Ginibre;
- β tend vers zero, alors on obtient un processus de Poisson.

La Figure 3 nous permet de voir que β permet de paramétrer la régularité de la réalisation d'un processus. Plus β est grand, plus le processus est régulier, plus β est petit, plus le processus est uniforme.

.2.4 Superposition de processus de β-Ginibre indépendants

Comme mentionné dans la proposition , la superposition de processus ponctuels de Poisson est un processus de Poisson. Le théorème ci-dessous nous donne un résultat de convergence en loi pour la superposition de processus de β-Ginibre indépendants :

Théorème .1 (Théorème de convergence des superpositions des réalisations des β-Ginibre [44])**.** *Pour tout $n \in \mathbb{N}^*$, soit Φ_n la superposition de n $\beta_{n,i}$-Ginibre indépendants $\{\Phi_{n,i}\}$ d'intensités $\lambda_{n,i} = \lambda_i/n$ et avec $\beta_{n,i} \in]0,1]$, pour tout $1 \leq i \leq n$. Supposons de plus que :*

(i) la suite $(\lambda_i)_{i\in\mathbb{N}^*} \subset \mathbb{R}_+^*$ est bornée et

(ii) $\lim_{n\to+\infty} \frac{1}{n}\sum_{i=1}^{n} \lambda_i = \lambda$.

Alors $(\Phi_n)_{n\in\mathbb{N}^*}$ converge en loi vers un processus de Poisson Φ d'intensité λ.

Nous présentons par la suite une méthode qui nous permet d'adapter le modèle du β-Ginibre à la réalité. C'est à dire une méthode de régression des paramètres λ et β. Selon les valeurs de λ et de β, il est possible de déduire des informations qualitatives sur le déploiement des réseaux des différents opérateurs.

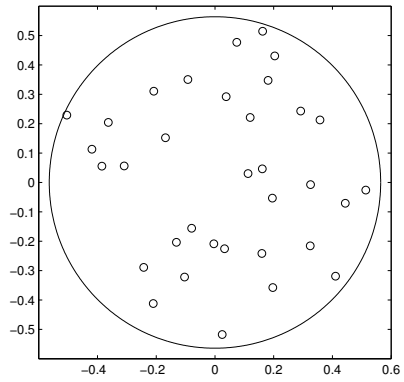

(a) 1/4-Ginibre

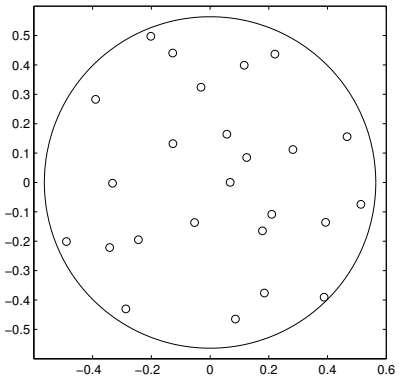

(b) 1/2-Ginibre

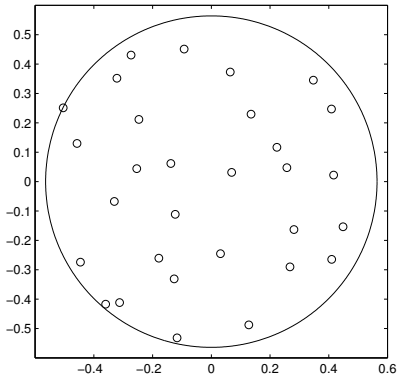

(c) 3/4-Ginibre

Figure 3: Exemples de réalisation de β-Ginibre d'intensité $\lambda = 30$ dans une boule de surface unité.

.3 Caractérisation des réseaux réels

.3.1 La fonction J

Afin d'analyser les propriétés statistiques du processus ponctuel formé par le déploiement d'un réseau mobile, nous utilisons la fonction J qui nous donne des informations quantitatives pour déterminer la valeur de β par régression, mais aussi qualitatives quant à la stratégie de déploiement des opérateurs. La fonction J est fonction de la distance inter-points $r > 0$ et caractérise le caractère répulsif ou attractif d'une réalisation d'un processus ponctuel. Nous en donnons ici les expressions analytiques pour les processus de Poisson, de Ginibre et de β-Ginibre. Le lecteur pourra se référer à l'ouvrage de Møller and al. [64] pour plus de détails théoriques sur cette statistique, ainsi qu'à l'article d'Haenggi et al. [33] pour l'obtention des expressions analytiques de J. On retient cependant quelques propriétés importantes:

Proposition .2.

- *Si pour une réalisation d'un processus ponctuel, il existe un intervalle de $\mathbb{R}_+^*$ tel que pour*

tout r appartenant à cet intervalle $J(r) > 1$, alors ce processus ponctuel est répulsif sur cet intervalle.

- *Si pour une réalisation d'un processus ponctuel, il existe un intervalle de $\mathbb{R}_+^*$ tel que pour tout r appartenant à cet intervalle $J(r) < 1$, alors ce processus ponctuel est attractif sur cet intervalle.*

Proposition .3 (Fonction J pour un processus ponctuel de Poisson)**.**

$$\forall r \in \mathbb{R}_+^* \;\; J(r) = 1.$$

Proposition .4 (Fonction J pour un processus de β-Ginibre)**.**

$$\forall r \in \mathbb{R}_+^* \;\; J(r) = \frac{1}{1 - \beta + \beta e^{-\frac{c}{\beta} r^2}}.$$

Nous remarquons que les définitions des fonctions J est cohérente avec le caractère répulsif du Ginibre et du β-Ginibre.

.3.2 Application à la ville de Paris

Méthode

A partir d'un échantillon données brutes, nous avons été en mesure d'estimer l'intensité ainsi que la fonction J de la réalisation du processus ponctuel sous-jacent, puis nous avons par régression déduit le paramètre β. Cette étude a été réalisée grâce à la librairie `spatstat` du langage `R` [7]. Nous prenons ici le déploiement des antennes SFR 3G dans la bande des 900 MHz. Dans un premier temps, nous sélectionnons une fenêtre correspondant à environ 60% de la surface de la commune de Paris. Ici, nous avons choisi un polygone qui épouse les limites de la commune, illustré en Figure 4. Pour plus de commodité, nous prenons par la suite des fenêtres rectangulaires. Le fenêtrage nous permet de réduire les effets de bord. L'intensité du processus sous-jacent est estimée de manière empirique. Puis le paramètre β est estimé par régression comme l'illustre la Figure 5. Dans notre cas, nous obtenons $\lambda = 1.91$ (antennes par kilomètre carré) et $\beta = 0.97$.

Interprétation des résultats

Les valeurs de β et λ nous donnent des informations sur les stratégies du déploiement du réseau. Voici les cas de figure pouvant se présenter:

- λ faible et β élevé signifient que le réseau est dans une première phase de développement. En effet, les opérateurs doivent dans un premier temps respecter les engagements de couverture du territoire et/ou de la population pris devant l'ARCEP. Ils disposent ainsi un nombre raisonnable d'antennes dans l'espace de la manière la plus régulière possible;

- λ élevé et β faible signifie que le réseau a été densifié à postériori. En effet, pour répondre aux impératifs de capacité de certains lieux de passage ou de forte densité de populations, les opérateurs ont été contraints de déployer de nouvelles antennes. Cette nouvelle répartition augmente la densité d'antennes par unité de surface, mais réduit la régularité du maillage initial.

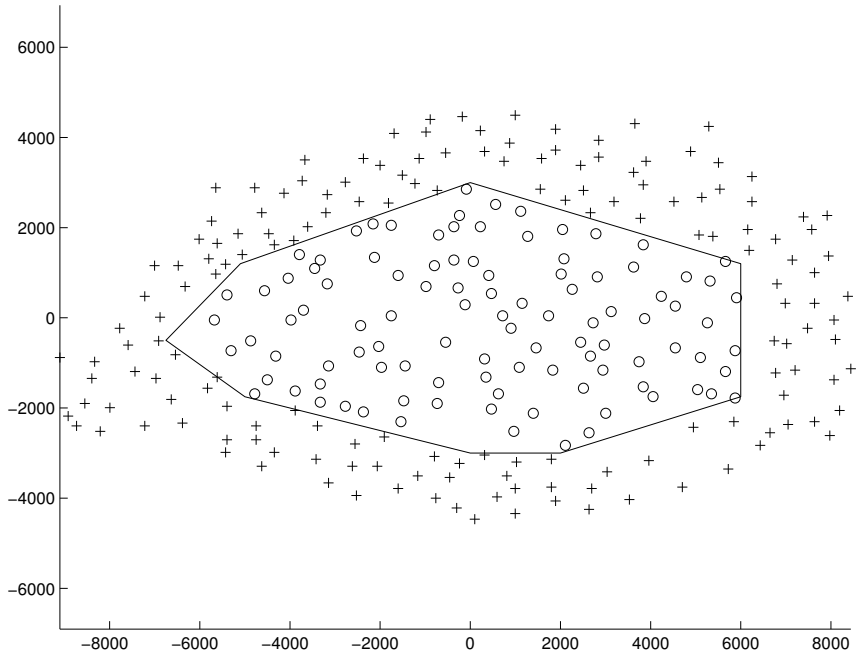

Figure 4: Exemple de sélection de fenêtre sur un déploiement d'un réseau 3G à Paris (SFR UMTS 900 MHz)

- λ et β élevés signifient que le réseau n'a pas été déployé par incréments et a été conçu dès le départ pour satisfaire à la fois des besoins en couverture du territoire mais aussi en capacité.

.3.3 Étude comparative des réseaux 3G

Nous étudions ici la répartition des antennes 3G sur le territoire dans trois cas pratiques: une zone urbaine très dense (Paris), une zone urbaine de province et une zone rurale, vide de population. Ces trois zones sont homogènes en termes de densité de population et sont caractéristiques du territoire Français. Le modèle mathématique précédent permet de nous donner une interprétation qualitative quant à la stratégie de déploiement appliquée par chaque opérateur. On comprend aisément qu'il existe une relation intrinsèque entre le déploiement des antennes 3G et la géographie du lieu considéré. Ainsi nous présentons ici trois scénarii type.

Zone urbaine dense: Paris

Paris est une zone urbaine unique en France. Centre culturel, économique et politique de la France, Paris est une ville qui s'est développée en grande partie avant la Seconde Guerre Mondiale. Ceci explique sa densité (plus de 21000 hab.km^{-2} sur 105 km^2 relativement uniforme sur toute sa surface. Le tissu urbain est en grande partie hérité du baron Haussman (grandes artères structurées en étoile formant des percées dans un réseau de rues plus étroites et anciennes). Des parcs (Luxembourg, Buttes de Chaumont, Tuileries...), mais aussi la Seine

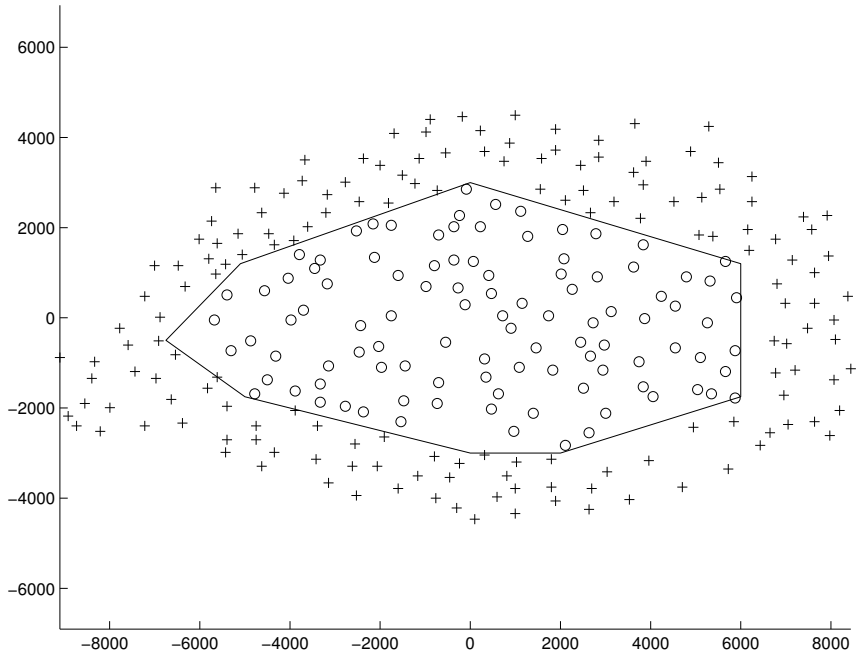

Figure 5: Exemple de régression d'une fonction J pour le réseau SFR UMTS 900MHz.

	LTE				UMTS			
	Orange	SFR	Bouygues	Free	Orange	SFR	Bouygues	Free
β	0.9	0.6	0.8	1.0	1	0.6	0.8	1.0
λ	4.23	4.17	5.44	1.60	4.99	5.27	6.19	1.60
N. ant.	149	147	189	56	174	185	216	56

Table 7: Paris

viennent aérer la ville. Enfin, Paris concentre des lieux de rassemblement (La Gare du Nord et la Gare Saint-Lazare sont respectivement les première et seconde gares d'Europe en termes de flux de voyageurs) et d'intérêts (lieux touristiques, grands magasins).
Ainsi, la densité d'antennes à Paris est aussi très élevée (environ 3.5 antennes par km^2 par opérateur). La répartition suit les grands boulevards et la Seine. Le nombre d'antennes est d'autant plus important dans un quartier donné que le flux ou la densité de population à cet endroit est élevé. Les trois opérateurs ont toutefois adapté des stratégies différentes quant au développement de leur réseau. Pour Orange, SFR et Bouygues Télécom, les sites utilisés pour la 3G sont pour la plupart déjà utilisés pour la 2G. Leur planification hérite de la stratégie de déploiement des antennes 2G.
Orange en tant qu'ancien opérateur historique (ce qui implique moyens humains et financiers conséquents) a lors de son déploiement 2G opté pour un réseau dense et régulièrement réparti sur la municipalité. Le déploiement de la 3G et de la 4G hérite de ces caractéristiques (Coefficient β élevé et un λ élevé). En ce qui concerne SFR et Bouygues, il semble que ces deux opérateurs aient déployé leur réseau plus progressivement qu'Orange. En effet, la valeur de β,

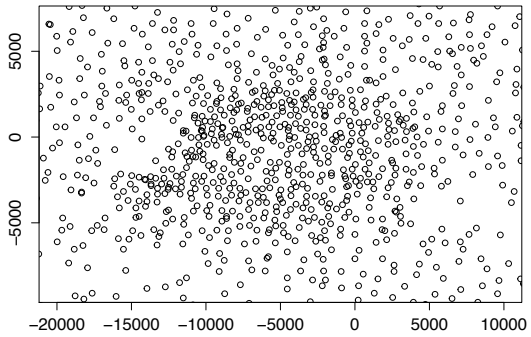

(a) Orange 3G

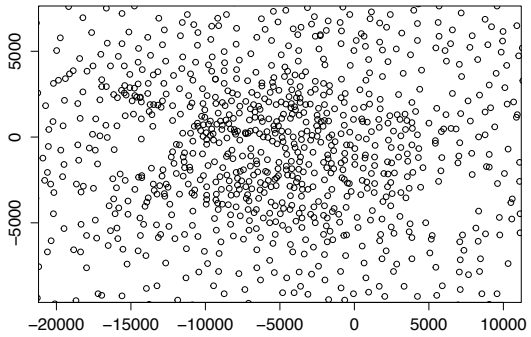

(b) SFR 3G

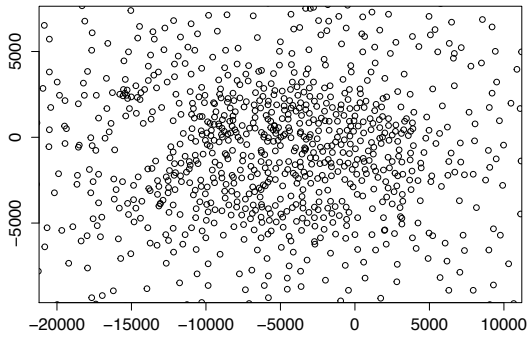

(c) Bouygues Télécom 3G

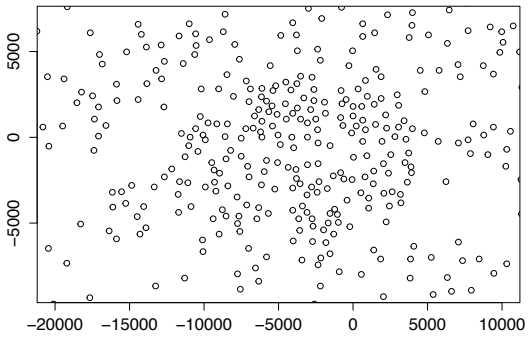

(d) Free 3G

Figure 6: Déploiement des réseaux 3G en Île-de-France

presque deux fois inférieure à celle d'Orange associée à une valeur plus élevée de λ suggère que le réseau a été déployé par incréments. Dans un premier temps, les objectifs de couverture ont primé (stratégie initiale de couverture), puis densification au niveau des *hot-spots* (stratégie de capacité). Free semble pour l'heure être dans la première phase de développement, avec un total de seulement 56 antennes (entre 3 et 4 fois moins que ses concurrents) réparties uniformément sur le territoire de la commune (β élevé). On remarquera que toutes les antennes de Free offrent les services 3G et 4G. Free cumule ici un retard à la fois en 3G et 4G puisque les réseaux de ses concurrents sont déjà arrivés à maturité à Paris dans ces deux technologies.

Zone urbaine de province

Contrairement à Paris, les zones urbaines de province (préfectures, sous-préfectures) sont des bassins de population dont la plupart se sont développés après la Seconde Guerre Mondiale. Les centre-villes sont en général densément peuplés. Ils sont constitués de rues étroites autour d'une église ou d'un beffroi. Le développement ultérieur de ces villes s'est fait par des zones pavillonnaires ou des barres d'immeubles qui restent moins denses et moins attractives que les centres eux-mêmes (les centres-villes sont des lieux de passages privilégiés) et dont le tissu

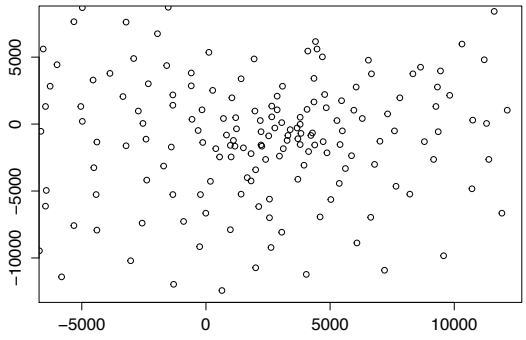

(a) Orange 3G

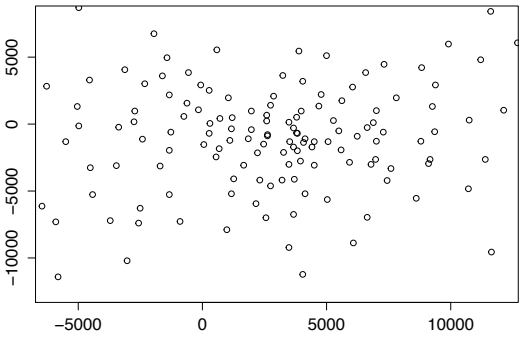

(b) SFR 3G

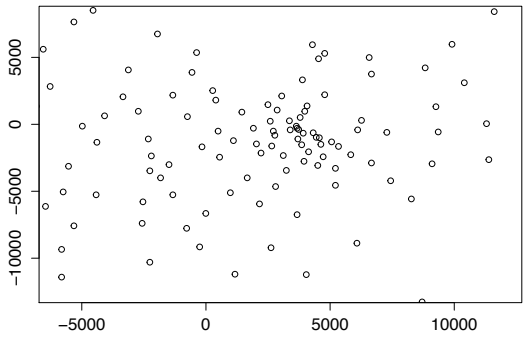

(c) Bouygues Télécom 3G

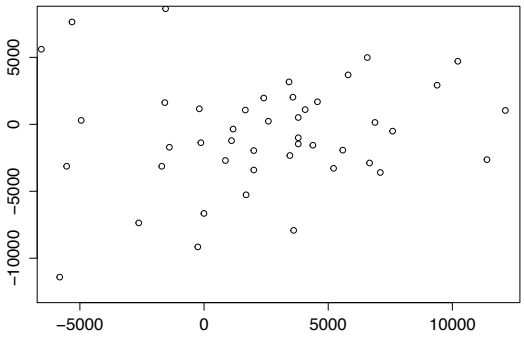

(d) Free 3G

Figure 7: Exemple de déploiement d'un réseau en zone urbaine de province. Ici est représenté la région bordelaise

	LTE				UMTS			
	Orange	SFR	Bouygues	Free	Orange	SFR	Bouygues	Free
β	1.0	1.0	0.4	0.8	0.7	0.8	0.4	0.8
λ	2.16	1.67	1.76	0.73	2.44	2.02	1.76	0.77
N. ant.	48	37	39	16	54	45	39	17

Table 8: Bordeaux

urbain a été dilaté car pensé pour la voiture. Chacun comprend alors que la répartition des antennes témoigne de cette réalité historique. Les antennes sont généralement réparties avec une très forte densité au centre des villes puis de manière plus diffuse dans les banlieues. Nous remarquons aussi que la répartition des antennes suit les axes de communications principaux. Afin de pouvoir comparer ces différents lieux nous avons choisi des zones de densités relativement homogènes, c'est-à-dire les centres-villes.
Free comme à Paris, est toujours dans une stratégie de couverture avec un nombre d'antenne

entre 2 et 4 fois inférieur à ses concurrents.

Zone rurale

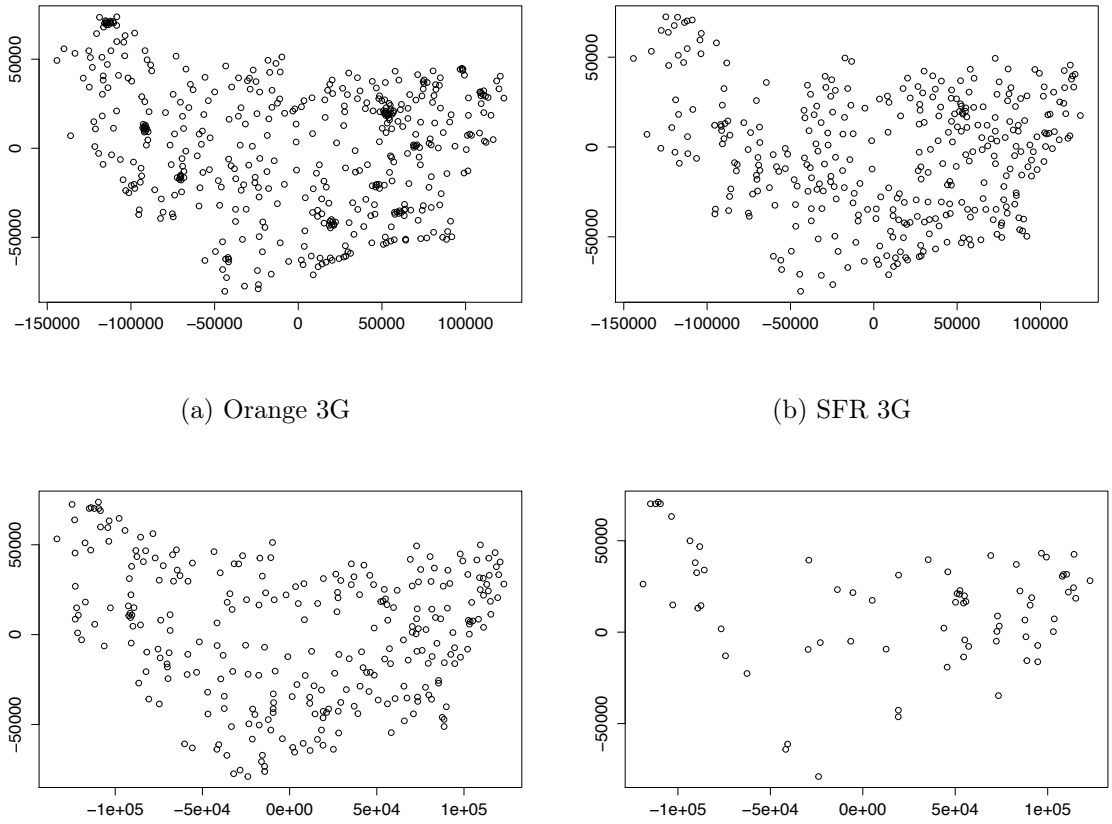

(a) Orange 3G

(b) SFR 3G

(c) Bouygues Télécom 3G

(d) Free 3G

Figure 8: Exemple de déploiement d'un réseau en zone rurale. Ici sont représentés les départements de la Haute-Saône, la Haute-Marne et des Vosges.

	LTE				UMTS			
	Orange	SFR	Bouygues	Free	Orange	SFR	Bouygues	Free
β	NA	NA	NA	NA	1.0	0.4	0.7	1.0
λ (10^{-3} ant/km^2)	0.63	0	1.56	1.56	16.7	16.7	10.7	2.50
N. ant.	2	0	5	6	53	57	34	8

Table 9: Vosges, Haute-Saône, Haute-Marne

Du point de vue régional ou départemental, l'espace est organisé autour de points attractifs (préfecture ou sous-préfecture), des routes et des vallées. Ainsi la densité d'antennes est plus forte à proximité des villes et des axes majeurs (autoroutes, nationales) Nous avons ici

étudié des zones *vides*, extrêmement peu denses avec des cellules dont le rayon peut atteindre une dizaine de kilomètres.
Pour tous les opérateurs, la couverture 4G est quasi-inexistante hors agglomération. La couverture 3G est au contraire mature pour Orange, SFR et Bouygues. Les conclusions précédentes sont aussi confirmées ici. Free se distingue par sa couverture 3G et 4G faible ou inexistante.

D'un point de vue national, le réseau 4G de tous les opérateurs n'est déployé de manière mature que dans les zones de densité urbaines fortes. Ainsi les quatre opérateurs sont dans une logique de couverture de population. Cette conclusion est aussi vraie pour le réseau 3G de Free. De plus, ce dernier opérateur n'est encore que dans la première phase du développement de son réseau 3G, car même dans les bassins de population, le nombre d'antennes déployés reste modeste comparé à ses concurrents.

Superposition des réseaux

D'un point de vue de l'utilisateur, un téléphone peut être attaché à n'importe quelle station de base, pourvue qu'elle appartienne à un réseau autorisé par son opérateur. Le tableau 10 nous présente les couples (β, λ) pour l'agrégat de toutes les antennes de chaque opérateur, ainsi que pour l'agrégat de toutes les stations de base. Ce dernier illustre le résultat du théorème .1 sur la superposition de réalisation indépendantes de β-Ginibre. Il est à noter qu'au sein du réseau de chaque opérateur, les sites 2G à 4G sont largement mutualisés. On observe aussi qu'environ 20% des sites sont aussi partagés par plusieurs opérateurs. Cette constatation est une conséquence directe de la rareté des emplacements géographiques et les barrières réglementaires à l'installation de nouveaux sites.

Table 10: Valeurs du couple (β, λ) par opérateur et de la superposition de tous les réseaux. L'intensité λ est exprimée en antennes par km^{-2}.

	Orange	SFR	Bouygues	Free	**Superposition**
β	0.9	0.7	0.8	0.9	**0.2**
λ	3.48	3.70	4.23	1.05	**10.28**
Nombre de sites	185	197	225	56	**547**

.3.4 Conclusion

La pertinence du modèle de β-Ginibre nous a permis d'étudier trois environnements : une zone urbaine dense, une zones suburbaine et une zone rurale. Chaque environnement a pu être caractérisé par le couple (β, λ). L'intensité λ donne la densité spatiale des antennes et est intrinsèquement liée au trafic utilisateur sous-jacent et le paramètre β qualifie l'*uniformité* ou la *régularité* d'un déploiement.

De l'observation des valeurs des couples (λ, β), deux stratégies de déploiement émergent.

- La première consiste en un déploiement permettant de satisfaire à la fois la couverture et la demande en trafic : les valeurs de λ varient entre 2.5 et 3.5 antennes par kilomètre carré (dans le scénario urbain) et avec β variant entre 0.8 et 1.

- La seconde stratégie consiste en un déploiement qui se réalise en deux phases : lors de la première phase, on effectue une couverture en signal. Les valeurs de λ varient alors entre 1 et 2 antennes par kilomètre carré et β entre 0.8 et 1 en scénario urbain. Lors de la seconde phase, la densité d'antennes augmente entre 2.5 et 3.5 antennes par kilomètre carré et β entre 0.5 et 0.8.

La superposition de tous les réseaux à Paris tend vers la réalisation d'un processus ponctuel de Poisson et illustre le Théorème de superposition des processus de β-Ginibre.

.4 Processus ponctuels et performances réseau

Les performances des réseaux sont souvent considérés à travers le prisme de la capacité point à point. En effet, le second théorème de Shannon lie la capacité C, la bande passante W et le rapport signal sur interférence et bruit (*SINR*) du lien :

$$C = W \log_2(1 + SINR)\,.$$

D'un point de vue du réseau, les interférences et plus particulièrement les interférences inter-site sont quantifiées dans le *SINR* et cette quantité est souvent étudiée dans le cas d'un déploiement hexagonal déterministe [37]. Nous avons cependant observé que les réseaux ont une nature stochastique intrinsèque que nous pouvions caractériser par le couple (β, λ). Ainsi dans cette partie nous proposons un cadre théorique permettant de lier le couple (β, λ) avec les performances du lien descendant d'un réseau OFDMA.

.4.1 Modèle du canal

Nous considérons le canal descendant d'un réseau LTE. Les réseaux sont déployés selon un processus de Poisson ponctuel ou un processus de β-Ginibre. Le pire cas est en termes d'interférences est envisagé : chaque cellule utilise la même fréquence que ses voisines. De plus, nous considérons que le canal descendant est découpé en une grille de blocs de ressources (RB), larges de 180kHz et d'une durée de 0.5 milliseconde. Le système est étudié dans un instantané d'une milliseconde. Pendant cet instantané, chaque station de base peut utiliser jusqu'à N_{avail} RBs. Ces blocs sont ensuite distribués aux utilisateurs actifs qui sont placés dans le plan selon un processus de Poisson ponctuel. Les stations de base ne coopèrent pas les unes avec les autres et sont toutes identiques et omni-directionnelles.

Soit Φ_u le processus de Poisson ponctuel de paramètre λ_u représentant la position des utilisateurs actifs. Soit Φ_b le processus de β-Ginibre d'intensité λ_b représentant la position des stations de base. On note ϕ_u et respectivement ϕ_b une réalisation de Φ_u et respectivement Φ_b. Pour un couple $(x, y) \in phi_u \times \phi_b$. On dénote $(G_{xy})_{(x,y)\in\phi_u\times\phi_b}$ une famille de variables aléatoires identiquement distribuées selon une loi exponentielle de paramètre 1. Cette famille représente l'évanouissement du canal. Ainsi nous définissons le modèle de canal suivant :

Définition .5 (Modèle de canal)**.** *La puissance reçue par un utilisateur à la position $x \in \phi_u$ depuis une station de base placée en $y \in \phi_b$ est donnée par :*

$$P(x, y) = P_t G_{xy} \,\|\, x - y \,\|^{-\gamma}, \tag{1}$$

où P_t est la puissance de transmission et γ l'exposant d'affaiblissement.

Nous faisons l'hypothèse que l'utilisateur s'attache à la station de base dont le signal est le plus fort. Ainsi on peut définir le *SIR* comme suit :

Définition .6 (*SIR*)**.** *Le SIR en voie descendante est donnée pour tout* $(x, \phi_b) \in E \times \mathfrak{N}_E$

$$SIR(x, \phi_b) = \max_{y_0 \in \phi_b} \frac{P(x, y_0)}{\sum_{y \in \phi_b} P(x, y) - P(x, y_0)}.$$

Blaszczyszyn et al. [13] et Natakta et al. [68] ont respectivement caractérisé le *SIR* d'un réseau déployé selon un processus ponctuel de Poisson et d'un processus ponctuel de β-Ginibre à travers le concept de probabilité de couverture.

Définition .7 (Probabilité de couverture)**.** *Pour tout* $\theta \geq 0$ *et un processus ponctuel stationnaire* Φ_b*, la probabilité de couverture* $\mathbb{P}(SIR \geq \theta)$ *est donnée par*

$$\mathbb{P}(SIR(\Phi_b) \geq \theta) = \int_{\mathfrak{N}_E} \mathbb{1}_{[-\infty, \theta]} \left(SIR(o, \phi_b) \right) \mathrm{d}\mathbb{P}_{\Phi_b}(\phi_b),$$

où $\mathbb{1}$ *est la fonction indicatrice.*

La probabilité de couverture peut être interprétée comme la proportion du réseau ayant un *SIR* supérieur à un certain seuil. Cette interprétation est raisonnable étant donné que l'on considère des processus stationnaires. Nous donnons les expressions analytiques pour le processus ponctuel de Poisson et le processus de β-Ginibre.

Proposition .5 (Probabilité de couverture pour le processus ponctuel de Poisson [13])**.** *Pour tout* $\theta \geq 1$ *et* $\gamma > 2$ *la probabilité de couverture pour les réseaux déployés selon un processus ponctuel de Poisson est donnée par :*

$$\mathbb{P}(SIR \geq \theta) = \frac{\gamma \sin(2\pi/\gamma)}{2\pi} \theta^{-2/\gamma}.$$

Proposition .6 (Probabilité de couverture pour le processus ponctuel de β-Ginibre [68])**.** *Pour tout* $\theta > 0$ *et* $\gamma > 2$ *la probabilité de couverture pour les réseaux déployés selon un* β*-Ginibre est donnée par :*

$$\mathbb{P}(SIR \geq \theta) = \beta \int_0^\infty e^{-s} \mathcal{M}(s, \theta) S(s, \theta) \, ds$$

$$où \ \mathcal{M}(s, \theta) = \prod_{j=0}^{\infty} \left(1 - \beta + \frac{\beta}{j!} \int_s^\infty \frac{t^j e^{-t}}{1 + \theta(s/t)^{\gamma/2}} \, dt \right)$$

$$et \ S(s, \theta) = \sum_{i=0}^{\infty} s^i \left((1 - \beta) i! + \beta \int_s^\infty \frac{t^i e^{-t}}{1 + \theta(s/t)^{\gamma/2}} \, dt \right)^{-1}.$$

Il est à noter que chacune des propositions .5 et .6 montrent que la probabilité de couverture ne dépend pas de l'intensité λ_b.

La figure 9 montre aussi qu'il existe un forte corrélation entre les propriété spatiales du réseau et de la qualité du signal moyenne du réseau. On constate, en effet qu'il y a jusqu'à 2dB de différence entre le processus ponctuel le plus *uniforme* et le plus *régulier*. Ainsi, le paramètre β a une influence quantifiable sur la qualité du signal. Grâce au second théorème de Shannon, nous savons que cette quantité est liée à la capacité du canal, qui elle est fixée par la demande de chacun des utilisateurs. Nous pouvons alors déduire le nombre de RBs qu'un utilisateur placé en un certain point x du plan, devrait obtenir du réseau pour garantir la capacité demandée.

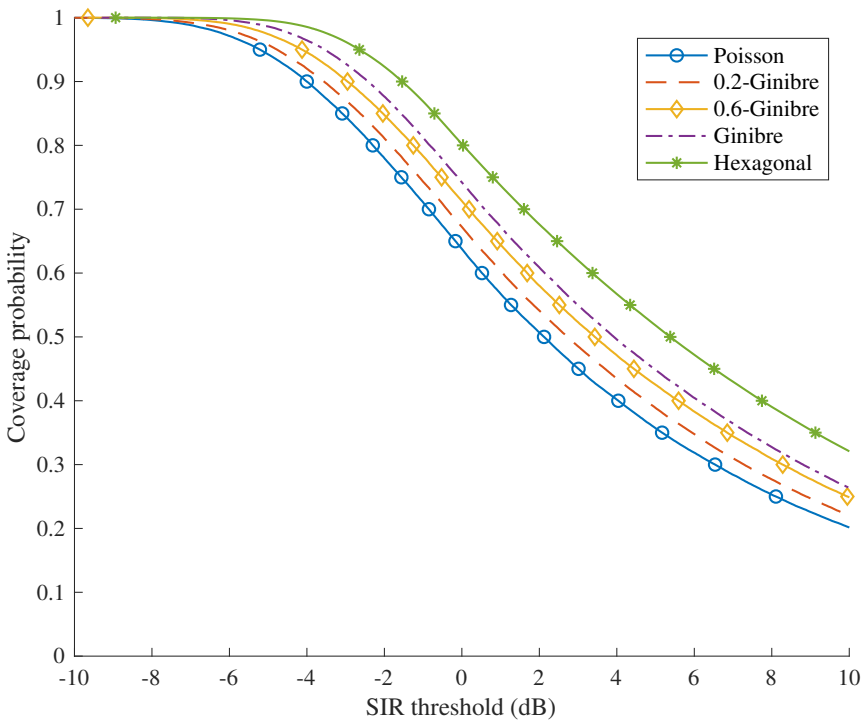

Figure 9: Probabilité de couverture $\mathbb{P}(SIR > \theta)$, pour $\gamma = 4$ et évanouissement indépendant.

Définition .8 (Nombre de RB potentiels à un point du plan)**.** *Le nombre de RB potentiel est le nombre de RB qui devrait être alloué à un utilisateur placé en x pour satisfaire ses besoins en capacité C. Pour tout $(x, \phi_b) \in E \times \mathfrak{N}_E$:*

$$n_r(x, \phi_b) = \min\left(\left\lceil \frac{C}{W_{rb} \log_2(1 + SIR(x, \phi_b))} \right\rceil, l_m \right), \tag{2}$$

où W_{rb} est la largueur spectrale du RB et où l_m est la quantité maximale de RB que l'on peut allouer à un utilisateur.

Par conséquent, pour toute réalisation d'utilisateurs actifs ϕ_u, le nombre total de RB qui devront être alloués dans le réseau déployé selon ϕ_b pour satisfaire la demande des utilisateurs dans un compact $A \in E$ est donnée par :

$$n_{tot}(\phi_u, \phi_b) = \int_{x \in A} n_r(x, \phi_b) \phi_u(\mathrm{d}x). \tag{3}$$

Il y a cependant une autre manière d'obtenir la quantité $n_{tot}(\phi_u, \phi_b)$. Soit la famille de fonctions $(a_l)_{1 \le l \le l_m}$, tel que pour chaque l et tout compact $A \subset E$, on a
$a_l : A \times \mathfrak{N}_E \to [0, 1]$,

$$a_l(x, \phi_b) = \begin{cases} \mathbb{1}_{[t_1, +\infty[}\left(SIR(x, \phi_b)\right) & \text{if } l = 1, \\ \mathbb{1}_{[0, t_{l_{m-1}}]}\left(SIR(x, \phi_b)\right) & \text{if } l = l_m, \\ \mathbb{1}_{[t_l, t_{l-1}]}\left(SIR(x, \phi_b)\right) & \text{otherwise,} \end{cases}$$

où t_l est le *SIR* nécessaire pour allouer l RB à un utilisateur. Selon le second théorème de Shannon :

$$t_l = 2^{C/lW_{rb}} - 1.$$

Le nombre de RB demandé par l'ensemble des utilisateurs peut donc prendre la forme :

$$n_{tot}(\phi_u, \phi_b) = \sum_{l=1}^{l_m} l \int_{x \in A} a_l(x, \phi_b) \phi_u(\mathrm{d}x).$$

Notons que cette quantité est calculée pour une réalisation d'un réseau donné ϕ_b et une réalisation d'utilisateurs ϕ_u. Ainsi, nous pouvons généraliser l'étude en considérant la variable aléatoire $n_{tot}(\Phi_u, \Phi_b)$, qui dépend de chacun des processus ponctuels des utilisateurs et des stations de base. Comme nous étudions l'influence du processus ponctuel relatif au déploiement du réseau, nous étudions l'espérance conditionnelle de $n_{tot}(\Phi_u, \Phi_b)$ relativement à la mesure $\mathrm{d}\mathbb{P}_{\Phi_b}$.

Définition .9 ($N_{tot}(\Phi_u)$)**.** *La variable aléatoire $N_{tot}(\Phi_u)$ est définie comme l'espérance conditionnelle par rapport au processus ponctuel Φ_b. Pour ϕ_u, une réalisation de Φ_u, il vient :*

$$\begin{aligned} N_{tot}(\phi_u) &= \mathbb{E}_{\Phi_b}[n_{tot}(\Phi_u, \phi_b) | \Phi_u = \phi_u], \\ &= \sum_{l=1}^{l_m} l \iint_{(x,\phi_b) \in A \times \mathfrak{N}_E} a_l(x, \phi_b) \mathrm{d}\mathbb{P}_{\Phi_b}(\phi_b) \phi_u(\mathrm{d}x). \end{aligned}$$

Nous pouvons caractériser la loi $N_{tot}(\Phi_u)$. Soit la famille $(\alpha_l)_{1 \leq l \leq l_m}$ définie par :

$$\alpha_l = \begin{cases} \mathbb{P}(t_1 < \mathit{SIR}(0, \Phi_b)) & \text{if } l = 1, \\ \mathbb{P}\big(t_{l_{m-1}} \geq \mathit{SIR}(0, \Phi_b)\big) & \text{if } l = l_m, \\ \mathbb{P}(t_l \leq \mathit{SIR}(0, \Phi_b) < t_{l-1}) & \text{otherwise.} \end{cases}$$

Proposition .7. *Pour un processus ponctuel stationnaire Φ_b et un processus de poisson Φ_u de paramètre λ_u, la variable aléatoire $N_{tot}(\Phi_u)$ observée dans un compact $A \subset E$ est un processus de Poisson composé tel que :*

$$N_{tot}(\Phi_u) = \sum_{l=1}^{l_m} l M_l,$$

où chaque M_l suit une loi de Poisson de paramètre $\lambda_u \alpha_l |A|$.

Connaissant la fonction caractéristique de chacun des M_l donnée par :

$$\forall t \in \mathbb{R}, \quad \Psi_l(t) = \exp\big(\alpha_l \lambda_u |A| \left(e^{it} - 1\right)\big),$$

nous pouvons en déduire la fonction caractéristique de $N_{tot}(\Phi_u)$.

Proposition .8 (Fonction caractéristique de $N_{tot}(\Phi_u)$)**.** *La fonction caractéristique Ψ de $N_{tot}(\Phi_u)$ est donnée par :*

$$\forall t \in \mathbb{R}, \quad \Psi(t) = \prod_{l=1}^{l_m} \Psi_l(lt). \tag{4}$$

Selon l'équation (4), nous pouvons calculer la distribution de $N_{tot}(\Phi_u)$, ainsi que sa fonction de répartition par convolution discrète des distributions de chaque terme lM_l:

$$\mathbb{P}(lM_l = \omega) = \begin{cases} 0 & \text{if } \omega \neq 0 \bmod l, \\ \exp(-m_l)\, m_l^q/q! & \text{if } \exists q \in \mathbb{N},\ \omega = ql, \end{cases}$$

où $m_l = \lambda_u \alpha_l |A|$.

.4.2 Application au dimensionnement

Afin de quantifier l'influence de la qualité du déploiement de chacun des types de réseau, nous proposons les métriques suivantes.

Définition .10 (La probabilité de dépassement de capacité)**.** *La probabilité de dépassement de capacité associé à un réseau déployé selon Φ_b et des utilisateurs placés selon Φ_u dans un compact $A \in E$ est donnée par :*

$$\mathbb{P}_{\Phi_u,\Phi_b}(n_{tot}(\Phi_u,\Phi_b) > N_{avail}\Phi_b(A))\,.$$

Cette définition n'étant pas pratique car dépendant de deux processus ponctuels, nous considérons la métrique moyennée respectivement par rapport à la mesure $\mathrm{d}\mathbb{P}_{\Phi_b}$.

Définition .11 (Probabilité de dépassement de capacité moyenne)**.** *La probabilité de dépassement de capacité moyenne associé aux réseaux déployés selon un β-Ginibre ou un processus ponctuel de Poisson Φ_b et pour des utilisateurs placés selon un processus ponctuel de Poisson Φ_u dans un compact $A \in E$ est donné par*

$$\mathbb{P}_{\Phi_u}(N_{tot}(\Phi_u) > N_{avail}\lambda_b|A|)\,.$$

Cette métrique dépend uniquement de la variable aléatoire $N_{tot}(\Phi_u)$ qui a été entièrement définie et caractérisée supra. Ainsi, nous pouvons étudier l'inégalité

$$\mathbb{P}_{\Phi_u}(N_{tot}(\Phi_u) > N_{avail}\lambda_b|A|) \leq \epsilon,$$

avec $\epsilon > 0$. Cette inégalité peut être étudié directement, mais grâce à l'inégalité de concentration [27], nous pouvons fournir une borne conservative à des fins d'ingénierie radio.

Théorème .2. *Pour tout réel $a > 0$, la borne supérieure est donnée par :*

$$\mathbb{P}_{\Phi_u}(N_{tot}(\Phi_u) \geq \mathbb{E}_{\Phi_u}[N_{tot}(\Phi_u)] + a) \leq \exp\left(-\frac{\int_A n_r^2(x)\lambda_u \mathrm{d}x}{l_m^2}\, \mathrm{g}\left(\frac{a\, l_m}{\int_A n_r^2(x)\lambda_u \mathrm{d}x}\right)\right),$$

où $g(\theta) = (1+\theta)\ln(1+\theta) - \theta$ pour tout $\theta > 0$.

.4.3 Résultats numériques

Les applications numériques sont effectuées sur des réseaux générés selon un processus de Poisson et selon un processus de β-Ginibre pour cinq valeurs de β. Nous considérons trois scénarios :

- Le seuil ϵ est fixé. Nous considérons le nombre de RB N_{avail} en fonction du l'exposant d'affaiblissement γ.

- Le seuil ϵ est fixé. Nous considérons la borne $\hat{N}_{avail}$ déduite de l'application du théorème .2 en fonction de l'exposant d'affaiblissement γ.
- Pour N_{avail} donné, la probabilité de dépassement de capacité est tracée en fonction de γ.

Table 11: Paramètres de simulation

P	1 W
λ_b	3.0 per km^2
λ_u	40 per km^2
l_m	10
C	1 Mb/s
W_{rb}	180 kHz
Exposant d'affaiblissement	from 2 to 5
Rayon du compact considéré	1.8 km

Les paramètres de simulation sont résumés dans la table 11. Les valeurs de λ_n et λ_u sont choisies comme observées en ville. Les utilisateurs sont identiques et demandent tous une capacité de 1 Mb/s.

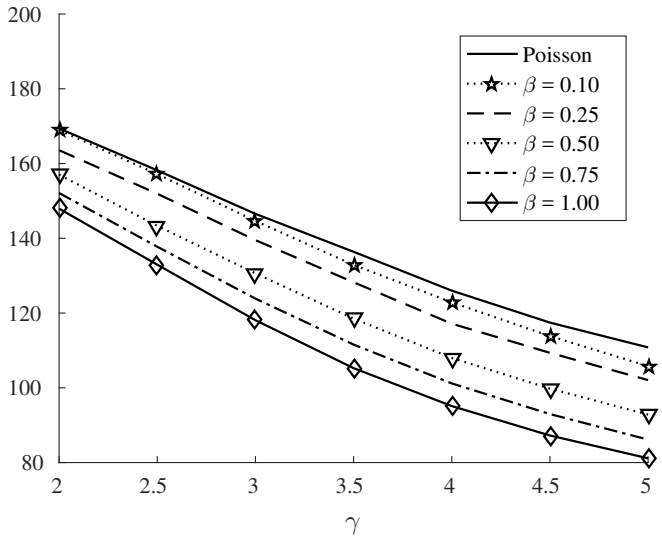

Figure 10: N_{avail} en fonction de γ pour une probabilité de dépassement bornée à $\epsilon = 10^{-2}$

Le graphique 10 illustre que le nombre moyen de RB devant être affecté à chaque antenne pour un seuil de dépassement de capacité donné décroît de 30% avec l'augmentation de l'exposant d'affaiblissement γ. En effet, plus les conditions radio sont difficiles, moins les cellules interfères les unes avec les autres. Ainsi chaque cellule aura en moyenne plus de surface avec un *SIR* élevé. De même, le graphique 12 nous montre que pour un nombre fixé de RB par antenne, la probabilité de dépassement de capacité décroît avec l'augmentation de γ. Le

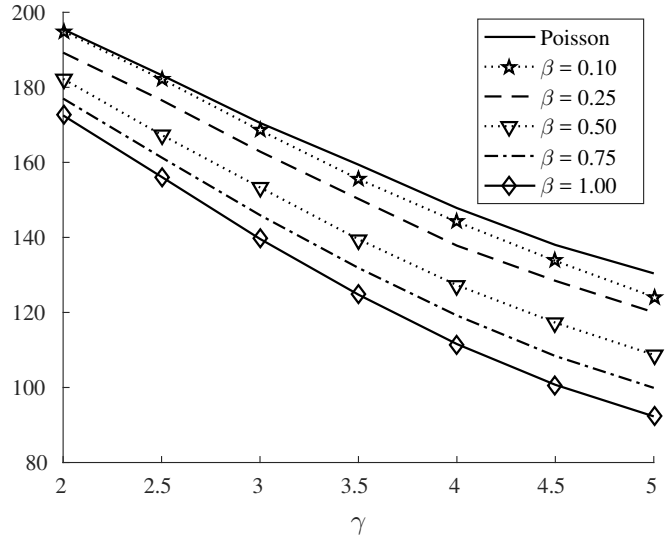

Figure 11: Borne supérieure $\hat{N}_{avail}$ en fonction de γ pour une probabilité de dépassement bornée à $\epsilon = 10^{-2}$

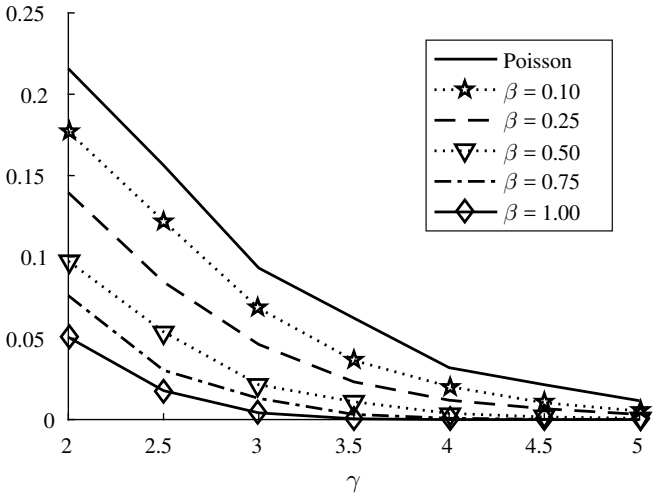

Figure 12: Probabilité de dépassement pour $N_{avail} = 100$ en fonction de γ

graphique 11 montre que la borne supérieure donnée par le théorème .2 est pessimiste et est supérieure de 10% par rapport au résultat exact. Pour chacun des scénarios, on constate que plus le paramètre β est élevé, meilleures sont les performances du réseau. On constate par ailleurs sur les graphiques 10 et 11 une amélioration des performances située entre 12% and 26% suivant la valeur de γ entre les cas Poisson et Ginibre. De plus, la probabilité de dépassement est divisée jusqu'à 4 entre un processus ponctuel de Ginibre et un processus ponctuel de Poisson.

.4.4 Conclusion

Dans cette partie nous avons étudié lien entre la qualité d'un déploiement réseau représenté par le paramètre β et les performances du réseau. Nous avons montré qu'il peut y avoir jusqu'à 25% entre un réseau déployé selon un processus de Poisson et un réseau déployé selon un processus de Ginibre.

.5 Nouveaux paradigmes pour l'allocation de ressources

Dans cette partie nous considérons toujours un réseau LTE en voie descendante. Lorsque la demande en RB dans le réseau dépasse le nombre de RB disponibles dans le réseau (scénario du dépassement de capacité), il est nécessaire dans un premier temps, de savoir combien de RB doivent être allouées à chaque utilisateur : c'est le problème de dimensionnement. Puis il est nécessaire de savoir pour chaque RB, quelle est la station de base servant quel utilisateur : c'est le problème d'allocation. Grâce au cadre théorique des équilibres de Cournot-Nash et du transport optimal, il nous est possible de répondre à ces deux défis en même temps.

.5.1 Modélisation du système

Comme précédemment, nous étudions un réseau cellulaire composé de stations de base omnidirectionnels placées dans le plan selon un processus ponctuel Φ_b (de Poisson ou de β-Ginibre) d'intensité λ_b. Chaque station de base dispose de N_{avail} RBs. Les utilisateurs sont placés selon un processus de Poisson ponctuel Φ_u d'intensité λ_u. On note par n le nombre de stations de base et par m le nombre d'utilisateurs dans le compact d'étude $A \subset E$.

Les réalisations des stations de base et des utilisateurs dans le compact A sont respectivement les ensembles de points $\phi_b = \{y_i\}_{1\leq i\leq n}$ et $\phi_u = \{x_j\}_{1\leq j\leq m}$. On note par N_j le nombre de RBs qu'un utilisateur x_j a besoin pour satisfaire la capacité désirée C, sachant qu'il est attaché à la station de base avec le meilleur *SINR* :

$$N_j = n_r(x_j, \phi_b) = \min\left(\left\lceil \frac{C}{W_{rb}\log_2(1+SINR(x_j,\phi_b))}\right\rceil, l_m\right).$$

Par conséquent, la demande totale de ressources est donnée par

$$n_{tot}(\phi_u, \phi_b) = \sum_{j=1}^{m} N_j.$$

Deux cas de figure peuvent se présenter :

1. Il y a dépassement de capacité du réseau : $n_{tot}(\phi_u, \phi_b) \geq N_{avail}\phi_b(A)$.
2. Il n'y a pas de dépassement de capacité du réseau : $n_{tot}(\phi_u, \phi_b) \leq N_{avail}\phi_b(A)$.

A partir d'ici nous ne nous attacherons qu'au premier cas de figure. Dans cette situation, ce sont les ressources réseau qui limitent le nombre de RB à allouer aux utilisateurs. Par conséquent, nous considérons que tous les RB disponibles sur le réseau sont utilisés.

Définition .12. *Soit μ_i la fraction de RB du réseau disponibles à la station de base placée en y_i :*

$$\mu_i = \frac{1}{n}.$$

Définition .13. *Soit ν_j^f la fraction de la demande en RB pour satisfaire l'utilisateur placé en x_j :*

$$\nu_j^f = \frac{N_j}{n_{tot}(\phi_u, \phi_b)}.$$

Définition .14. *Soit ν_j la fraction des RB du réseau alloué à un utilisateur placé en x_j :*

$$\nu_j = \frac{n_j^a}{N_{avail}\phi_b(A)},$$

où n_j^a est le nombre de RB alloué à un utilisateur placé en x_j.

Définition .15. *Soit π_{ij} la proportion de RB disponibles dans le réseau utilisée entre la station de base placée en y_i et l'utilisateur placé en x_j. La quantité π_{ij} vérifie :*

$$\sum_{i=1}^{n} \pi_{ij} = \nu_j,$$

et

$$\sum_{j=1}^{m} \pi_{ij} = \mu_i.$$

Dans ce modèle, nous considérons qu'un utilisateur peut être servi par plusieurs stations de base, ce qui introduit une certaine forme de coopération. Ainsi ces définitions traduisent le fait que du point de vue d'un utilisateur, le nombre total de RB alloués à cet utilisateur est égal à la somme des blocs de ressources provenant de chaque station de base. De même, le nombre total de RBs d'une station de base est égal aux RBs alloués à ses utilisateurs.

Soit $\mathcal{P}([1,n])$ l'ensemble des mesures de probabilité sur $[1,n]$. Les quantités $\boldsymbol{\mu} = (\mu_1, \ldots, \mu_n)$, $\boldsymbol{\nu} = (\nu_1, \ldots, \nu_m)$ et $\boldsymbol{\pi} = (\pi_{1,1}, \ldots \pi_{nm})$ sont des mesures de probabilité discrètes. La mesure de probabilité $\boldsymbol{\mu}$ (respectivement $\boldsymbol{\nu}$) appartient à l'ensemble $\mathcal{P}([1,n])$ (respectivement $\mathcal{P}([1,m])$. La mesure de probabilité $\boldsymbol{\pi}$ appartient à l'ensemble $\Sigma(\boldsymbol{\mu}, \boldsymbol{\nu})$ et sa première (respectivement sa seconde) marginale est égale à $\boldsymbol{\mu}$ (respectivement $\boldsymbol{\nu}$).

Comme le réseau doit dimensionner les ressources allouées à chaque utilisateur, il faut introduire une métrique pour caractériser la différence entre le nombre de ressources allouées à un utilisateur et les ressources demandées par chaque utilisateur. Cette métrique doit également saisir l'équité globale de la politique d'allocation au niveau du réseau. Nous introduisons donc la fonction d'équité suivante.

Définition .16 (Fonction d'équité)**.** *La fonction d'équité est donnée par*

$$s(\boldsymbol{\nu}) = {}^t(\boldsymbol{\nu} - \boldsymbol{\nu}^f)(\boldsymbol{\nu} - \boldsymbol{\nu}^f),$$

où $\boldsymbol{\nu}^f = \left(\nu_1^f, \ldots, \nu_m^f\right)$ et ${}^t\boldsymbol{\nu}$ est la transposé de $\boldsymbol{\nu}$.

La fonction d'équité représente la distance quadratique entre la proportion de ressources demandée et la proportion allouée. L'équité entre les utilisateurs est assurée puisque la proportion de ressources plutôt que le nombre absolu de ressources est prise en compte. Le choix d'une fonction quadratique donne également de bonnes propriétés d'optimisation. En effet, elle est intrinsèquement convexe sur $\mathbb{R}^n$.

Soit c_{ij} le coût de transmission d'un RB entre la station de base placée en y_i et l'utilisateur placé en x_i tel que

$$c_{ij} = \frac{\sum_{k=1}^{n} P(x_j, y_k) - P(x_j, y_i) + N_0 W_{rb}}{P(x_j, y_i)}.$$

Le coût c_{ij} est l'inverse du *SINR* calculé pour le canal radio entre une station de base en y_i et un utilisateur en x_j.

Définition .17 (Fonction de coût)**.** *Pour une mesure de probabilité $\boldsymbol{\pi} \in \Sigma(\boldsymbol{\mu}, \boldsymbol{\nu})$, le coût total d'allocation des ressources est donné par*

$$W_c(\boldsymbol{\pi}) = \sum_{(i,j)} c_{ij}\, \pi_{ij}.$$

Définition .18 (Le problème joint de dimensionnement et d'allocation)**.** *Le problème joint de dimensionnement et d'allocation est formulé selon le problème d'optimisation suivant :*

$$\boldsymbol{\pi}^* = \underset{\pi \in \Sigma(\boldsymbol{\mu}, \boldsymbol{\nu})}{\operatorname{argmin}} W_c(\boldsymbol{\pi}) + s(\boldsymbol{\nu}),$$

où l'optimum $\boldsymbol{\pi}^*$ vérifie:

$$\begin{aligned}
&\forall 1 \leq i \leq n,\ \sum_{j=1}^{m} \pi_{ij}^* = \mu_i, \\
&\forall 1 \leq j \leq m,\ \sum_{i=1}^{n} \pi_{ij}^* = \nu_j \leq \nu_j^f, \\
&\forall (i,j),\ \pi_{ij} \geq 0.
\end{aligned}$$

Ce problème d'optimisation vise à minimiser conjointement la fonction de coût et la fonction d'équité. En plus du terme d'équité, la fonction de coût fournit l'allocation des ressources en prenant en compte la coopération entre les stations de base. Cela signifie que toute station de base peut fournir des RBs à n'importe quel utilisateur. Cependant, il est peu probable que des RBs soient transférés depuis des stations de base éloignées d'un utilisateur donné. En effet, le coût augmente avec la distance et les interférences, ce qui prévient un tel comportement. Les trois contraintes du problème d'optimisation concernent l'allocation des RBs entre les stations de base et les utilisateurs. Comme nous considérons le réseau dans un état de dépassement de capacité : la contrainte sur la famille de $(\mu_i)_{1 \leq i \leq n}$ est saturée, ce qui signifie que tous les RBs de chaque antenne sont alloués aux utilisateurs. La seconde contrainte n'est pas saturée, ce qui signifie que la demande de chaque utilisateur peut ne pas être entièrement satisfaite.

.5.2 Caractérisation du problème d'optimisation

Le problème d'optimisation de la définition .18 est en fait un problème de Cournot-Nash comme définit dans les travaux de Blanchet et al. [11]. Il est en effet la somme du terme de coût W_c qui contrôle l'allocation des ressources et du terme d'équité s qui contrôle de dimensionnement des ressources des utilisateurs. Cependant, le problème d'optimisation n'étant pas continu par rapport à la mesure de Lebesgue, il n'est pas possible d'appliquer les résultats de Blanchet et al.

Résolution exacte

Lemme .1. *Le problème d'optimisation est un problème d'optimisation quadratique :*

$$\boldsymbol{\pi}^* = \underset{\boldsymbol{\pi}}{\operatorname{argmin}} {}^t\boldsymbol{\pi} H \boldsymbol{\pi} + {}^t\mathbf{L}\boldsymbol{\pi},$$

tel que :

$$\begin{aligned} &T_n\boldsymbol{\pi} = \boldsymbol{\mu}, \\ &T_m\boldsymbol{\pi} \leq \boldsymbol{\nu}^f, \\ &\forall 1 \leq l \leq nm,\ \pi_l \geq 0, \end{aligned}$$

où :

$$\begin{aligned} T_n &= \mathbf{1}_{1,m} \otimes \mathbf{Id}_n, \\ T_m &= \mathbf{Id}_m \otimes \mathbf{1}_{1,n}, \\ H &= {}^tT_mT_m = \mathbf{Id_m} \otimes \mathbf{1}_{n,n}, \\ \mathbf{L} &= \mathbf{c} - 2T_m\boldsymbol{\nu}^f. \end{aligned}$$

L'opérande $\otimes$ représente le produit Kronecker. La matrice $\mathbf{Id_m}$ correspond à la matrice d'identité de dimension m et la matrice $\mathbf{1}_{m,n}$ est la matrice de 1 avec m lignes et n colonnes.

Ce lemme est la reformulation vectorielle de la définition .18. Puisque H est une matrice semi-définie positive et que $\boldsymbol{\pi}^*$ est une mesure de probabilité, la limite du domaine d'optimisation est assurée. L'existence d'une solution est donc garantie. Une telle formulation peut-être implémentée dans un solveur quadratique. Cependant, la matrice H n'étant pas de rang plein, la solution n'est pas nécessairement unique et trouver une solution peut être NP-difficile [74]. Dans le paragraphe suivant, nous présentons une approximation, qui fournit une solution en temps polynomial.

Équilibres approchés

Le lemme .1 met en évidence la structure algébrique du problème d'optimisation : le couplage induit par le fait qu'il existe une correspondance entre les probabilités $\boldsymbol{\mu}$ et $\boldsymbol{\nu}$, définit la matrice H. La représentation de H en tant que produit Kroneker ($H = \mathbf{Id_m} \otimes \mathbf{1}_{n,n}$) montre la superposition sous-jacente du problème d'allocation et du dimensionnement des ressources. Le facteur $\mathbf{Id_m}$ représente l'allocation des ressources et le facteur $\mathbf{1}_{n,n}$ représente l'allocation optimal de ressources pour chaque utilisateur. La formalisation quadratique ne peut toutefois pas être complètement séparée en raison du terme de coût $\mathbf{c}$ qui caractérise de manière unique la qualité du signal entre une station de base et un utilisateur. Considérant que la plupart des ressources sont allouées sur le lien du coût minimal c_j^{min}, défini par $c_j^{min} = \min_i c_{ij}$, la stratégie simplifiée suivante est appliquée:

- Tout d'abord, nous résolvons le problème de dimensionnement des ressources avec le coût exprimé sous la forme d'un vecteur $\mathbf{c}^{min}$ des coefficients c_j^{min},
- Puis, nous résolvons l'allocation de ressources entre les stations de base et les utilisateurs avec la fonction de coût.

Afin de résoudre le problème de dimensionnement des ressources, la matrice de coût est remplacée par le vecteur de coût $\mathbf{c}^{min}$. La résolution de ce problème n'est considérée que du point de vue de l'utilisateur, ce qui équivaut à trouver la mesure $\boldsymbol{\nu}$ qui satisfait le problème d'optimisation quadratique indépendamment de la mesure $\boldsymbol{\mu}$.

Définition .19. *Le problème simplifié est donné par :*

$$\boldsymbol{\nu}^* = \underset{\boldsymbol{\nu}}{\operatorname{argmin}} {}^t\boldsymbol{\nu} H \boldsymbol{\nu} + {}^t\tilde{\mathbf{L}}\boldsymbol{\nu},$$

tel que :

$${}^t\mathbf{1}_{1,m} \cdot \boldsymbol{\nu} = 1 \text{ and } \nu_j \geq 0,$$

avec :

$$H = \mathbf{Id}_m, \text{ and } \tilde{\mathbf{L}} = \mathbf{c}^{min} - 2\boldsymbol{\nu}^f.$$

Lemme .2. *La fonction d'utilité du problème d'optimisation simplifié est équivalente à une équation d'hypersphère.*

En effet, le problème d'optimisation simplifié peut être écrit sous la forme suivante:

$$\boldsymbol{\nu}^* = \underset{\boldsymbol{\nu}}{\operatorname{argmin}} {}^t\boldsymbol{\nu} H \boldsymbol{\nu} + {}^t\tilde{\mathbf{L}}\boldsymbol{\nu} + \frac{1}{4}{}^t\tilde{\mathbf{L}}\tilde{\mathbf{L}},$$

tel que :

$${}^t\mathbf{1}_{1,m} \cdot \boldsymbol{\nu} = 1 \text{ and } \nu_j \geq 0,$$

On note par $\mathcal{C}$, l'enveloppe convexe définie par les contraintes. La constante ajoutée ne modifie pas les optimums et par conséquent, ce problème est équivalent au problème d'optimisation simplifié. De plus, la fonction d'utilité est l'équation d'une hypersphère du centre $\boldsymbol{\nu}^0 = -\tilde{\mathbf{L}}/2$ et la valeur de la fonction objectif correspond à son rayon.

Théorème .3. *La solution $\boldsymbol{\nu}^*$ est unique et est de la forme :*

$$\boldsymbol{\nu}^* = \boldsymbol{\nu}^0 - \frac{{}^t\mathbf{u}(\boldsymbol{\nu}^0 - \mathbf{M})}{(m-k)}\mathbf{u},$$

où k est le nombre de coordonnées nulles de $\boldsymbol{\nu}^*$, $\mathbf{u} = \mathbf{1}_{m-k,1}$, $\boldsymbol{\nu}^0 = -\tilde{\mathbf{L}}/2$ et $\mathbf{M} = \mathbf{u}/(m-k)$.

Une fois déterminée la solution au dimensionnement, il suffit de résoudre le problème d'allocation formulé comme suit :

$$\boldsymbol{\pi}^* = \underset{\pi \in \Sigma(\boldsymbol{\mu}, \boldsymbol{\nu}^*)}{\operatorname{argmin}} W_c(\boldsymbol{\pi}),$$

où l'optimum $\boldsymbol{\pi}^*$ vérifie:

$$\forall 1 \leq i \leq n, \ \sum_{j=1}^{m} \pi_{ij}^* = \mu_i,$$

$$\forall 1 \leq j \leq m, \ \sum_{i=1}^{n} \pi_{ij}^* = \nu_j^*,$$

$$\forall (i,j), \ \pi_{ij}^* \geq 0.$$

Ceci est un problème de transport optimal au sens de Monge-Kantorovitch. Comme ce problème est linéaire, une solution peut être déterminé par l'algorithme du simplexe en un temps polynomial. Ainsi on en déduit le résultat suivant pour le problème approché :

Théorème .4. *Un optimum du problème approché peut être trouvé en un temps polynomial.*

.5.3 Numerical analysis

Au niveau du système, trois indicateurs sont analysés.

- Le ratio de satisfaction des utilisateurs :

$$r_u = \frac{1}{m} \sum_{j=1}^{m} \frac{n_j^a}{N_j},$$

dans le cas d'un dépassement de capacité. Il représente la moyenne du rapport entre le nombre de RB alloués par le réseau à chaque utilisateur et le nombre de ressources demandées par chaque utilisateur. Si le réseau n'est pas en dépassement de capacité,

$$r_u = 1.$$

- Le ratio d'occupation du réseau :

$$r_n = 1.$$

dans le cas d'un dépassement de capacité. Dans le cas contraire,

$$r_n = \frac{1}{n} \sum_{j=1}^{n} \frac{n_j^u}{N_{avail}}.$$

C'est la proportion des ressources totales disponibles utilisées dans le réseau.

- Le ratio de coopération :

$$r_c = \frac{1}{m} \sum_{j=1}^{m} \mathbb{1}_{\left[\left[\sum_{i=1}^{n} \mathbb{1}_{[\pi_{ij} \neq 0]}\right] > 1\right]},$$

est la proportion d'utilisateurs qui reçoivent des RBs provenant de plusieurs stations de base.

Nous définissons le point de fonctionnement optimal du réseau comme l'intersection de la courbe de satisfaction de l'utilisateur et de la courbe d'occupation du réseau. Dans la section suivante, ce point est identifié pour les solutions exactes et approchées de Cournot-Nash. Sa position relative est étudiée dans plusieurs cas de déploiement de réseau.

Les paramètres de simulation sont résumés dans le tableau 12. Les courbes des graphiques 13, 14a et 14b correspondent à l'espérance de chaque indicateur par rapport aux processus ponctuels des stations de base Φ_b et des utilisateurs Φ_u.

Comparaison des équilibres de Cournot-Nash exacts et approchés

Dans le graphique 13, r_n, r_u et r_c sont tracés pour les équilibres exacts de Cournot-Nash en fonction du rapport de densité λ_u/λ_b en traits pleins. En utilisant la fonction Matlab `quadprog`, une itération pour le nombre maximum d'utilisateurs prend environ 3 secondes pour calculer sur un ordinateur portable 8 cœurs datant de fin 2014. Ce chiffre a été produit avec 500 itérations. Le point de fonctionnement optimal du réseau est atteint pour un ratio de densité de 21 et pour un taux de satisfaction des utilisateurs (ou une occupation du réseau)

Table 12: Paramètres de simulation

P	1 Watt
λ_b	10 antennes par km^2
λ_u	10 à 500 utilisateurs par km^2
l_m	10
C	500 kb/s
W_{rb}	180 kHz
N_{avail}	100
Exposant d'affaiblissement γ	3
Évanouissement lent	10 dB
Rayon du réseau	1.8 km

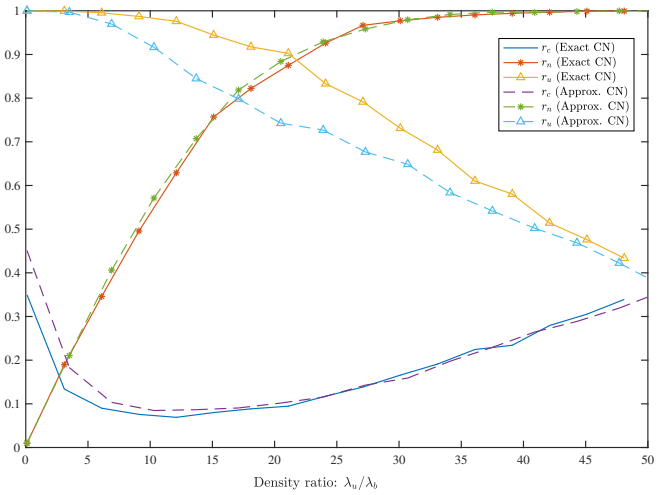

Figure 13: Comparaison des équilibres de Cournot-Nash exacts et approchés pour un 1/4-Ginibre.

de 89%. La proportion de coopération atteint un minimum au voisinage du point de fonctionnement optimal, avec environ 10% des utilisateurs en coopération. La forme en U de la courbe de coopération met également en évidence le passage d'un réseau à faible probabilité de dépassement à un réseau avec une forte probabilité de dépassement. Du point de vue du modèle, une faible charge réseau et une charge réseau élevée sont des situations identiques: il existe un grand déséquilibre entre la quantité de RB disponible à allouer et la quantité de RB pouvant être alloués. Par conséquent, la proportion minimum de coopération est atteinte lorsque la densité d'utilisateurs actifs est de 5 à 15 fois supérieure à la densité de la station de base, zone où la probabilité de dépassement est la même que celle de ne pas être en dépassement.

Une comparaison entre les solutions approchées et les solutions exactes est également donnée dans le graphique 13. Le transport optimal a été résolu avec la fonction `intlinprog`. Une itération pour une densité de 500 utilisateurs et 10 stations de base par unité de carré est calculée en environ 350 ms. Le point de fonctionnement optimal du réseau est atteint pour un

ratio de densité de 17 et pour un taux de satisfaction des utilisateurs (ou une occupation du réseau) de 80%. Le cas approché se révèle donc être une limite pessimiste de la solution exacte de Cournot-Nash, qui peut être utilisée pour une estimation pessimiste des performances du réseau. C'est un bon compromis entre complexité de calcul et précision, puisque le calcul est environ dix fois plus rapide que l'algorithme exact, alors que l'erreur est inférieure à 5% sur l'ensemble des indicateurs. La proportion de coopération et les comportements d'occupation du réseau sont similaires aux courbes exactes.

Impact du déploiement du réseau sur le point de fonctionnement optimal du réseau

Nous considérons des réseaux composés d'antennes dessinées selon un processus de points β-Ginibre ou Poisson avec la même intensité λ_b.

Dans les graphiques 14a et 14b, l'impact de la régularité est étudié. Les courbes des processus ponctuels Poisson et β-Ginibre sont tracées pour les équilibres exacts et approchés de Cournot-Nash. Quatre processus ponctuels β-Ginibre sont considérés avec quatre valeurs de β : 0,25, 0,50, 0,75 et 1. Les résultats sont donnés dans le tableau 13.

Table 13: Points de fonctionnement optimal en fonction du facteur β.

	Exact CN		CN approché	
Processus ponctuel	λ_u/λ_b	r_u or r_n	λ_u/λ_b	r_u or r_n
Poisson	21	88%	17	80%
$\beta = 0.25$	22.5	88%	19	82%
$\beta = 0.50$	25	90%	21	84%
$\beta = 0.75$	27.5	92%	22.5	85%
$\beta = 1$	29	94%	24	87%

Pour les équilibres exacts et approchés de Cournot-Nash, le rapport de densité et la satisfaction de l'utilisateur du point de fonctionnement optimal augmentent conjointement avec la valeur du paramètre β. Cela s'explique par le fait que la qualité globale du *SINR* dans le réseau augmente avec la régularité du déploiement.

.5.4 Conclusion

Dans cette partie nous avons proposé un nouveau cadre théorique basé sur les équilibres de Cournot-Nash pour résoudre le problème joint du dimensionnement et de l'allocation de ressources dans le réseau. Les résultats nous révèlent qu'il existe un point optimal de fonctionnement du réseau et que ce point de fonctionnement est atteint pour un rapport de densité plus élevé lorsque le réseau est régulièrement déployé.

.6 Travaux futurs

Les processus de ponctuels β-Ginibre fournissent de nombreuses informations sur les stratégies de performance et de déploiement du réseau. À cet égard, nous avons précisément caractérisé les performances du réseau pour la liaison descendante. Les limites du modèle de processus de ponctuels β-Ginibre sont dues en partie au fait que le réseau, que nous souhaitons caractériser, doit avoir des propriétés spatiales homogènes. Au niveau régional, d'autres processus peuvent

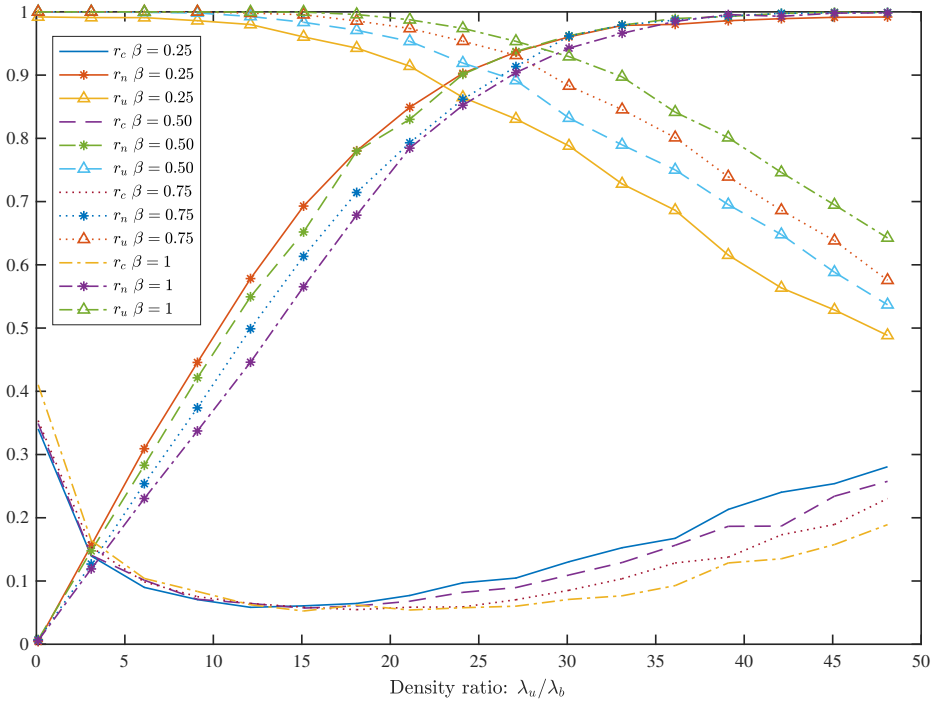

(a) Équilibre de Cournot-Nash exact

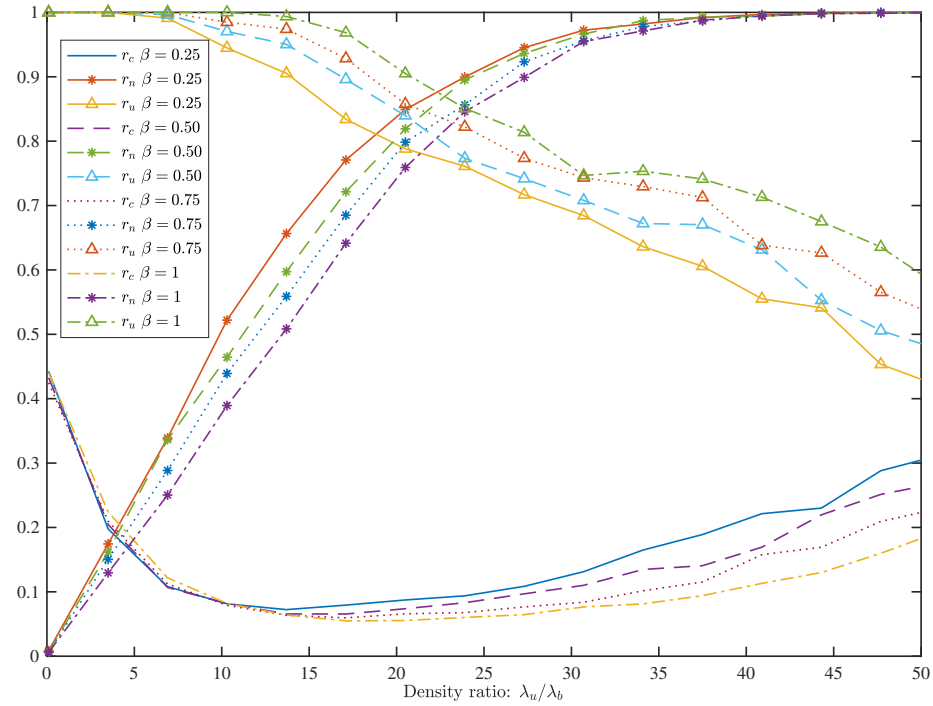

(b) Équilibre de Cournot-Nash approché

Figure 14: Équilibres obtenus pour β =0.25, 0.50, 0.75 and 1

être étudiés. En ce qui concerne l'analyse des performances, la théorie des files d'attente pourrait être introduite pour caractériser le lien entre la densité des abonnés et la densité d'antennes.